REDUCED-ORDER MODELLING AND SIMULATION OF INTEGRATED AC-DC SYSTEMS USING GAM-TYPE DYNAMIC PHASOR SOLUTION APPROACH

by

Xing Liang

B.Eng, Southwest Jiaotong University, 2017

A THESIS SUBMITTED IN PARTIAL FULFILLMENT OF

THE REQUIREMENTS FOR THE DEGREE OF

MASTER OF APPLIED SCIENCE

in

THE FACULTY OF GRADUATE AND POSTDOCTORAL STUDIES

(ELECTRICAL AND COMPUTER ENGINEERING)

THE UNIVERSITY OF BRITISH COLUMBIA

(Vancouver)

September 2019

The following individuals certify that they have read, and recommend to the Faculty of Graduate and Postdoctoral Studies for acceptance, a thesis/dissertation entitled:

Reduced-order Modelling and Simulation of Integrated AC-DC Systems Using GAM-type Dynamic Phasor Solution Approach

submitted by Xing Liang in partial fulfillment of the requirements for

the degree of Master of Applied Science

in The Faculty of Graduate and Postdoctoral Studies

Examining Committee:

Dr. Juri Jatskevich, Electrical and Computer Engineering
Supervisor

Dr. William Dunford, Electrical and Computer Engineering
Supervisory Committee Member

Dr. Jose Marti, Electrical and Computer Engineering
Supervisory Committee Member

Abstract

Modelling and transient simulation of electric power systems and their components is enabling field of research much needed for planning, design, and operation of present and future evolving electrical grids and systems. The line-commutated-rectifiers (LCRs) are commonly used in integrated AC-DC energy conversion systems, where they are also known as the source of harmonics. Recently, a full-order parametric dynamic phasor (PDP) modelling methodology has been proposed in the literature for efficient transient simulation of the LCR systems including harmonics. Although this modelling approach is able to capture any desired number of harmonics, this increased accuracy also comes at an additional computational cost. The main objective of this thesis is to improve the numerical efficiency of transient simulation of the LCR systems with harmonics using the parametric dynamic phasor (PDP) modelling methodology.

In this thesis, a reduced-order PDP model is proposed to reduce the computational cost and enable faster simulations. The fundamental DPs are represented by differential equations, while high-order DPs are represented by algebraic equations. Moreover, the harmonic ripples that may exist in the DC subsystem have also been incorporated to increase the modelling fidelity of the new approach. The superior performance of the new technique is validated on several examples of integrated AC/DC power systems (including three-phase transformer and synchronous machine). Rigorous case studies demonstrate that the reduced-order PDP model of integrated AC/DC systems is capable of accurately tracking the steady-state and transient responses, while providing higher numerical efficiency compared to the conventional detailed model and the prior established full-order PDP models.

Lay Summary

Modelling and transient simulation of electric power systems and their components is enabling field of research much needed for planning, design, and operation of present and future evolving electrical grids and systems. The extensive utilization of line-commutated-rectifiers (LCR) in AC-DC energy conversion systems has been a challenge for modelling of power networks accurately and efficiently using existing simulation tools. The proposed innovative reduced-order parametric dynamic phasor (PDP) modelling approach is demonstrated to offer significant computational advantages for modelling and simulations of integrated AC-DC power systems with LCRs compared to the conventional detailed modelling and the prior established full-order PDP approaches. It is envisioned that such modelling technique can be integrated into many industry-grade transient simulation tools and become very useful to many researchers and practitioner engineers for conducting various power studies.

Preface

Many of the research results presented in this thesis have been published in conference proceedings and/or will be submitted for peer review. In all publications, I am the primary contributor for deriving equations, developing models, performing case studies and analyzing simulation results. My supervisor, Dr. Juri Jatskevich, has provided guidance and instructive comments throughout the process of conducting research, paper writing and revisions. The co-authors of my publications include our former graduate students Dr. Yingwei Huang and Dr. Seyyedmilad Ebrahimi who provided their instructions on research and editorial comments on manuscripts of my publications.

Chapter 3 is based on the following conference paper that has been published:

X. Liang, Y. Huang, J. Xia and J. Jatskevich, "Reduced-order Parametric Dynamic Phasor Modeling of Line-commutated-rectifier Systems," in *Proc. IEEE PES General Meeting.*, Atlanta, USA, Aug. 2019.

Chapter 4 is based on the following conference paper that has been published:

X. Liang, Y. Huang, S. Ebrahimi and J. Jatskevich, "Reduced-Order Parametric Dynamic Phasor Modeling of AC Distribution Systems with Rectifier Loads," *2019 IEEE 28th International Symposium on Industrial Electronics (ISIE)*, Vancouver, BC, Canada, 2019, pp. 165-170.

Chapter 5 is based on the following journal paper to be submitted:

X. Liang, Y. Huang, S. Ebrahimi and J. Jatskevich, "Reduced-Order Parametric Dynamic Phasor Modeling SM-Rectifier Systems Including DC ripples," to be submitted.

Table of Contents

List of Tables

List of Figures

List of Symbols

In this thesis, scalars are written using italic fonts [e.g., i_{as}], and vectors and matrices are denoted by bold letters [e.g., $\boldsymbol{e}_{abcs}$, $\mathbf{R}_s$]. To distinguish the representation of different types of signals discussed in this thesis, the lowercase letters are used to denote the time-domain instantaneous signals [e.g., $i_{as}(t)$], the uppercase letters used to denote the SFA-type DPs [e.g., $I_{as}(t)$], and the angle brackets “<>” are used to denote the GAM-type DPs [e.g., $<i_{as}>_k (t)$]. The angle brackets “<>” notation for the GAM-type DPs has been first proposed in [71], and since that has been commonly used in related literature. The conventional steady state fundamental-frequency phasors used in Chapter2 are demoted by the uppercase letters in italic font [e.g., I_{as} (ω_s)].

Only basic variables are aggregated in this section: all other variable are defined explicitly throughout the thesis.

e_{xfd}	Scaled field winding voltage (synchronous machine)
J	Combined machine-load moment of inertia (in kg·m^2)
ω_s	System fundamental frequency (in rad/s)
s	Laplace variable

List of Abbreviations

AC	Alternating current
AAVM	Analytical average-value model
AVM	Average-value model
CCM	Continuous-conduction mode
CP	Constant parameter (model)
CPU	Central processing unit
d axis	Direct axis
DC	Direct current
DAEs	Differential Algebraic Equations
DCM	Discontinuous-conduction mode
DER	Distributed energy resource
DP	Dynamic phasor
emf	Electromotive force
EMTP	Electromagnetic transient program
FFT	Fast Fourier transform
GAM	Generalized average modelling
HVDC	High-voltage direct current
LCR	Line-commutated rectifier
LTE	Local Truncation Error
MSS	Multi-steady-states (approach)
ODE	ordinary differential equation

PAVM	Parametric average-value model
PC	Personal computer
PDP	Parametric dynamic phasor (model)
q axis	Quadrature axis
SFA	Shifted-frequency analysis
SM	Synchronous machine
SV	State variable (-based programs)
TD	Time domain (model)
VBR	Voltage-behind-reactance (model)

Acknowledgements

First of all, I would also like to thank the entire faculty, staff, and my fellow graduate students at UBC for their support during my studies in Canada. I would like to express my enduring appreciation to my supervisor, Dr. Juri Jatskevich, who offered me the great opportunity of pursuing Master of Applied Science (MASc) program in the Department of Electrical and Computer Engineering at UBC. It was a great honor and pleasure to be supervised by such a knowledgeable and hard-working professor, whose passion, vision and expertise in electric power systems have inspired me to do research and deeper enrich my experience. The encouragement I have received from such a kind and caring supervisor has endlessly contributed to my study.

I would like to thank Dr. William Dunford and Dr. Jose Marti for dedicating their valuable time to serve on my examining committee, and for all their useful comments and feedback that have improved my thesis.

I am very grateful, that during my graduate work at UBC, I have been a member of the Electric Power and Energy Systems (EPES) research group, where I have spent plenty of time with my lab colleagues. I am particularly thankful to Yingwei Huang, Navid Amiri and Seyyedmilad Ebrahimi, for helping me with my papers and many discussions of my research and their prior related work; and to Jiayue Xu and Zhi Qu for their advice during my graduate study. I also would like to thank Mohammad Mahdavyfakhr, Dexter Lin, Shuan Dong, Bo Chen, Javier Tarazona, Zejun Yang, Ahmed Sherwali, Sina Chiniforoosh, Wonbae Choi, Xinyu Zhang, Xiaotong Wang, Jinhui Xia, Shaobo Yin, Hadi Aghazadeh, Zeqi Hong, Jianzhen Qu, Jin Zhao, and many others, for having a good inspiring time working in the same EPES research group at UBC.

Finally, the special gratitude is owed to my parents and other family members, who have supported me throughout my years of education.

Dedication

To my wonderful parents

Chapter 1: Introduction

1.1 Motivation

Modern power systems are quickly evolving, while facing unprecedented technological changes in all aspects of energy generation, transmission, distribution, and consumption. Renewable energy sources are now supplementing or replacing many older fossil-fuel power plants, due to economical, ecological, and political factors. In 2016, the renewables accounted for nearly 62% of the net addition to the global power generating capacity [1]; and as of 2017, wind and solar, for the first time, exceeded 10% of the total electricity generation in the United States [2]. Unlike traditional power plants, these distributed energy resources (DERs) are usually interfaced with AC grid using power electronic converters with fast responding capabilities and extended controllability. Moreover, the advent of smart grid technologies [3] has promoted the proliferation AC and DC technologies into microgrids [4]-[5], interfacing of DERs and energy storage systems, and controllable loads [6].

At the same time, electronic devices are increasingly used in integrated AC-DC systems, such as power network of Kaiser building in UBC as depicted in Figure 1.1 [7]. Reconfiguration of the traditional power network to incorporate intermittent distributed energy sources introduces high degree of uncertainty and variability [8], since more electronics are introduced into system. For instance, the line-commutated rectifiers (LCRs) are commonly used in medium- and high-power industrial applications, such as distributed generation [9]-[10], classic high-voltage DC (HVDC) transmission systems [11], electrical subsystem of vehicles [12], aircraft [13] and ships [14]. Numerous challenges arise due to non-linear properties of power electronic components. Although

LCRs are reliable and less costly, they are also known as a source of harmonics in AC systems, causing lower power quality and unfavorable impact on other equipment [9]. In addition, these harmonics tend to aggravated by the oscillatory interactions between the switching operation of power converters, the dynamic controller systems, and the impedance of the interconnected systems [15]-[17]. To investigate these phenomena, researchers and engineers worldwide are conducting large number of computer studies. Accurate and efficient modelling of each system component is therefore critical at all stages of design, analysis, monitoring, control, and energy management to ensure the secure, reliable and optimized operation of the integrated AC-DC power systems [6].

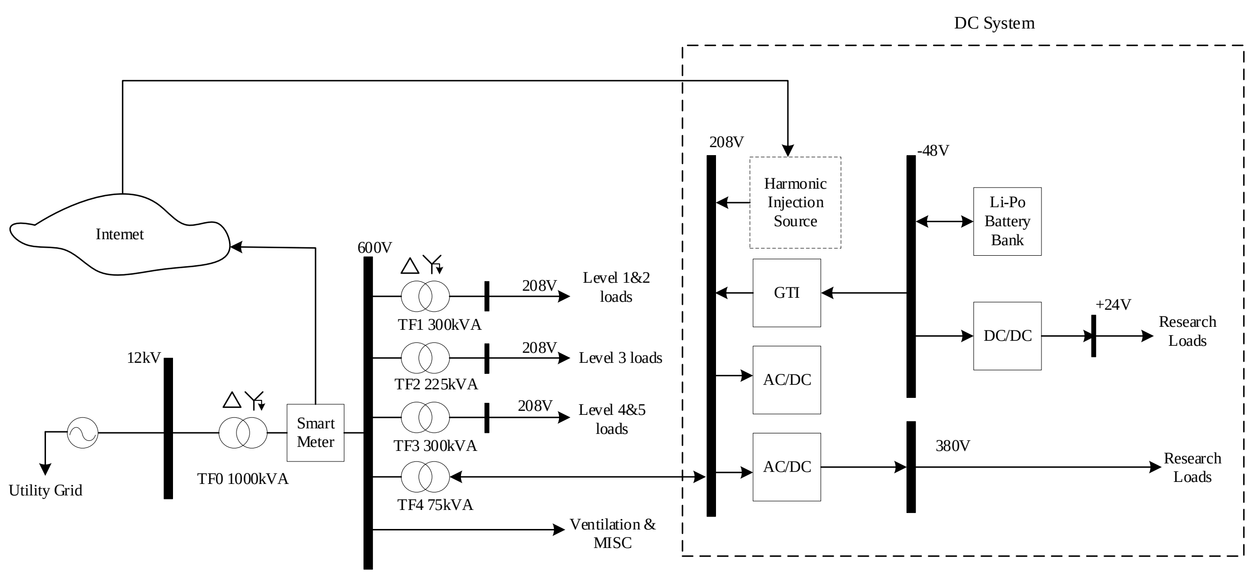

Figure 1. 1 An example of simplified single-line diagram of electrical system in Kaiser building at UBC depicting AC and DC subsystems [7].

The study of power system transients has been an active area of research for many decades, and various analysis tools and simulators have been developed for different objectives, time scales, types of disturbances, etc.[18]-[20]. The conventional detailed models of switching converters and

LCRs can be readily developed using built-in components available in many electromagnetic transient (EMT) simulation programs such as PSCAD [6] or Matlab/Simulink toolboxes such as Simscape Electrical [21] and PLECS [22]. To capture fast and detailed transients in time-domain, such simulation tools have to run at very small time step sizes. So, long simulation times are typically required due to the heavy computational burden resulted from switching devices such as rectifiers. Consequently, there is a significant need for accurate and efficient modelling and simulation techniques that are applicable for general-purpose system-level transient studies of integrated AC-DC power systems.

1.2 Literature Review

1.2.1 Dynamic Phasor (DP) Type Modelling Approaches

To overcome computational cost while retaining accuracy, an alternative modelling approach referred to in the literature as the dynamic phasor (DP) solution, uses hybrid time-phasor representation of power system signals. There are two types of DP theories, namely the shifted-frequency analysis (SFA) [23]-[24] and the generalized averaging method (GAM) [25]. This thesis focuses on generalized averaging method type of DP.

1.2.1.1 Shifted-Frequency Analysis (SFA)

Shifted-frequency-analysis originates from modulation techniques in signal processing theory [26], where time-domain instantaneous signal is represented as a band-pass formed by the sum of closely-spaced sine wave around fundamental frequency (50/60Hz)[23]-[24],[27]. This type of dynamic phasor, defined as complex envelope of analytic signal in signal processing is obtained as an analogous low-pass representation of the original band-pass instantaneous signal [23]. The frequency of power system signals can be down-shifted to around 0 Hz from around fundamental frequency, which allows larger time step selection [6]. This kind of dynamic phasor solution has been applied to various power-electronics-based systems. However, this low-pass representation of time-domain signal with harmonics will shift the entire spectrum by $-\omega_s$, and thus small times stepms may still be required to represent the high frequency harmonics.

1.2.1.2 Generalized Averaging Method (GAM)

To account for high-order harmonics existing in AC-DC power systems, the generalized averaging method (GAM-type) dynamic phasor has been proposed in [25], and it is defined as the time varying Fourier coefficients of a ‘sliding window’ of the time-domain signal with a period of $T_s = \frac{2\pi}{\omega_s}$ [28]. For the GAM-type dynamic phasor, the frequency content can be shifted to 0 Hz accordingly for each selected harmonic, thus permitting larger time step sizes to be used. Also, the GAM enables to select frequency components of interest to construct an adequate approximation of the original time-domain waveform. Recent publications [28]-[30] demonstrate the accuracy and numerical efficiency of the GAM-type DP models of synchronous machine rectifier systems. Although including harmonics leads to better accuracy, more state variables are added to the overall model, which increases the computational cost of simulations. Therefore, this thesis investigates a reduced-order DPs modelling method in order to reduce the computational cost.

1.2.2 Modelling of AC-DC Power System Components

In addition to modelling approaches, the simulation performance of the integrated AC-DC power system is highly dependent on the proper modelling of each system component. As illustrated in Figure 1.1, a representative AC-DC energy conversion system includes rotating machines, AC/DC converters, line-commutated-rectifiers (LCRs), transformers, loads, etc. Models of electric machines and power converters are typically the bottleneck in most simulation programs [31]-[33], and therefore are considered in this thesis.

1.2.2.1 Modelling of Line-Commutated Rectifiers (LCRs)

Owing to low cost, high reliability, and simplicity, the line-commutated-rectifiers (LCRs) are widely used in a myriad of industrial and commercial applications [10], including the input stage of variable frequency drives (VFDs) [9]-[10], DERs [34], electric systems of vehicles, ships and aircrafts [35], and over 70% of today's HVDC transmission systems [36], etc. However, the LCRs contribute considerable harmonics into system, which causes various operating modes of LCRs [22], [38]. Numerically accurate and efficient models of LCRs are therefore needed for predicting system-level transients as well as varying harmonics under different loading conditions.

A variety of modelling approaches of AC/DC power converters have been proposed, including exact linear time varying modelling [39]-[40], sample-data modelling [41], and dynamic-average-value models (AVMs) [42]. The AVMs of LCRs can be mainly classified into two categories: analytical AVMs (AAVMs) [42] and parametric AVMs (PAMs) [43]-[44]. Applying the GAM methodology to time-domain AVMs, has attracted significant attention with the goal to develop LCR models that possesses good accuracy and superior efficiency.

One existing DP model of LCRs proposed in [21] has applied the GAM approach to AAVMs. Nevertheless, the obvious shortcoming is that analytical switching functions used for rectifier modes are incapable of approximating the actual waveforms of currents and voltages very accurately. Besides, analytical DP models derived for only the continuous conduction mode are inadequate for the LCRs where various operating modes exist depending on load conditions.

Recently, inspired by the parametric average-value modelling (PAVM) [44], a parametric DP (PDP) model has been established in [21]. The PDP model is proven to effectively predict the system dynamics including ac harmonics under different operating modes. However, this PDP model doesn't consider DC ripples that may exist in DC subsystem. Therefore, extending the established PDP model to augment the DC ripples is also considered in this thesis.

1.2.2.2 Modelling of Electric Machines

Synchronous machines are present in almost every bulk/islanded power system as the main source of electrical energy, as well as being the functional unit for power stability or reactive power support [20], [42]. Depending on the interfacing circuit with the power network, the machine models can be generally classified into three categories: coupled-circuit phase-domain (PD) models [42]; classical *qd* models [20], [42]; and the so-called voltage-behind-reactance (VBR) models [45]-[49].

The PD models using *abc* phase coordinates can be directly interfaced with external power systems. However, the inductances in PD models are time-varying due to rotor position in salient-pole synchronous machines, which requires costly calculations per time step, and greatly complicate the analysis of machine dynamics [42],[50].

The classical approach is based on Park's [51] *qd* model, where the parameters of the transformed equivalent circuits in *qd* coordinates are time-invariant. As such, the *qd* models become default (built-in) models in most of state-of-art simulators today due to their simplicity and high efficiency. However, in SV-based programs, when interfaced with external inductive *abc*-phase network requiring inputs of voltages [50], the *qd* models represent voltage-input current-output components, which cause incompatibility. In EMTP-Type simulators, this interfacing issue also exists by requiring prediction of machine state variables (stator currents, speed voltages, field voltage, etc.), thus leading to limited accuracy and requiring small time-steps [50].

To achieve direct machine-network interface while attaining good numerical efficiency, the VBR models [45]-[49] have been proposed with a circuit configuration of an equivalent voltage source behind a reactance [19]-[20]. In VBR models, the stator states are in *abc* phases, while the rotor variables are formulated in *qd* coordinates. However, due to dynamic saliency, these models have rotor-position-dependent time-varying inductances. In order to solve this problem, a constant-parameter VBR models (CP-VBR) where an additional artificial damper winding is added to *q*-axis has been proposed in [46]-[48]. Owing to its advantages, the CP-VBR models have been used with SFA-based DP modelling [52]. This thesis also investigates the performance of CP-VBR machine models with and GAM-Type DPs.

1.3 Research Objectives

This thesis proposes a reduced-order parametric dynamic phasor (PDP) modelling for several types of AC-DC systems: 1) LCR benchmark system; 2) AC distribution system with transformer and rectifier loads; and 3) integrated SM-fed rectifier system. All three cases validate the beneficial properties of reduced-order PDP modelling approach in terms of saving computational cost and allowing larger time steps, while retaining good accuracy in prediction of system transients. The detailed objectives are summarized below:

Objective 1: Developing reduced-order parametric dynamic phasor (PDP) modelling methodology and demonstrating it on a generic integrated AC-DC system.

So far, the full-order parametric dynamic phasor (PDP) modeling technique has been developed for AC-DC systems. As part of this thesis, the reduced-order PDP model is proposed to speed up the simulation and save computations by eliminating the dynamics of high-order components in ac side. Using the combination of state equations to represent the fundamental DPs and the algebraic equations to represent the higher-order harmonics has not been considered in the previous literature.

Objective 2: Extending Objective 2 to modelling a typical AC distribution system with three-phase transformer and rectifier loads.

In this objective, the proposed reduced-order PDP model is first applied to AC distribution system with a three-phase ΔY transformer. A general reduced-order DP modelling method is innovatively developed for three-phase transformers considering various wiring configurations.

Objective 3: Develop methodology for predicting the DC-side ripples existing in SM-rectifier systems based on parametric DP methodology.

The previously formulated PDP modelling technique assumes no harmonics exist in DC side, which is not the case in practice. Therefore, a new set of parametric functions is constructed to include any desired orders of harmonics in DC side. Moreover, the modified model of DC system is developed to augment harmonic orders of the interest. Also, the reduced-order DP technique is applied to CP-VBR model of synchronous machine.

Chapter 2: System Modelling Methodologies

To set the stage for the proposed models, this chapter presents the fundamentals of dynamic phasor (DP-type) modelling methodologies, including the traditional system modelling methods along with signal representations in power system simulations. Next, two types of DP representations are set forth, including the shifted frequency analysis (SFA) and the generalized averaging method (GAM). The difference between various signal representations in terms of modelling basic power system components are demonstrated for comparison.

2.1 Signal Representations in Power System Simulations

Power system transients studies have been studied for decades using different simulation tools and programs developed for different size of networks, range of time scales of transients, and even different types of disturbances [18]-[20]. Focusing on high-frequency and relatively-fast phenomena in power systems, the so-called electromagnetic transients (EMT) programs (and EMTP) are used, which are generally divided into two categories: nodal-analysis-based tools (hereafter referred to as EMTP-type [31], [53]) and state-variable (SV-based) tools [32], [33].

The EMTP approach has been first introduced by Dr. H. W. Dommel in 1960s, which is a discretized time-domain solution method. Therein, the continuous-time differential equations are replaced with discretized difference equations through a certain type of discretization method, typically implicit trapezoidal rule [54]. As a result, the modelling accuracy partly depends on time step size. In EMTP type simulation tools, the time step size is typically fixed, and for typical power systems studies in may be in the range of microseconds (1 – 100μs). For instance, the model of inductor in EMTP is derived in (2.1) using trapezoidal rule:

$$
\begin{cases}
v_L(t) = L\dfrac{d}{dt}i_L(t), \\
\int_{t-\Delta t}^{t} v_L(t)dt = L\left[i_L(t) - i_L(t-\Delta t)\right], \\
\dfrac{v_L(t)+v_L(t-\Delta t)}{2}\Delta t = L\left[i_L(t) - i_L(t-\Delta t)\right], \\
v_L(t) = \dfrac{2L}{\Delta t}i_L(t) + [-v_L(t-\Delta t) - \dfrac{2L}{\Delta t}i_L(t-\Delta t)], \\
v_L(t) = \dfrac{2L}{\Delta t}i_L(t) + e_{h_L}(t).
\end{cases}
\tag{2.1}
$$

Each component in the system is discretized following a similar process as in (2.1), and then the overall equations are combined into a system of nodal equations, which is solved at each time step. The details of EMTP-type modelling approach can be found in numerous references [31], [53].

The state-variable-based (SV-based) representation is also briefly discussed in this section. The dynamics of system can be expressed by a set of first order ODEs in the sate-space formulation as:

$$
\begin{cases}
\dfrac{d}{dt}\mathbf{x} = \mathbf{f}(\mathbf{x},\mathbf{u},t), \\
\mathbf{y} = \mathbf{g}(\mathbf{x},\mathbf{u},t).
\end{cases}
\tag{2.2}
$$

Here, $\mathbf{x}$ is state vector, $\mathbf{u}$ is input vector, t is time, and $\mathbf{y}$ is output vector. In some cases, where system is time-invariant and linear (and/or piecewise linear), (2.2) can be expressed in matrix-form as the standard state-space formulation as

$$
\begin{cases}
\dfrac{d}{dt}\mathbf{x} = \mathbf{A}\mathbf{x} + \mathbf{B}\mathbf{u}, \\
\mathbf{y} = \mathbf{C}\mathbf{x} + \mathbf{D}\mathbf{u}.
\end{cases}
\tag{2.3}
$$

Here, **A**, **B**, **C**, D are the state-space matrices. The eigenvalues of matrix A represent system's dynamic modes [20].

Various numerical integration methods such as ordinary differential equations (ODE) solvers in MATLAB/Simulink [32] can be used to solve (2.2) and (2.3). The selection of proper ODE solvers depends on the problem type (continuous/discrete states, stiff/non-stiff) and requirement for accuracy and efficiency. The variable-step embedded ode solvers usually use a pair of methods in order to estimate the Local Truncation Error (LTE) at every time step and make the automatic time-step adjustment. Those ode solvers are designed to adjust the time step to achieve the required accuracy within the user-specified error tolerances. The commonly used ode solvers [72]-[75] are summarized in Table 2.1.

Table 2. 1 Commonly used ode solvers in Matlab/Simulink.

Stiffness of system	Solvers	Step Method	Formula	Performance
Non-stiff	ode45	One-step	Runge-Kutta (4,5)	Good for most non-stiff systems
	ode23	One-step	Runge-Kutta (2,3)	More efficienct than ode45 at crude tolerances
	ode113	Multi-step	Adams-Bashforth-Moulton	More efficienct than ode45 at stringent tolerances
Stiff	ode15s	Multi-step	Numeical Differentiation Formulas	Good for most stiff and differential-algebraic problems
	ode23s	One-step	Rosenbrock (order 2)	More efficienct than ode15s at crude tolerances for stiff problem of small size
	ode23t	One-step	Trapezoidal Rule	Good with moderately stiff
	ode23tb	One-step on first stage and Multi-step on second stage	Trapezoidal Rule at first stage and Backwad Differentiation Formula (order 2) at second stage	More efficienct than ode15s at crude tolerances

In the computer studies presented in this thesis, without loss of generality, the ode23tb solver has been chosen because it provides good accuracy and stability. This solver has very good efficiency in solving stiff problems using an implicit Runge-Kutta pair method (2, 3). Therein, one-step trapezoidal rule is used at the first stage, and it is followed by the second stage with Backward Differentiation Formula (order 2). The process can be repeated cyclically to obtain a method with two internal steps and no memory [76].

In addition to simulation tools, the representation of signals also factors in simulation efficiency and accuracy.

2.1.1 Time Domain Instantaneous Signal

The instantaneous time-domain signals are commonly used in EMT programs (both EMTP-Type and SV-based tools). Generally, a sinusoidal AC power system variable in steady state can be expressed as

$$u(t) = \mathrm{U}\cos(\omega_s t + \theta). \tag{2.4}$$

Here, ω_s represents the system fundamental frequency, U and θ denote magnitude and angle of the signal, respectively.

By the means of instantaneous signals, system components can be modelled in detail in measurable variables and easily compared with field tests [23]. However, the selection of maximum time step size depends on the highest appearing frequency, which be established based on the Nyquist criterion or sampling theorem,

$$\Delta t_{\max} = \frac{1}{2 f_{\max}}. \tag{2.5}$$

Therefore, the simulation efficiency is limited by system harmonics that needed to be represented. Due to this limitation, this representation may not be appropriate for large time step sizes [23].

2.1.2 Conventional Fundamental-Frequency Phasors

The concept of phasor uses a vector which rotates counterclockwise at a uniformed speed ω_s so as to make one complete revolution per period [55]-[56]. This vector is commonly known as phasor. As shown in Figure 2.1, the fundamental frequency phasor of power system signal $u(t)$ in (2.4) is defined as

$$U(\omega_s) = \mathrm{U}\cos\theta + \mathrm{j}\cdot\mathrm{U}\sin\theta = \mathrm{U}\angle\theta = \mathrm{U}\cdot e^{\mathrm{j}\theta}, \tag{2.6}$$

where $U(\omega_s)$ denotes the phasor representation at fundamental-frequency ω_s, while U is peak magnitude of sinusoidal waveform, and θ is the angle made with the reference rotating vector. The reference rotating vector can be chosen arbitrary, and all other phases are determined thereby.

The time instantaneous signal is retrieved by

$$u(t) = \mathrm{U}\cos(\omega_s t + \theta) = \mathrm{Re}(\mathrm{U}e^{\mathrm{j}(\omega_s t+\theta)}) = \mathrm{Re}(\mathrm{U}e^{\mathrm{j}\theta}e^{\mathrm{j}(\omega_s t)}) = \mathrm{Re}(U(\omega_s)e^{\mathrm{j}(\omega_s t)}). \tag{2.7}$$

The projections of this revolving vector upon horizontal axis represents the instantaneous value of the time-domain waveform [56].

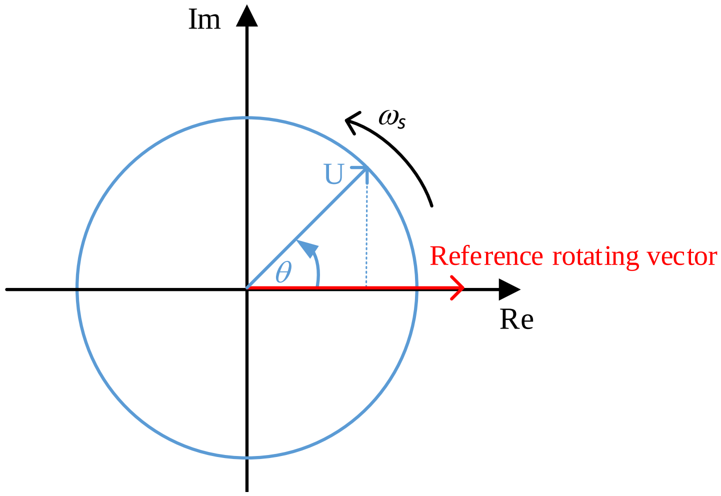

Figure 2. 1 Phasor with angular speed.

With the measure magnitudes and phase quantities of sinusoidal voltage and current waveforms, the power flow in transmission lines can be conveniently obtained [19]. Besides, it can be used for advanced protection and monitoring, for example, of ambient and disturbance conditions in power system such as generator trips and system separation [19]. Moreover, fundamental-frequency phasor facilitates the solution of interconnecting transmission network with synchronous machines [20].

The unbalanced system of *n* related phasors can be resolved into *n* systems of balanced phasors called symmetrical components of the original phasors [20] is another important application of phasors in terms of analysis of unbalanced power systems. Notwithstanding the advantages of the fundamental-frequency phasors, this type of signal representation has difficulties dealing with power system containing different harmonics.

2.1.3 Dynamic Phasor (DP) Type Representation

To overcome the limitations of the conventional steady state phasors, this section explains a hybrid time-phasor signal representation suitable to model integrated AC-DC power systems, using SFA- and GAM-type DP approaches.

2.1.3.1 Shifted-Frequency Analysis (SFA)

The concept of SFA-type DPs originates from signal processing theory, where the carrier signal is modulated to a narrow-band signal [24]. Although power system transient phenomena are typically characterized by frequency spectra, yet as the system returns to a steady state, the spectrum becomes centered on the fundamental frequency ω_s, with its bandwidth generally less than ω_s [23]. Using Fourier analysis, a band-pass signal can be visualized as the sum of an infinite number of closely spaced sine waves, as shown in Figure 2.2, and mathematically formulated as (2.8)

$$u(t) = \lim_{\Delta\omega \to 0} \sum_{i=-\infty}^{\infty} a_i \cos[(\omega_s + i\Delta\omega)t + \theta_i]. \tag{2.8}$$

Applying trigonometric identity, the above signal can be rewritten as

$$u(t) = u_I(t)\cos(\omega_s t) - u_Q(t)\sin(\omega_s t), \tag{2.9}$$

where

$$u_I(t) = \lim_{\Delta\omega \to 0} \sum_{i=-\infty}^{\infty} a_i \cos[(i\Delta\omega)t + \theta_i] \tag{2.10}$$

$$u_Q(t) = \lim_{\Delta\omega \to 0} \sum_{i=-\infty}^{\infty} a_i \sin[(i\Delta\omega)t + \theta_i] \tag{2.11}$$

Thus, instantaneous time signal is represented by two low-pass signals $u_I(t)$ and $u_Q(t)$ and two carrier signals, cos $\omega_s t$ and sin $\omega_s t$. As the two carriers are of the same frequency (but are out of phase by 90 degrees), the two low-pass signals are named as in-phase and quadrature components of the band-pass signal $u(t)$, respectively. After this modulation, these two low-pass signals have identical two-sided amplitude spectra, the same as the positive amplitude spectrum of $u(t)$ but shifted down to zero by the fundamental frequency ω_s [27]. Thus, the SFA-type DP of instantaneous signal $u(t)$ is defined as

$$U(t) = u_I(t) + \mathrm{j}u_Q(t). \tag{2.12}$$

In signal processing, $U(t)$ is also regarded as the complex envelope of the instantaneous time signal. Analytical signal is listed as another representation of instantaneous time signal $u(t)$, which is linked to SFA-type DP through

$$\hat{U}(t) = U(t)e^{\mathrm{j}\omega_s t}. \tag{2.13}$$

Substituting (2.12) into (2.13) yields

$$\begin{aligned}\hat{U}(t) &= [u_I(t) + \mathrm{j}u_Q(t)]\cdot[\cos(\omega_s t) + \mathrm{j}\cdot\sin(\omega_s t)] \\ &= u_I(t)\cos(\omega_s t) - u_Q(t)\sin(\omega_s t) + \mathrm{j}\cdot[u_I(t)\sin(\omega_s t) + u_Q(t)\cos(\omega_s t)] \\ &= u(t) + \mathrm{j}\cdot\mathrm{H}[u(t)],\end{aligned} \tag{2.14}$$

where the Hilbert transform is defined as [57]

$$\mathrm{H}[u(t)] = \frac{1}{\pi}\int_{-\infty}^{\infty}\frac{u(t)}{t-\tau}d\tau. \tag{2.15}$$

The SFA-type DP can be obtained as the frequency modulation of the analytical signal $\hat{U}(t)$ by -ω_s from its original frequency, while the instantaneous signal can be reconstructed as the real part of the analytical signal $\hat{U}(t)$. This process is commonly referred to as shifted-frequency analysis (SFA) [24], [27], which is illustrated in Figure 2.3 and summarized in the following equations:

$$U(t) = \hat{U}(t) \cdot e^{-\mathrm{j}\omega_s t} = \{u(t) + \mathrm{j} \cdot \mathrm{H}[u(t)]\} \cdot e^{-\mathrm{j}\omega_s t}. \tag{2.16}$$

$$u(t) = \mathrm{Re}[\hat{U}(t)] = \mathrm{Re}[U(t) \cdot e^{\mathrm{j}\omega_s t}]. \tag{2.17}$$

From Figure 2.3, it is seen that the original signal is modulated to a signal around frequency of 0 Hz. Therefore, according to Nyquist criterion (2.5), now the possible maximum sampling step size can be very large, which enables a flexible selection of time step size during simulation.

In SFA-type of DPs, the analytical signal is described by a low-pass signal around fundamental frequency. However, power systems have a wide frequency spectrum under real operations, for which the accuracy of SFA-type of DPs may be compromised is the large time steps are used.

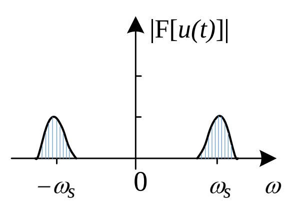

Figure 2. 2 Discrete frequency spectrum of a band-pass signal *u*(*t*) as the sum of a number of sine waves.

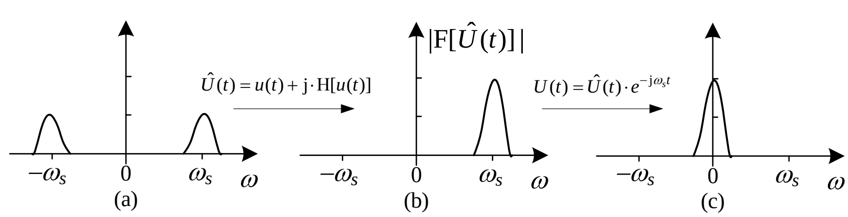

Figure 2. 3 Frequency spectra of band-pass signals in different representations during process of SFA: (a) instantaneous time signal *u*(*t*); (b) analytical signal $\hat{U}(t)$; and (c) SFA-type DP *U*(*t*).

2.1.3.2 Generalized Averaging Method (GAM)

To overcome the limitations of SFA-type DPs, a different DP representation called the generalized averaging method (GAM) may be considered that can account for wide-band signals with high frequency components. In AC/DC systems, a time-domain instantaneous signal u(t) can be viewed as a waveform $u(\tau)$ over a sliding window with period of $T_S = 2\pi/\omega_s$, as depicted in Figure 2.4. This sliding window time-domain waveform $u(\tau)$ can be expressed by Fourier series [6], [25] as

$$u(\tau) = \sum_{k=-\infty}^{\infty} \langle u \rangle_k (t) e^{\mathrm{j}k\omega_s \tau}, \tag{2.18}$$

where $\tau \in (t - T_s,\ t]$. The time varying $u(\tau)$ is assumed nearly periodic. The k-th order GAM-Type DP is defined as the k-th Fourier coefficient $<u>_k(t)$, as

$$\langle u \rangle_k (t) = \frac{1}{T_s} \int_{t-T_s}^{t} u(\tau) e^{-\mathrm{j}k\omega_s \tau} d\tau. \tag{2.19}$$

As described in (2.19), the GAM-type DPs of time-domain signal is depicted in Figure 2.5, where the frequency content of each single order components is shifted to 0 Hz accordingly by its harmonic frequency. In this way, large time step size may be allowed in modelling of any order components in power systems.

In addition, the GAM-type DPs enable a selection of a number of DPs of interest (i.e., selection of k), to achieve a balance between accuracy and computational cost, since the inclusion of higher-order components adds to the modelling complexity but leads to better approximation of the original time-domain waveform. The reconstruction of the original instantaneous signal can be achieved through [58]

$$u(t) = \mathrm{Re}\left[\sum_{k=-K}^{K} \langle u \rangle_k (t) e^{\mathrm{j}k\omega_s t}\right] = 2 \cdot \mathrm{Re}\left[\sum_{k=0}^{K} \langle u \rangle_k (t) e^{\mathrm{j}k\omega_s t}\right]. \tag{2.20}$$

Here, k ={1,2,3,…, K} denotes the set of selected orders of GAM-type DPs, and K determines the degree of accuracy (i.e., total number of harmonics).

Moreover, several operation relationships of GAM-type DPs, which are required to enable transferring the state equations of a linear time-periodic system to the dynamic phasor domain [25], are listed as followings,

$$\langle u \rangle_{-k} = \langle u \rangle_k^*, \tag{2.21}$$

$$\langle uv \rangle_k = \sum_i \langle u \rangle_{k-i} \cdot \langle v \rangle_i, \tag{2.22}$$

$$\left\langle \frac{du}{dt} \right\rangle_k = \frac{d}{dt}\langle u \rangle_k + \mathrm{j}k\omega_s \langle u \rangle_k. \tag{2.23}$$

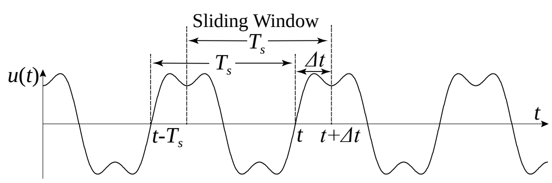

Figure 2. 4 The illustration of time-domain signal over a sliding window.

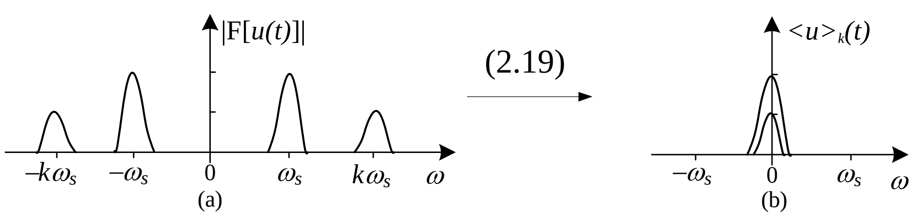

Figure 2. 5 Frequency spectrum of power system signal in different representations: (a) instantaneous signal, and (b) GAM-type DP.

From power system simulation perspective, the use of GAM-Type DPs can be helpful in reducing the number of time steps and retaining accuracy by properly selecting the orders of interest (i.e. total number of harmonics of interest). In this way, one should anticipate a trade-off between the simulation accuracy and modelling complexity. Typically, only the fundamental component and first few dominant harmonics are selected for common system-level modelling and analysis.

2.2 Modelling Basic *RLC* Components

To better apply DPs to power system studies, the basic *RLC* components are represented in different types of signal approaches, as summarized in Table 2.1. For example, the procedure of developing power system models in dynamic-phasor-domain can be summarized as follows.

1) Obtain time-domain equations using instantaneous signal representation;
2) Rewrite time-domain signals in dynamic-phasor-domain by apply the definition of corresponding type of dynamic phasor. For SPA-Type DPs, the DPs can be obtained using (2.17); and For GAM-Type DPs, the DPs can be obtained using (2.20).
3) Manipulate and simplify the DPs models derived in step 2) by using features (2.21-2.23);

The following is the example of how to derive capacitor model in GAM-Type dynamic phasor domain.

$$
\begin{aligned}
& i_C(t) = C\frac{d}{dt}v_C(t) \\
& 2\cdot \mathrm{Re}\left\{\sum_{k=0}^{K}\langle i_C(t)\rangle_k \cdot e^{\mathrm{j}k\omega_s t}\right\} = 2\cdot C\cdot \mathrm{Re}\left\{\sum_{k=0}^{K}\left\langle \frac{d}{dt}v_C(t)\right\rangle_k \cdot e^{\mathrm{j}k\omega_s t}\right\} \\
& \sum_{k=0}^{K}\langle i_C(t)\rangle_k \cdot e^{\mathrm{j}k\omega_s t} = C\cdot \sum_{k=0}^{K}\left\langle \frac{d}{dt}v_C(t)\right\rangle_k \cdot e^{\mathrm{j}k\omega_s t} \\
& \langle i_C(t)\rangle_k = C\cdot\left\{\frac{d}{dt}\langle v_C(t)\rangle_k + \mathrm{j}k\omega_s\langle v_C(t)\rangle_k\right\}
\end{aligned}
\tag{2.24}
$$

It is noted that SFA-Type DPs and GAM-Type DPs are hybrid time-phasor signals, so that the DPs are complex-value variables with both real and imaginary parts in state-space formulation [6].

Table 2. 2 Basic *RLC* components formulations in different signal representations.

Signal Representation	Resistor R	Inductor L	Capacitor C
Instantaneous Signal	$v_R = Ri_R(t)$	$v_L = L\frac{d}{dt}i_L(t)$	$i_C = C\frac{d}{dt}v_C(t)$
Conventional Phasor	$V_R(\omega_s) = RI_R(\omega_s)$	$V_L(\omega_s) = \mathrm{j}\omega_s LI_L(\omega_s)$	$I_C(\omega_s) = \mathrm{j}\omega_s CV_C(\omega_s)$
SFA-Type DP	$V_R(t) = RI_R(t)$	$V_L(t) = \mathrm{j}\omega_s LI_L(t) + L\frac{d}{dt}I_L(t)$	$I_C(t) = \mathrm{j}\omega_s CV_C(t) + C\frac{d}{dt}V_C(t)$
GAM-Type DP	$\langle v_R\rangle_k(t) = R\langle i_R\rangle_k(t)$	$\langle v_L\rangle_k(t) = \mathrm{j}k\omega_s L\langle i_L\rangle_k(t) +$ $L\frac{d}{dt}\langle i_L\rangle_k(t)$	$\langle i_C\rangle_k(t) = \mathrm{j}k\omega_s C\langle v_C\rangle_k(t) +$ $C\frac{d}{dt}\langle v_C\rangle_k(t)$

Chapter 3: Reduced-order Parametric Dynamic Phasor (PDP) Modelling of AC-DC Networks

This chapter begins with parametric dynamic phasor modelling of line-commutated-rectifier, which interfaces the AC and DC subsystems. Next, the modelling of DC subsystem in dynamic phasor domain is presented. Then, a reduced-order dynamic phasor modelling technique is proposed for AC network with the purpose of simplifying the AC subsystem to achieve higher numerical efficiency, while to retain accuracy. The computer studies validate the proposed reduced-order parametric dynamic phasor methodology in accurately predicting steady-state and transient responses under a wide range of operating modes, while highlighting its computational advantages over the traditional detailed model and the previously established full-order parametric dynamic phasor model.

3.1 Parametric Dynamic Phasor (PDP) Modelling

The LCRs are commonly found as the input stage in low-to medium-power variable frequency drives and motor loads that are widely used in industrial and commercial applications [22], [59]. These loads, commonly referred as front-end rectifier loads [22], [60], and may appear in large numbers in distribution systems, industrial facilities [22], [61] distributed generation [22], [62], transportation [22], [63], as well as arc furnaces [22], [64]. Depending on the application, the source can be a distribution feeder (or a transformer) as in Case I, or a rotating machine (generator) as in Case II, as depicted in Figure 3.1.

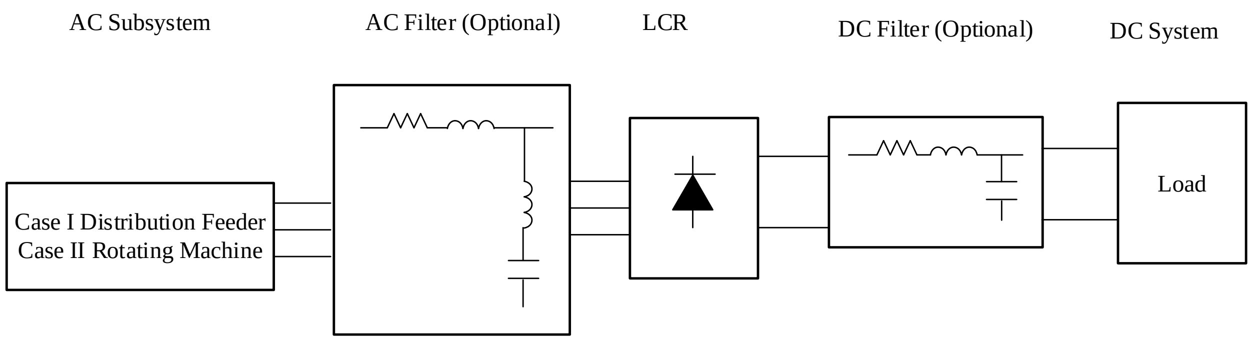

Figure 3. 1 Typical configuration of a front-end rectifier load system.

Though LCRs are wide-used in power system, they are also known to cause harmonics in AC systems, leading to lower power quality, and unfavorable impact on other equipment [21]. Therefore, it has been of particular interest to power engineering community to develop models of LCR systems that can accurately predict their harmonics in a wide range of operating conditions, and at the same time, are computationally efficient and applicable for large-scale system-level transient studies.

Besides conventional detailed models of LCRs developed in time-domain, various DP models of LCRs have been set forth in the literature [6], [21]. In the analytical DP (ADP) models, the LCR is represented by a series of switching functions to relate the AC and DC subsystems [21]. However, the different modes of LCRs require different sets of switching functions, which makes this approach additionally complicated [22]. Recently, inspired by the parametric average-value modelling (PAVM) approach [44], a parametric DP (PDP) model has been established in [21]. The PDP model is proven to effectively predict the system dynamics including harmonics under different operating modes (i.e. from open- to short-circuit).

For comparison with the previous publications [6], the same generic integrated AC-DC system which has been validated with detailed models, dynamic average-value models, and hardware [22], [43]-[44], [57], is considered in this section, as depicted in Figure 3.2. Therein, a diode rectifier is assumed to be supplied by the AC network represented by its Thevenin equivalent voltage source $\boldsymbol{e}_{abcs}$, series resistance r_{th} and inductance L_{th}. The existence of shunt filters has no dramatic effect on modelling of such rectifier systems [22]-[38], and that is why only series filters are considered in this generic benchmark system. The series filter is optional with resistor r_{ac} and inductor L_{ac}. The DC subsystem consists of optional DC filter and an equivalent resistive load R_{load}. As depicted in Figure 3.1, this integrated AC-DC system can generally be broken into three parts, namely the AC subsystem, the DC subsystem, and the LCR which interfaces both subsystems. Since LCR relates the AC side and DC side variables, this chapter begins with modelling of the LCRs.

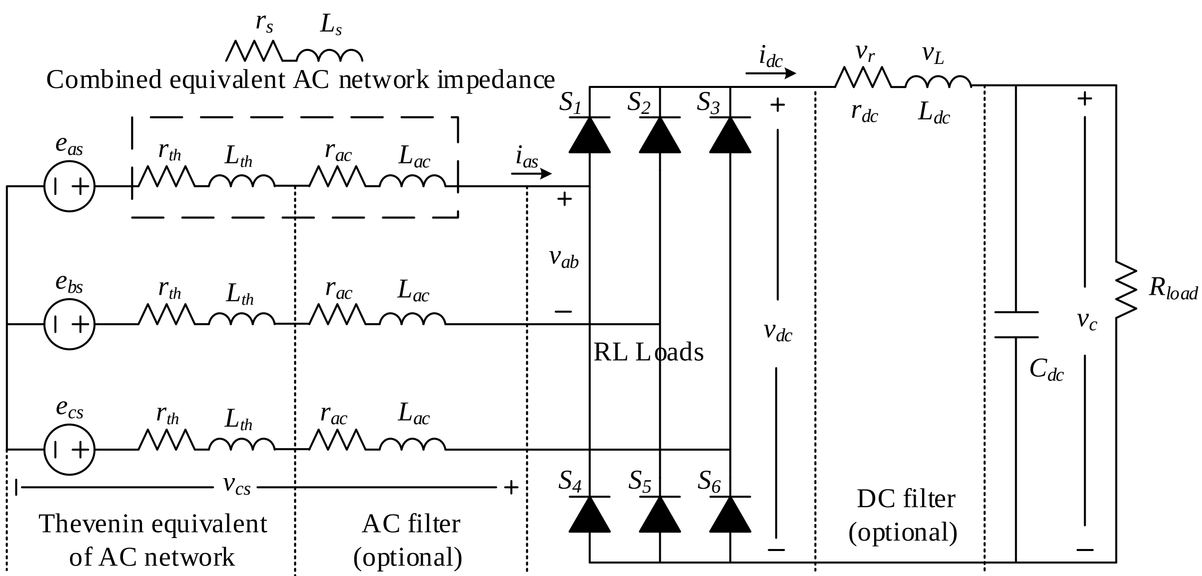

Figure 3. 2 The considered generic integrated AC-DC system.

3.1.1 Parametric Dynamic Phasor (PDP) Modelling of LCRs

Inspired by the parametric approach [43]-[44] to model AC and DC dynamics of the LCR system under various operating conditions, the parametric relationships of AC and DC variables are established in dynamic phasor domain in [6]. Assuming a symmetrical AC system, the relationships between magnitude of DP of phase *a* variables and dc-side DP are expressed as

$$\left|\langle v_{as}\rangle_k\right| = \alpha_k(\cdot)\left|\langle v_{dc}\rangle_0\right|, k \in K; \tag{3.1}$$

The angle relationships between AC currents and voltages are established as

$$\varphi_k(\cdot) = \mathrm{ang}(\langle v_{as}\rangle_k) - \mathrm{ang}(\langle i_{as}\rangle_1), k \in K; \tag{3.2}$$

Assuming an ideal DC system without any harmonics/ripple, only the 0-th order DPs are established at the DC side as

$$\begin{cases} \left|\langle i_{dc}\rangle_0\right| = \beta_0(\cdot)\left|\langle i_{as}\rangle_1\right| \\ \langle i_{dc}\rangle_0 = \left|\langle i_{dc}\rangle_0\right| \end{cases}. \tag{3.3}$$

Combining (3.1) and (3.2), the AC side DPs are obtained as,

$$\begin{cases} \langle v_{as}\rangle_k = \alpha_k(\cdot)\left|\langle v_{dc}\rangle_0\right| e^{\mathrm{j}(\mathrm{ang}(\langle i_{as}\rangle_1)+\varphi_k)} \\ \langle v_{as}\rangle_k = \langle v_{bs}\rangle_k e^{\mathrm{j}(\frac{2k\pi}{3})} = \langle v_{cs}\rangle_k e^{\mathrm{j}(\frac{-2k\pi}{3})} \end{cases}, k \in K. \tag{3.4}$$

Due to the assumed symmetry, the DPs for phase *b* and phase *c* are obtained by a phase shift of ±2*k*π/3, respectively. In (3.1)-(3.4), $\alpha_k(\cdot)$, $\beta_0(\cdot)$, and $\varphi_k(\cdot)$ are the parametric functions dependent on the switching conditions of the LCR system. In (3.4) the set *K*={1,5,7} denotes the selected AC harmonics of interest, since 1st, 5th and 7th orders are considered dominant in AC subsystem. The selection of desired harmonics can be facilitated by Fourier analysis tools in Matlab/Simulink [32]. For the purpose of simplifying the models, only the fundamental AC current is assumed to affect the DC current.

For consistency with the previous related models, the dynamic impedance z is used as input argument of parametric functions [44]. These parametric functions are determined in terms of dynamic impedance z which is defined as [21].

$$z = \frac{\left|\langle v_{dc} \rangle_0\right|}{\left|\langle i_{as} \rangle_1\right|}. \tag{3.5}$$

Finally, the PDP model of the LCR can be established using (3.3), (3.4), and (3.5), along with parametric functions $\alpha_k(z)$, $\beta_0(z)$, and $\varphi_k(z)$.

3.1.2 Constructing Parametric Functions

A detailed simulation under study is utilized to obtain the functions $\alpha_k(z)$, $\beta_{k_{dc}}(z)$, $\varphi_k(z)$ and $\varphi_{k_{dc}}(z)$ numerically, using approaches similar to those in [43]-[44].

Since GAM-Type DPs become constant in steady state [25], a straightforward approach is considered where the detailed simulation can be run in various steady-state conditions corresponding to the operating points of interest, while the fast Fourier Transform (FFT) of time-domain waveforms of variables are tabulated and saved [6], [43]-[44]. The system is connected to a resistive load that varies in a wide range for various operating conditions. The stored data points at different operating modes with subsequent proper curve fitting are utilized [6]. This method of constructing parametric functions is herein referred to as the multi-steady-states (MSS) approach, which requires to run the detailed simulations in a loop to calculate the steady state solutions for the desired number of points.

3.2 DP Modelling of DC Subsystem

For the purpose of this section, only the 0-th order DP is considered in DC subsystem, under the assumption of ideal operation. In such case, the DP representation of DC subsystem is directly compatible with the time-domain model, which is preferable for interfacing considerations [6]. Considering DC filter, the DC subsystem is formulated in time-domain as [44]

$$\begin{cases} v_{dc} = v_c + r_{dc} i_{dc} + v_L \\ C_{dc} \cdot \dfrac{d}{dt} v_c = i_{dc} - \dfrac{v_c}{R_{load}} \\ \dfrac{d}{dt} v_L = \dfrac{1}{\tau}(L_{dc} \dfrac{d}{dt} i_{dc} - v_L) \end{cases}, \tag{3.6}$$

The derivative of inductor voltage v_L comes from the transfer function commonly used to represent inductor in dc side of integrated AC/DC systems, as shown in (3.7).Transfer function (3.7) is used in model implementation, while for mathematically description of model in time domain, the inductor is expressed using the differential equation.

$$H_L(s) = \frac{s \cdot L_f}{\tau s + 1} \tag{3.7}$$

Where τ is a time constant small enough to be negligible at switching frequency (i.e. τ =10μs is used in this thesis). The reason for formulating τ into model is to avoid numerical differentiation [43]-[44].

Transforming time domain equations to dynamic phasor domain yields

$$\begin{cases} \langle v_{dc} \rangle_0 = \langle v_c \rangle_0 + r_{dc} \langle i_{dc} \rangle_0 + \langle v_L \rangle_0 \\ C_{dc} \cdot \dfrac{d}{dt} \langle v_c \rangle_0 = \langle i_{dc} \rangle_0 - \dfrac{\langle v_c \rangle_0}{R_{load}} \\ \dfrac{d}{dt} \langle v_L \rangle_0 = \dfrac{1}{\tau}(L_{dc} \dfrac{d}{dt} \langle i_{dc} \rangle_0 - \langle v_L \rangle_0) \end{cases}, \tag{3.8}$$

From (3.6) and (3.8), the direct interface between the LCR system and the DC subsystem is achieved since two sets of equations are input-output compatible.

3.3 DP Modelling of AC Subsystem

Typically, the LCR have one discontinuous conduction mode (DCM) and three continuous conduction modes (CCM-1, CCM-2, and CCM-3), respectively depending on the load conditions [22]. Phase currents in ac subsystem will be highly distorted when the LCR operates in DCM, which usually occurs at light load conditions [10]. Since the 1st, 5th, and 7th order components are dominant in AC subsystem [6], it is appropriate to select these orders of DPs to represent the AC subsystem. For the DC subsystem, in the implementation considered in this section, only the 0-th order DP component is considered for modeling its dynamics.

3.3.1 Full-order DP Modelling of Thevenin AC Equivalent Circuit

The AC subsystem dynamics can be expressed in time-domain as

$$L_s \frac{d}{dt}\mathbf{i}_{abcs} + r_s\mathbf{i}_{abcs} + \mathbf{v}_{abcs} = \mathbf{e}_{abcs} \tag{3.9}$$

Throughout this document, the subscript "*abcs*" denotes the three stationary phases *as*, *bs*, *cs* of AC subsystem variables. Applying the GAM approach [6], the *k*th order DP equation yields

$$L_s \frac{d}{dt}\langle \mathbf{i}_{abcs} \rangle_k + (r_s + \mathrm{j}k\omega_s L_s)\langle \mathbf{i}_{abcs} \rangle_k + \langle \mathbf{v}_{abcs} \rangle_k = \langle \mathbf{e}_{abcs} \rangle_k, k \in K. \tag{3.10}$$

Here, $K=\{1,5,7\}$as aforementioned. Since $<\mathbf{i}_{abcs}>_k$, $<\mathbf{v}_{abcs}>_k$, and $<\mathbf{e}_{abcs}>_k$ are vectors of complex variables, to facilitate operations using regular simulation programs that does calculations of only real variables, (3.9) is decomposed into real and imaginary parts as

$$\frac{d}{dt}\begin{bmatrix}\langle \mathbf{I}_{abcs,r}\rangle_k \\ \langle \mathbf{I}_{abcs,i}\rangle_k\end{bmatrix}=\begin{bmatrix}\langle \mathbf{E}_{abcs,r}\rangle_k \\ \langle \mathbf{E}_{abcs,i}\rangle_k\end{bmatrix}-\begin{bmatrix}\langle \mathbf{V}_{abcs,r}\rangle_k \\ \langle \mathbf{V}_{abcs,i}\rangle_k\end{bmatrix}-\begin{bmatrix}r_s & -k\omega_s L_s \\ k\omega_s L & r_s\end{bmatrix}\begin{bmatrix}\langle \mathbf{I}_{abcs,r}\rangle_k \\ \langle \mathbf{I}_{abcs,i}\rangle_k\end{bmatrix}. \tag{3.11}$$

Here subscripts "*r*" and "*i*" are used to denote the real and imaginary components, respectively.

For the full-order PDP model [21], the 1st, 5th, and 7th order DPs of AC subsystem are expressed using full-order differential equations. For the considered example benchmark system, this formulation results in 18 state variables in the AC subsystem (which has appropriate computational cost). Additionally, any fast transient changes may excite transient ringing/oscillations in DP domain [58], which also leads to reduction of time step size. Therefore, a reduced-order dynamic phasor modelling of AC subsystem has been proposed in [65].

3.3.2 Reduced-order DP Modelling of Thevenin AC Equivalent Circuit

In reduced-order modelling, it is assumed that transients are dominated by the first-order DP, whereas the higher-order DPs dynamics may be neglected. This reduced-order PDP model can eliminate the ringing in DP domain and reduce the number of state variables. For the proposed reduced-order PDP model, only the first-order DPs dynamics are considered and represented by differential equations, and the remaining higher-order (harmonic) DPs are expressed by algebraic equations. The differential equation for the fundamental component is formulated as

$$\frac{d}{dt}\begin{bmatrix}\langle \mathbf{I}_{abcs,r}\rangle_1 \\ \langle \mathbf{I}_{abcs,i}\rangle_1\end{bmatrix}=\begin{bmatrix}\langle \mathbf{E}_{abcs,r}\rangle_1 \\ \langle \mathbf{E}_{abcs,i}\rangle_1\end{bmatrix}-\begin{bmatrix}\langle \mathbf{V}_{abcs,r}\rangle_1 \\ \langle \mathbf{V}_{abcs,i}\rangle_1\end{bmatrix}-\begin{bmatrix}r_s & -k\omega_s L_s \\ k\omega_s L & r_s\end{bmatrix}\begin{bmatrix}\langle \mathbf{I}_{abcs,r}\rangle_1 \\ \langle \mathbf{I}_{abcs,i}\rangle_1\end{bmatrix}. \tag{3.12}$$

The algebraic equation for harmonic components becomes

$$0=\begin{bmatrix}\langle \mathbf{E}_{abcs,r}\rangle_k \\ \langle \mathbf{E}_{abcs,i}\rangle_k\end{bmatrix}-\begin{bmatrix}\langle \mathbf{V}_{abcs,r}\rangle_k \\ \langle \mathbf{V}_{abcs,i}\rangle_k\end{bmatrix}-\begin{bmatrix}r_s & -k\omega_s L_s \\ k\omega_s L & r\end{bmatrix}\begin{bmatrix}\langle \mathbf{I}_{abcs,r}\rangle_k \\ \langle \mathbf{I}_{abcs,i}\rangle_k\end{bmatrix}, k=5,7 \tag{3.13}$$

It is seen in (3.12) that the dynamics are removed from higher order DPs, which can be solved implying a steady state in harmonics. Also, in this reduced-order PDP model, there are only 6 state variables in the ac subsystem, all of which are coming from (3.11).

3.4 Implementation

The full-order parametric dynamic phasor (PDP) model of the LCR benchmark system can be summarized into three subsystems: 1) full-order dynamic phasor model of the AC network represented by a Thevenin equivalent circuit with equations (3.11); 2) parametric dynamic phasor (PDP) model of the LCR formulated as a set of parametric functions listed in (3.3)-(3.5); and 3) the DC subsystem modeled with only 0th order GAM-Type DPs as (3.6). Figure 3.3 illustrates the interconnections among three subsystems.

However, in the implementation of reduced-order model shown in Figure 3.4, the AC network is modeled using equation (3.12) and (3.13) in reduced-order PDP model with exclusion of high-order dynamics; and the rest subsystems are the same with the full-order model. In particular, 5th and 7th DPs are represented without dynamics by algebraic expressions.

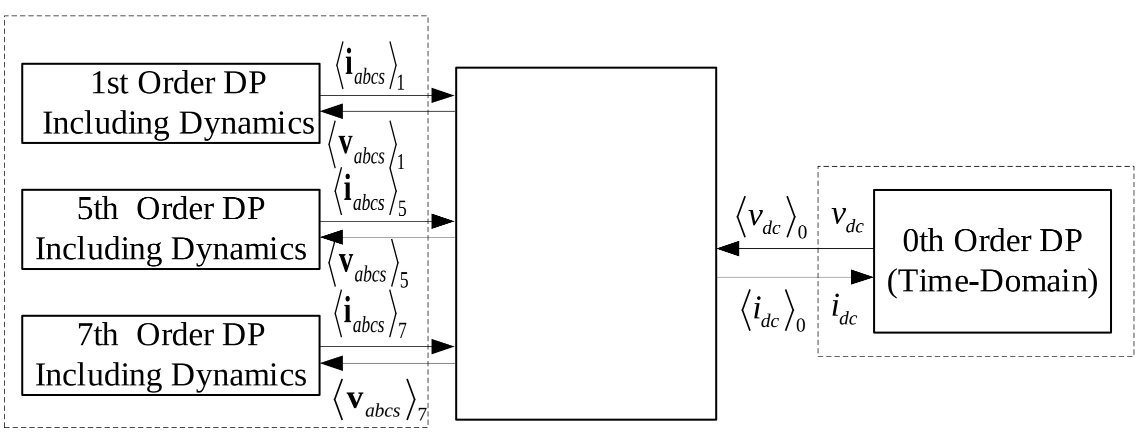

Figure 3. 3 Implementation of the full-order PDP model of a generic AC-DC system.

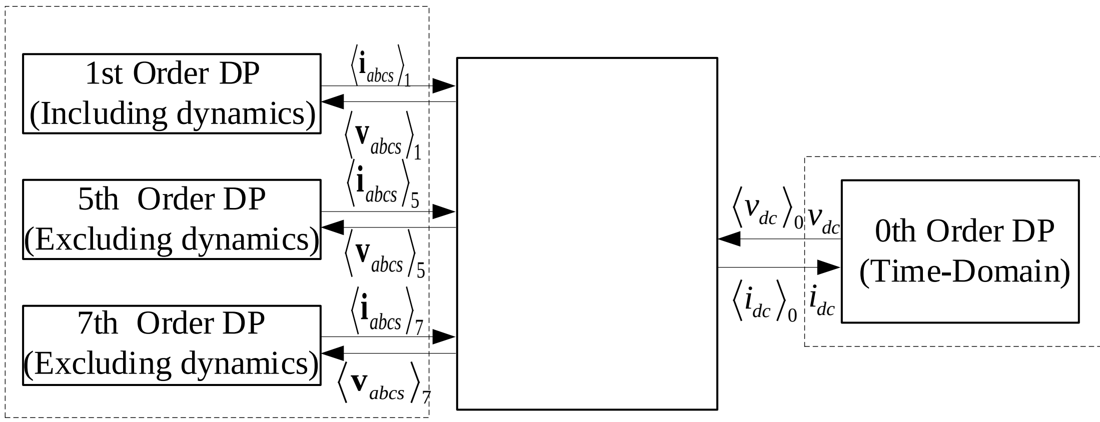

Figure 3. 4 Implementation of reduced-order PDP model of a generic AC-DC system.

It is also noted that higher-order components, beyond of 7th, can be augmented in the AC subsystem of either full-order model or reduced-order model when needed.

3.5 Computer Studies

To evaluate the numerical property of the proposed model, the full-order PDP model [21] and the reduced-order PDP model of integrated AC-DC system shown in Figure. 3.5 have been implemented in MATLAB/Simulink. The system parameters are summarized in Appendix A. For the studies in this chapter, the 1st, 5th, and 7th order DPs are included, whereas more terms may be included if desired. The detailed switching model of the considered benchmark system has also been implemented as the reference [21].

A transient computer study is selected to span a wide range of operating conditions. In the following study, the LCR system is assumed to operate in steady state with DC load of 950Ω, which corresponds to operation in DCM. At t = 0.25s, the DC load is changed down to 150Ω; and at t = 0.5s, the load is further reduced down to 10 Ω; and finally at t = 0.75s, the DC load resistance is reduced to 0.1 Ω; respectively, and the simulation runs until t = 1s. The corresponding simulation results are shown in Figure 3.5. In this study, the system first transits from DCM to CCM-1, then to CCM-2, and finally reaches steady state in CCM-3. For consistency, all case studies are conducted on a PC with a 3.4GHz Intel i7-2600 CPU.

3.5.1 Variable-Time-Step Study

First, the subject models are solved using the ode23tb solver [6] with max/min time step of 0.1ms and 100ns, respectively; and relative and absolute tolerance of $1e^{-4}$. To give a general view of the transient predicted by the subject models, the trajectories of phase a and DC currents and voltages are shown in Figure 3.5(a). A zoom-in view showing the system response under first load change is plotted in Figure 3.5(b). From these two figures, it is observed that both two PDP models, by including 5th and 7th harmonics, are capable of producing the results that match well the detailed model (reference solution). Moreover, even though the dynamics of high-order components are eliminated in the reduced-order PDP model, it has invisible impact on accuracy of predicting responses in both AC and DC subsystems.

To investigate the numerical efficiency of the subject models, a 10s transient study covering all four operating modes by varying load is considered here. In the variable-step study, the two PDP models are executed for 1s using the ode23tb solver with max step size set to 5ms, min step size to 100ns, and relative and absolute tolerances set to 1e-3, respectively.

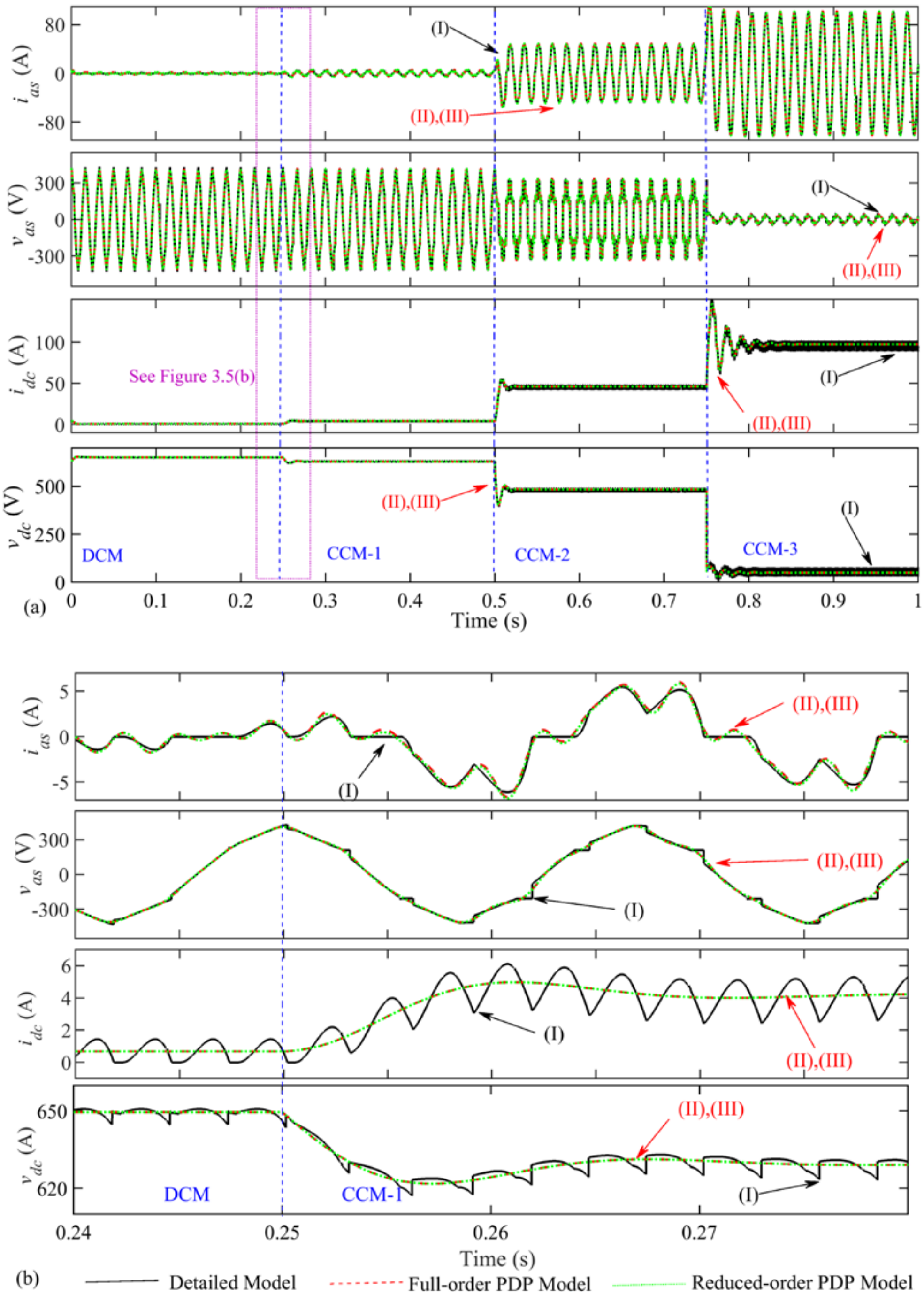

Figure 3. 5 System response to changes in load resistance as predicted by the subject models: (a) the entire simulation response due to three consecutive changes, and (b) magnified view during the first transient from DCM to CCM-1.

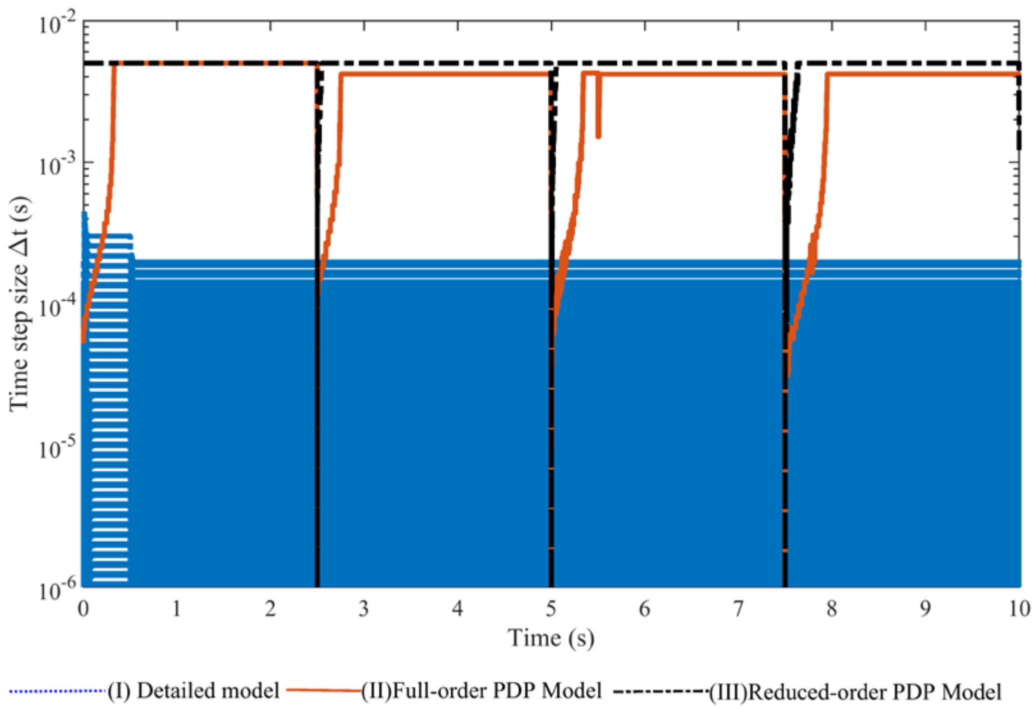

Figure 3. 6 Simulation step size chosen by the subject models in variable-time-step study.

To study the efficiency, the time step sizes chosen during the course of simulation by the subject models are demonstrated in Figure 3.6. Therein, it is seen that both full- and reduced-order PDP models use small time steps at the beginning of each transient period caused by the change in the DC load, while larger time step sizes are used during steady state for both PDP models. When the load abruptly changes, the ode solver can automatically adjust the time step sizes based on error tolerance setting to achieve the required accuracy and/or "catch" the events.

However, after the transients, the step size of the reduced-order model increases more quickly until it reaches the specified maximum time step size of 5ms. The full-order PDP model also increases its time steps right after the load changes, but it increases more slowly and almost reach the maximum time step size.

Furthermore, the corresponding numerical statistics for the three subject models are summarized in Table 3.1, which includes the total CPU time, the total number of steps, and the average time step used by each model. As it can be seen in Table 3.1, the two PDP models have superior numerical efficiency than the detailed model with less number of steps taken and less CPU time.

At the same time, it is noted that proposed reduced-order PDP model takes significantly fewer steps (2,229 vs. 10,466) and executes much faster (0.77s vs. 1.91s) than the full-order model. Due to the constantly excited transients which are present in all higher-order DPs (harmonics), the variable time step of the full-order PDP model cannot significantly increase and the average time step is only 955.47μs. At the same time, the reduced-order PDP model has the transients of the fundamental component only (since the harmonic DPs are solved algebraically assuming their steady state), and its average time step is much higher (4486.31μs vs. 955.47μs), as summarized in Table 3.1.

Table 3. 1 Numerical efficiency of the subject models for variable time step study of 10 seconds.

Model	**No. of Time Steps**	**Total CPU Time, s**	**Average Time Step, μs**
Detailed Model	81117	8.69	123.28
Full-order PDP	10466	1.91	955.47
Reduced-order PDP	2229	0.77	4486.31

3.5.2 Fixed-Time-Step Study

In this section, the full- and reduced-order PDP models are executed with fixed time step Δt = 5 μs using the ode14x solver. The total CPU time taken and the CPU time per step are summarized in Table 3.2 for the two subject models. As seen in Table 3.2, the reduced-order PDP model is also 28.5% computationally less expensive than full-order PDP model.

Table 3. 2 Numerical efficiency of two PDP Models for fixed time step study of 10 seconds.

Model	No. of Time Steps	Total CPU Time, s	CPU Time per Step, μs
Full-Order PDP	200001	93.410	467.05
Reduced-Order PDP	200001	66.786	333.93

As it can be seen in Tables 3.1 and 3.2, the reduced-order PDP model is computationally more effective with either variable-step or fixed-step solvers. This improved numerical efficiency is achieved by the algebraic representations of the high-order DPs. To better demonstrate this point, the transients observed in the 5th and 7th order DPs of the phase a current during the 1s simulation study of Figure 3.5(a) are shown in Figure 3.7.

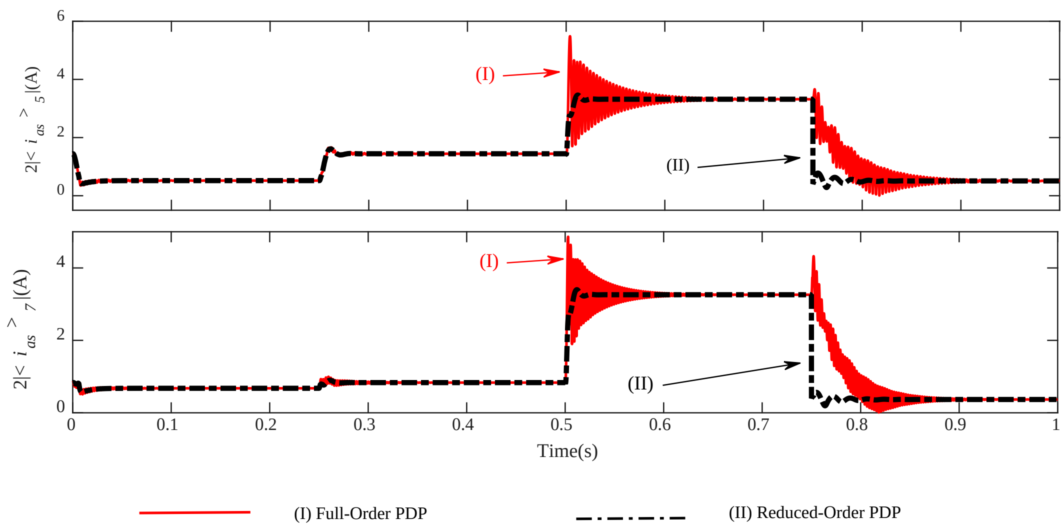

Figure 3. 7 Transients observed in 5th and 7th order DPs of the phase a current during load changes corresponding to 1s study.

As is seen in Figure 3.7, the 5th and 7th order DPs have significant ringing especially when the LCR system enters the CCM-2 and CCM-3 modes. These fast transients in harmonic DPs do not allow the full-order PDP model to increase its time step significantly and uses more sampling points. In contrast, these 5th and 7th order ringing transients are removed in the reduced-order PDP model, thus enabling this model to rapidly increase its time step. In addition to that, the proposed reduced-order PDP model is also computationally cheaper per time step since it uses fewer state variables.

To investigate the accuracy of subject models, in this section, the study focuses on the time interval of 0.245s – 0.275s, i.e., the mode transition from DCM to CCM-1. Here, the models are solved using the ode14x implicit solver with different selected fixed time step sizes.

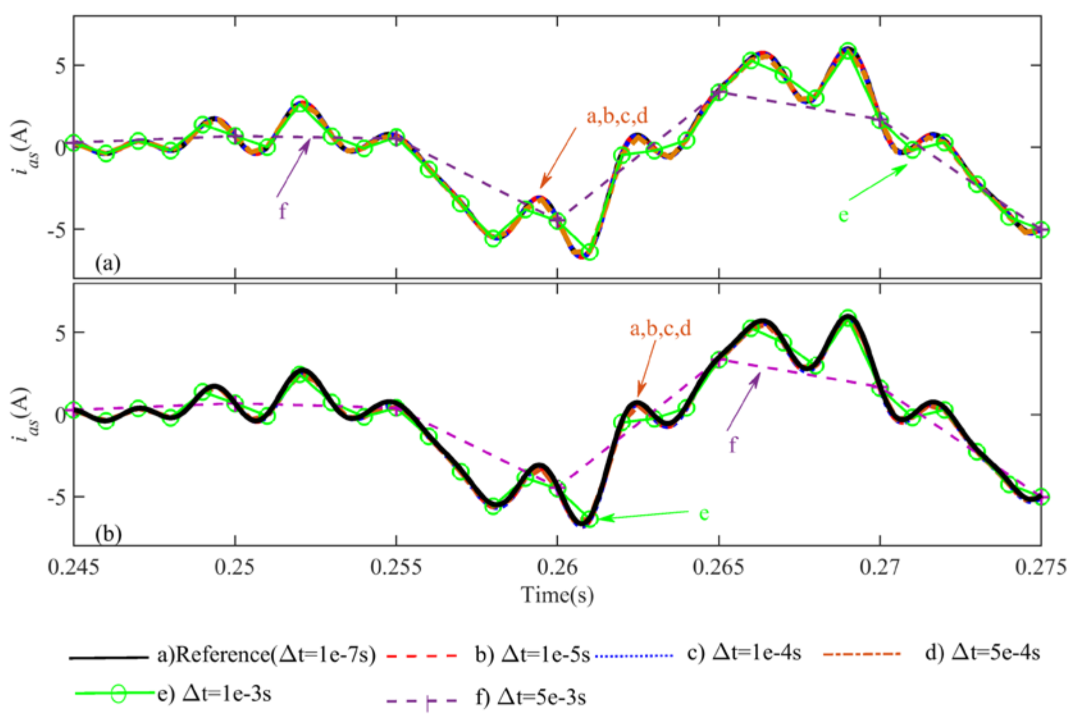

Figure 3. 8 Current trajectory predicted by the two PDP models using fixed time steps: (a) full-order PDP, and (b) proposed reduced-order PDP.

Since the accuracy of full-order PDP model has been established in [21], its solution with very small fixed time step of 0.1μs is assumed as reference. The current trajectories predicted by the subject models using different fixed time step are demonstrated in Figure 3.8. As it can be seen in Figure 3.8, both PDP models achieve very similar accuracy during this transient interval. Specifically, even when the time steps are larger than the waveform ripple, i.e. 1ms and 5ms, respectively, the solution points produced by the PDP models lay on top of the reference solution trajectory.

To give a quantitative evaluation of accuracy comparison, the 2-norm error and infinity-norm (i.e. the max) error are tabulated in Table 3.3. As it can be seen in Table 3.3, it is seen that the proposed reduced-order PDP model is less accurate compared to the full-order PDP model. However, errors calculated from the reduced-order PDP model at different time step sized are less dispersive than those of the full-order model, which reflects the potential of larger allowable time step size taken by the reduced-order PDP model.

Table 3.3 Comparison of accuracy by two PDP models for fixed time step study.

Time Step Size, ms	Full-Order PDP		Reduced-Order PDP	
	2-Norm Error	Infinity-Norm Error	2-Norm Error	Infinity-Norm Error
0.01	0.0993	0.0050	1.2773	0.2319
0.1	0.5731	0.0346	1.3110	0.2349
0.5	1.0139	0.0784	1.3466	0.2371
1	1.1055	0.0946	1.3559	0.2373
5	1.2097	0.1292	1.5069	0.2449

Chapter 4: Reduced-order PDP Modelling of A Typical AC Distribution System with Transformer and Rectifier Loads

Three-phase transformers are commonly used in distribution systems. This chapter begins with dynamic phasor modelling of transformers using GAM-Type DPs solution. Next, the afore-proposed reduced-order parametric dynamic phasor modelling approach is applied to AC distribution system with a $\Delta_1 y_{g0}$ three-phase transformer. Computer studies have revealed advantages of the reduced-order parametric dynamic phasor methodology used in AC distribution system through the fact that new model demonstrated improvement of numerical efficiency without losing accuracy.

4.1 DP Modelling of Three-phase Transformers

4.1.1 Single-phase Transformers

In a practical transformer, windings have resistance, not all windings link the same flux, permeability of the core material is not infinite, and core losses occur when the core material is subjected to time-varying flux [66]. In this thesis, the transformer is modelled using its equivalent electrical circuit, since in the way the two sides of transformer can be easily interfaced with the rest of the power network. For the purpose of this thesis, the core losses are neglected. The equivalent circuit of a single-phase transformer is depicted as Figure 4.1. As shown in Figure 4.1, all variables and components are referred to the secondary side based on the following relationships:

$$
\begin{cases}
v'_{w1} = \dfrac{v_{w1}}{a} \\
i'_{w1} = a \cdot i_{w1} \\
r'_1 = \dfrac{r_1}{a^2} \\
L'_{l1} = \dfrac{L_{l1}}{a^2} \\
L'_m = \dfrac{L_m}{a^2}
\end{cases}
\quad . \tag{3.14}
$$

Here, a ($=N_1/N_2$) is turns ratio of the single-phase transformer. This is done for the reason that electronic loads are commonly connected to the secondary side in distribution systems. The inductance L'_{l1} represents the referred leakage inductance at the primary side, accounting for the effect of leakage flux. The referred winding resistance of the primary side is denoted as r'_1. In a practical magnetic core having finite permeability, a magnetizing current i_m is required to establish a flux in the core. This effect can be represented by a magnetizing inductance L_m.

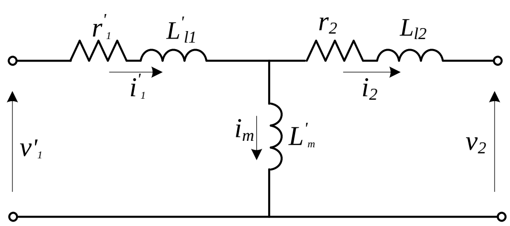

Figure 4. 1 Equivalent circuit of single-phase transformer based on physical reasoning.

4.1.2 Three-phase Transformers

In three-phase power system, three-phase transformers are required to step up or step down voltages at various stages. A three-phase transformer can be built by suitably connecting a bank of three single-phase transformers, or by constructing a three-phase transformer on a common magnetic structure [66]. In this thesis, the three-phase transformer is assumed to be comprised of a bank of three single-phase transformers.

4.1.2.1 Transformer Windings Configurations

A set of three similar single-phase transformers may be connected to form a three-phase transformer in the way that the primary and secondary windings may be connected in either Wye (Y) or Delta (Δ) configurations. There are therefore four possible connections for a three-phase transformer: Y- Δ, Δ-Y, Δ- Δ, and Y-Y. Additionally, the interconnection between windings and bushings are determining the phase shift across a transformer. Generally, assuming a maintained positive sequence rotation, in actual practice almost all connections can be seen in 6 variations of wye connections and 6 different ways of delta connections listed in Figure 4.2 and Figure 4.3 [37], given a set of three windings W_1, W_2, W_3, and three transformer phase bushing U, V, W. The # refers to the phase angle, as viewed on a 12 hour clock, of winding W_1 relative to the voltage applied to U bushing with a balanced three-phase positive sequence voltage.

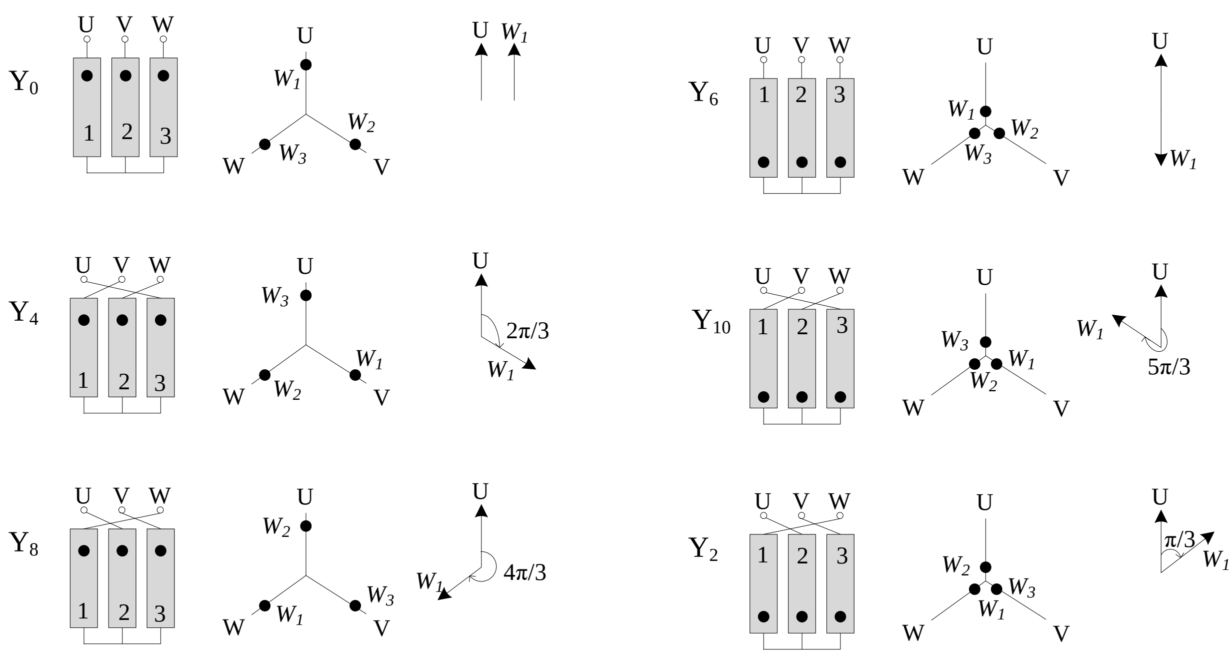

Figure 4. 2 Six ways to wire a Wye winding.

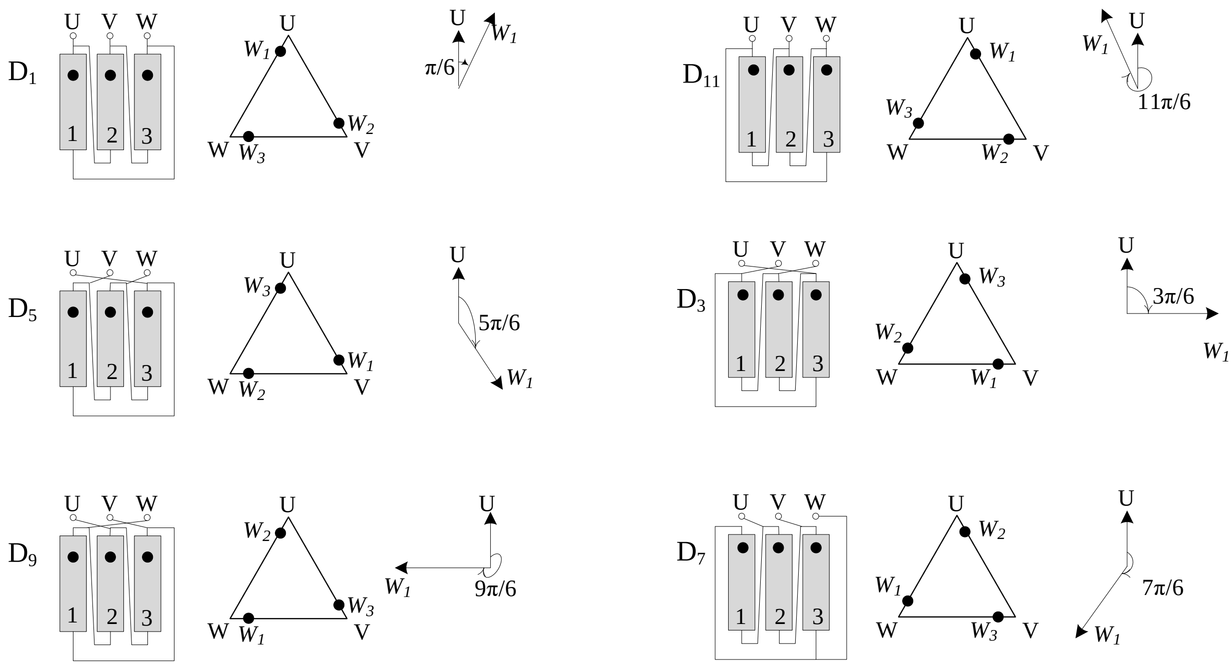

Figure 4. 3 Six ways to wire a Delta winding.

4.1.2.2 Phase Shift and Magnitude Difference

1) *Phase shift between bushing variables and winding variables*

From the listed winding connections, it is seen that some of three-phase transformer connections will result in a phase shift between the bushing voltages and the winding voltages. The angular relationship will be the angel difference of variables between phase U variables and winding W_1, as illustrated in Figure 4.2 and Figure 4.3. Since the positive sequence is defined as UVW, W_1 may lag the phase U by a certain angle denoted in Figure 4.2 and Figure 4.3.

2) *Magnitude difference between bushing variables and winding variables*

In Y-connections, no magnitude differences exists between the bushing variables and the winding variables, since the windings are connected between the bushing nodes and the neutral points, as depicted in Figure 4.2. Since the positive bushing sequence is assumed to be maintained, the different connections leads to nothing but phase shift of variables between the bushings and the windings, and the magnitudes are equivalent between the bushings and the windings. The relationship between the bushing variables and the winding variables are expressed as

$$\begin{cases} v_U = v_{w1} \cdot e^{\mathrm{j}\theta_{Y_\#}} \\ i_U = i_{w1} \cdot e^{\mathrm{j}\theta_{Y_\#}} \end{cases}. \tag{3.15}$$

Here, v_U and i_U represent the voltage and current of the bushing U respectively, while v_{w1} and i_{w1} represent the voltage and current of the winding W_1 respectively. The angle $\theta_{Y_\#}$ denotes the phase shift between the bushing variables and the winding variables; and $Y_\#$ refers to the wiring configuration.

On the one hand, in Δ-connections, the windings are connected between two bushing nodes, by which the winding voltages can be regarded as the line-to-line voltages with the magnitude of $\sqrt{3}$ times the phase bushing variables. On the other hand, the current flowing through each single winding flows through two bushings, for which the magnitude of the winding current is only $\frac{1}{\sqrt{3}}$ times the phase bushing variables. The relationship between the bushing variables and the winding variables are expressed as

$$\begin{cases} v_U = \dfrac{1}{\sqrt{3}} v_{w1} \cdot e^{\mathrm{j}\theta_{D_\#}} \\ i_U = \sqrt{3} i_{w1} \cdot e^{\mathrm{j}\theta_{D_\#}} \end{cases} \tag{3.16}$$

Here, v_U and i_U represent the voltage and current of the bushing U respectively, while v_{w1} and i_{w1} represent the voltage and current of the winding W_1 respectively. The angle $\theta_{D_\#}$ denotes the phase shift between the bushing variables and the winding variables; and $Y_\#$ refers to the wiring configuration.

4.1.3 Equivalent Circuit of Three-phase Transformers

In a three-phase transformer bank, the three single-phase transformers are practically identical. Under a balanced load and source, the voltages and currents on both primary and secondary sides are balanced, too. The voltages and currents in one phase are the same as those in other phases, except that there is a phase displacement of 120 degrees. Therefore, for the purpose of this thesis, one phase is sufficient to determine the variables on the two sides of the transformer. A single-phase equivalent circuit can be conveniently obtained if all sources, transformer windings, and load impedances are considered to be Y-connected.

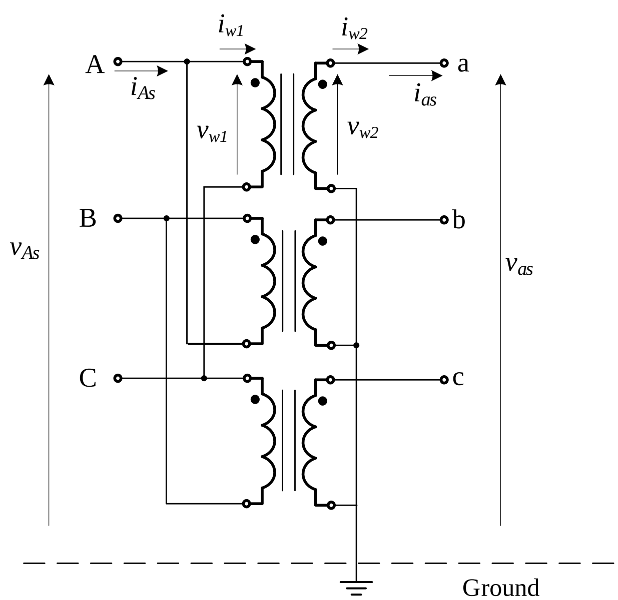

Figure 4. 4 Windings configuration of $\Delta_1 Y_{g0}$ three-phase transformer bank.

The Δ-connections are also commonly used in practice. In such cases, the equivalent circuit is obtained based on the winding variables (not the phase variables). In this way, the phase shift of the line-to-line voltages between primary side and secondary side caused by different leakage flux is automatically included in the model, which is reflected through the inclusion of L'_{l1} and L'_{l2}. In addition, the phase shift of the line-to-line voltages between the primary side and the secondary side caused by different connections is displayed in the way of phase shift between the phase variables and the winding variables at each side. Therefore, this method of deriving the equivalent circuit does not require transformed Y representation of the actual circuit before constructing the single phase equivalent circuit.

For instance, the equivalent circuit of $\Delta_1 Y_{g0}$ three-phase transformer (bank) is demonstrated in Figure 4.5. As depicted in Figure 4.4, the primary side is connected in Δ_1, for which the phase variables are different from the winding variables; and the secondary side is connected in Y_0. Based on classical magnetically coupled circuit modelling of transformers, it is reasonable to derive the model using the winding variables.

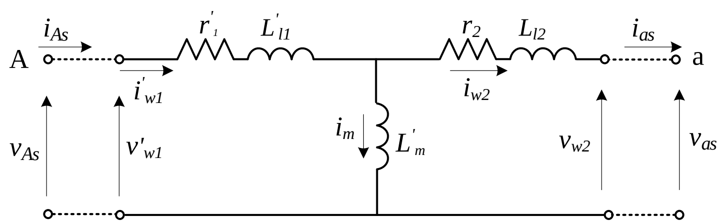

Figure 4. 5 Equivalent circuit of three-phase transformer bank.

In Figure 4.5, v_{As} and i_{As} represent the phase A voltage and current at the primary side; and v_{as} and i_{as} represent the phase A voltage and current at the secondary side. Additionally, v'_{w1} and i'_{w1} represent the referred voltage and current of winding 1 at the primary side; while v_{w2} and i_{w2} represent the voltage and current of winding 2 at the secondary side. The referred variables and components of transformer can be obtained similar to (3.24), as follows:

$$\begin{cases} v_{w1}^{'} = \dfrac{v_{w1}}{a} \\ i_{w1}^{'} = a \cdot i_{w1} \\ r_1^{'} = \dfrac{r_1}{a^2} \\ L_{l1}^{'} = \dfrac{L_{l1}}{a^2} \end{cases} . \tag{3.17}$$

The phase shift and magnitude difference should be added to attain the phase variables, as addressed in Section 4.1.2.2. In the $\Delta_1 Y_{g0}$ connection, the relationships between the phase variables and the winding variables are expressed as

$$\begin{cases} i_{As} = \sqrt{3} i_{w1}^{'} e^{j\frac{\pi}{6}} \\ v_{As} = \dfrac{1}{\sqrt{3}} v_{w1}^{'} e^{j\frac{\pi}{6}} \end{cases} \tag{3.18}$$

$$\begin{cases} i_{as} = i_{w2} \\ v_{as} = v_{w2} \end{cases} \tag{3.19}$$

Equation (4.5) represents the relationship between the phase variables and the winding variables at primary side (Δ_1-connection); and (4.6) represents the relationships between the phase variables and the winding variables at secondary side (Y_0-connection).

4.1.4 Modelling of Three-phase Transformers using GAM-Type DPs

Based on Figure 4.3, the T-equivalent circuit of transformer is modelled in time domain as

$$\begin{cases} L_{l1}^{'} \dfrac{d}{dt} i_{w1}^{'} + r_1^{'} i_{w1}^{'} + L_m^{'} \dfrac{d}{dt} (i_{w1}^{'} - i_{w2}) = v_{w1}^{'}, \\ -L_{l2} \dfrac{d}{dt} i_{w2} - r_2 i_{w2} + L_m^{'} \dfrac{d}{dt} (i_{w1}^{'} - i_{w2}) = v_{w2}. \end{cases} \tag{3.20}$$

Applying the GAM approach to (4.5), the DP equations for the k-th order harmonic variables can be expressed as

$$\begin{cases} \langle v'_{w1} \rangle_k = (L'_{l1} + L'_m)\left(\frac{d}{dt}\langle i'_{w1} \rangle_k + \mathrm{j}k\omega_s \langle i'_{w1} \rangle_k \right) + r_1 \langle i'_{w1} \rangle_k - L'_m \left(\frac{d}{dt}\langle i'_{w2} \rangle_k + \mathrm{j}k\omega_s \langle i'_{w2} \rangle_k \right) \\ \langle v_{w2} \rangle_k = (-L_{l2} - L'_m)\left(\frac{d}{dt}\langle i_{w2} \rangle_k + \mathrm{j}k\omega_s \langle i_{w2} \rangle_k \right) - r_2 \langle i_{w2} \rangle_k + L'_m \left(\frac{d}{dt}\langle i'_{w1} \rangle_k + \mathrm{j}k\omega_s \langle i'_{w1} \rangle_k \right) \end{cases}. \tag{3.21}$$

As addressed in Chapter 3, the dynamics of high-order harmonics is negligible in reduced-order DP model, so that the following expression are obtained as

$$\begin{cases} \langle v'_{w1} \rangle_1 = (L'_{l1} + L'_m)\left(\frac{d}{dt}\langle i'_{w1} \rangle_1 + \mathrm{j}k\omega_s \langle i'_{w1} \rangle_1 \right) + r_1 \langle i'_{w1} \rangle_1 - L'_m \left(\frac{d}{dt}\langle i'_{w2} \rangle_1 + \mathrm{j}k\omega_s \langle i'_{w2} \rangle_1 \right) \\ \langle v_{w2} \rangle_1 = (-L_{l2} - L'_m)\left(\frac{d}{dt}\langle i_{w2} \rangle_1 + \mathrm{j}k\omega_s \langle i_{w2} \rangle_1 \right) - r_2 \langle i_{w2} \rangle_1 + L'_m \left(\frac{d}{dt}\langle i'_{w1} \rangle_1 + \mathrm{j}k\omega_s \langle i'_{w1} \rangle_1 \right) \end{cases};$$
$$\begin{cases} \langle v'_{w1} \rangle_k = (L'_{l1} + L'_m)\left(\mathrm{j}k\omega_s \langle i'_{w1} \rangle_k \right) + r_1 \langle i'_{w1} \rangle_k - L'_m \left(\mathrm{j}k\omega_s \langle i'_{w2} \rangle_k \right) \\ \langle v_{w2} \rangle_k = (-L_{l2} - L'_m)\left(\mathrm{j}k\omega_s \langle i_{w2} \rangle_k \right) - r_2 \langle i_{w2} \rangle_k + L'_m \left(\mathrm{j}k\omega_s \langle i'_{w1} \rangle_k \right) \end{cases}, k > 1. \tag{3.22}$$

The interface between the transformer and the rest of power network can be achieved through relationships between the winding variables and the phase variables in (4.5) and (4.6). Applying the GAM approach to (4.5) and (4.6), the interface of dynamic phasors is obtained as

$$\begin{cases} \langle i_{As} \rangle_k = \sqrt{3}\langle i'_{w1} \rangle_k e^{\mathrm{j}(\frac{k\pi}{6})} \\ \langle v_{As} \rangle_k = \frac{1}{\sqrt{3}}\langle v'_{w1} \rangle_k e^{\mathrm{j}(\frac{k\pi}{6})} \end{cases}, \tag{3.23}$$

$$\begin{cases} \langle i_{as} \rangle_k = \langle i_{w2} \rangle_k \\ \langle v_{as} \rangle_k = \langle v_{w2} \rangle_k \end{cases}. \tag{3.24}$$

4.2 Dynamic Phasor (DP) Modelling of AC Distribution System with Three-phase $\Delta_1 Y_{g0}$ Transformer

As addressed in Section 3.1, the LCR loads can connect to a distribution feeder or a transformer. This section analyzes the performance of reduced-order parametric dynamic phasor model of an AC distribution system with LCR loads, in terms of accuracy and computational cost. The considered AC distribution system with rectifier loads is depicted in Figure 4.6. The AC network is represented by a Thevenin equivalent circuit consisting of voltage source $\boldsymbol{e}_{abcs}$ and series line impedances (r_s, L_s). The parallel resistors (r_{s1}) represent other loads that draw part of power from the AC network. Here, a $\Delta_1 Yg_0$ transformer regulates (steps up/down) the voltage to provide power to the rectifier loads and some other loads represented by parallel impedances (r_{s2}, L_{s2}). A low-pass *RLC* filter smoothens the rectified current and voltage to feed a DC network that is represented here by a resistive load R_{load}. The system parameters are summarized in Appendix B.

As addressed in Section 3.1.1, a single phase of AC subsystem may be considered for simplicity. In order to simplify the model and improve simulation speed, the single-phase (phase *a*) equivalent circuit of the AC network is demonstrated in Figure 4.7.

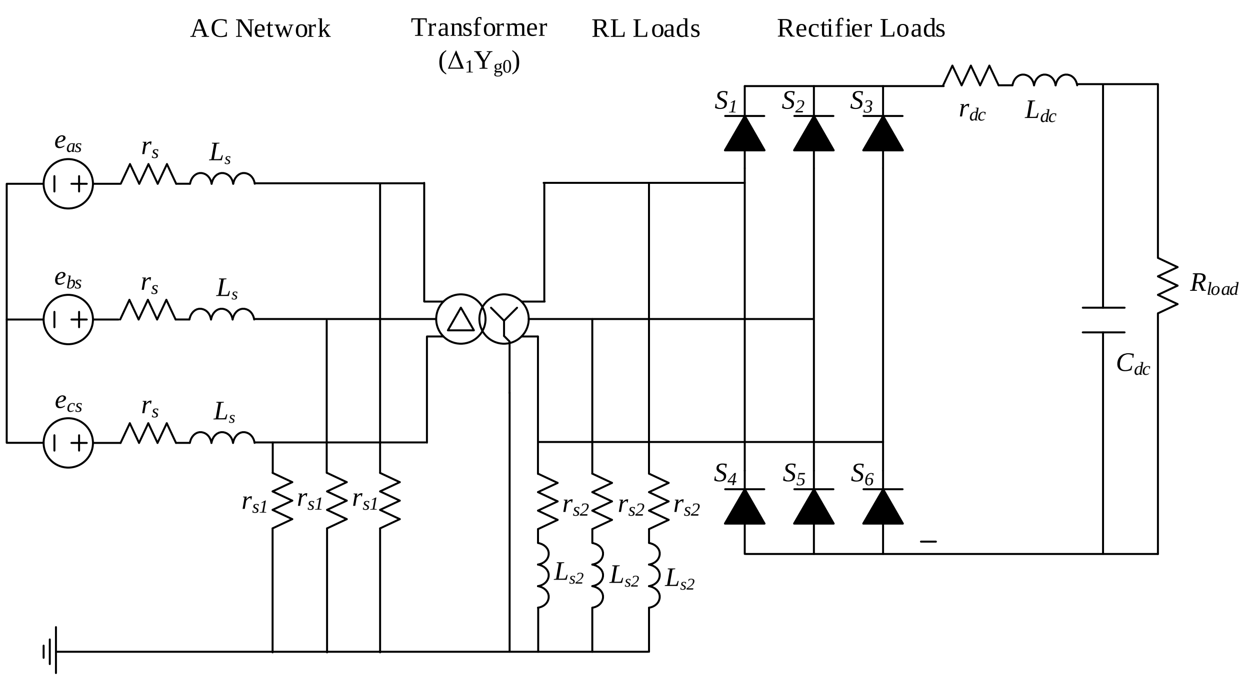

Figure 4. 6 The considered generic AC distribution system with transformer and rectifier load.

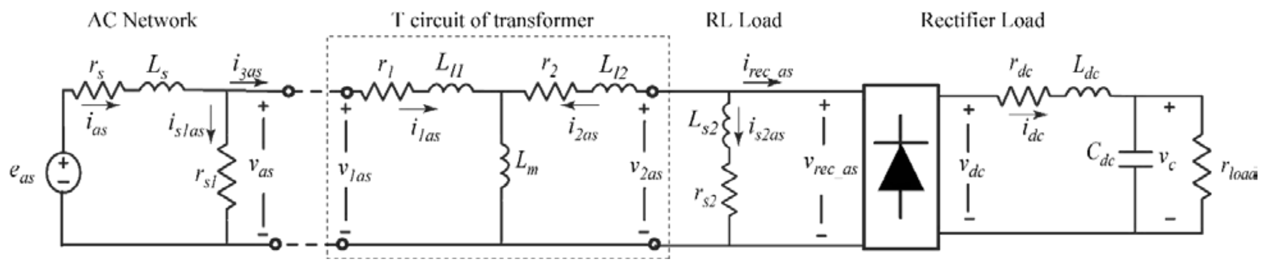

Figure 4. 7 Single-phase equivalent circuit of the considered AC distribution system.

The entire system can be broken down into four parts, namely the AC network, T-circuit of transformer, the *RL* load, and the rectifier load. The resistance r_1 and r_2, the leakage inductance L_{l1} and L_{l2}, the voltage v_{1as} and v_{2as}, and the current i_{1as} and i_{2as} are related to primary and secondary windings of the transformer, respectively, and L_m is the mutual inductance. The parameters of three-phase transformer are summarized in Appendix B. Due to Δ-connection at the primary side, the winding voltage v_{1as} and current i_{1as} are different from the phase *a* voltage v_{as} and current i_{3as}. Therefore, the angle shift and scaling of magnitude should be added accordingly. With 30-degree shift and $\sqrt{3}$ scaling of the currents and voltages in the single-phase equivalent circuit, the relationship between the variables at the delta connection are as follows:

$$\begin{cases} \langle v_1 \rangle_k = \sqrt{3}\langle v_{as} \rangle_k \, e^{\mathrm{j}(\frac{-k\pi}{6})} \\ \langle i_3 \rangle_k = \sqrt{3}\langle i_1 \rangle_k \, e^{\mathrm{j}(\frac{k\pi}{6})} \end{cases}, k \in K. \tag{3.25}$$

Herein, $<v_1>_k$, and $< i_1>_k$, are the referred *k*-th harmonic voltage and current of the Y-equivalent of the transformer winding, while $<i_3>_k$, and $<v_{as}>_k$ are the *k*-th harmonic voltage and current of the phase *a* of AC network, respectively.

4.2.1 Full-order DP Modelling

The AC distribution system is broken down into four parts as seen in Figure 4.5. Then the DP model consists of four parts as well. The AC network dynamics can be expressed in time-domain as

$$\begin{cases} L_s \dfrac{d}{dt} i_{as} + r_s i_{as} + v_{as} = e_{as} \\ \quad v_{as} = r_{s1}(i_{as} - i_{3as}) \end{cases}. \tag{3.26}$$

The subscript "*as*" denotes phase *a* variables stationary variables. Applying the GAM approach [25], the DP equation for the *k*-th order harmonics can be expressed as

$$L_s \frac{d}{dt}\langle i_{as}\rangle_k + (r_s + r_{s1} + \mathrm{j}k\omega_s L_s)\langle i_{as}\rangle_k - r_{s1}\langle i_{3as}\rangle_k = \langle e_{as}\rangle_k . \tag{3.27}$$

The T-circuit of transformer is modeled in time-domain as

$$\begin{cases} L_{l1} \dfrac{d}{dt} i_{1as} + r_1 i_{1as} + L_m \dfrac{d}{dt}(i_{1as} + i_{2as}) = v_{1as}, \\ L_{l2} \dfrac{d}{dt} i_{2as} + r_2 i_{2as} + L_m \dfrac{d}{dt}(i_{1as} + i_{2as}) = v_{2as}. \end{cases} \tag{3.28}$$

Similar to (4.14), applying the GAM approach to (4.15), the DP equations for the k th order harmonic variables of the transformer can be expressed as

$$\begin{cases} \langle v_{1as}\rangle_k = (L_{l1} + L_m)\left(\dfrac{d}{dt}\langle i_{1as}\rangle_k + \mathrm{j}k\omega_s\langle i_{1as}\rangle_k\right) + r_1\langle i_{1as}\rangle_k + L_m\left(\dfrac{d}{dt}\langle i_{2as}\rangle_k + \mathrm{j}k\omega_s\langle i_{2as}\rangle_k\right), \\ \langle v_{2as}\rangle_k = (L_{l2} + L_m)\left(\dfrac{d}{dt}\langle i_{2as}\rangle_k + \mathrm{j}k\omega_s\langle i_{2as}\rangle_k\right) + r_2\langle i_{2as}\rangle_k + L_m\left(\dfrac{d}{dt}\langle i_{1as}\rangle_k + \mathrm{j}k\omega_s\langle i_{1as}\rangle_k\right). \end{cases} \tag{3.29}$$

Since the secondary-side of transformer has Y-connection, its variables can be directly interfaced with the rectifier and the *RL* load, and can be modeled as

$$\begin{cases} v_{rec\_as} = v_{2as}, \quad i_{rec} = -i_{s2as} - i_{2as} \\ v_{rec\_as} = r_{s2} i_{s2as} + L_{s2} \cdot \dfrac{d}{dt} i_{s2as} \end{cases}. \tag{3.30}$$

Applying the GAM approach to (4.17), the DP equations for the k-th order harmonic variables of rectifier load can be expressed as

$$\begin{cases} \left\langle v_{rec\_as} \right\rangle_k = \left\langle v_{2as} \right\rangle_k, \quad \left\langle i_{rec\_as} \right\rangle_k = -\left\langle i_{s2as} \right\rangle_k - \left\langle i_{2as} \right\rangle_k \\ \left\langle v_{rec\_as} \right\rangle_k = r_{s2} \left\langle i_{s2as} \right\rangle_k + L_{s2} \cdot \left(\dfrac{d}{dt} \left\langle i_{s2as} \right\rangle_k + jk\omega_s \left\langle i_{s2as} \right\rangle_k \right) \end{cases}. \tag{3.31}$$

It is worth mentioning that since $\langle i_{as} \rangle_k$, $\langle v_{as} \rangle_k$, and $\langle e_{as} \rangle_k$ are vectors of complex variables, to facilitate operations using regular simulation programs, (4.14),(4.16), and (4.18) are decomposed into real and imaginary parts [67]. The model for the AC distribution system has been defined by (4.14), (4.16), and (4.18). The currents $\langle i_{rec\_as} \rangle_k$ are input to the rectifier model, and the voltages $\langle v_{rec\_as} \rangle_k$ coming out of the rectifier PDP model are the input to the AC distribution system model.

4.2.2 Reduced-order DP Modelling

In reduced-order PDP modeling technique [65], it is assumed that the system transients are dominated by the first-order DP (fundamental frequency components of variables), whereas the higher-order DPs (harmonic components of variables) dynamics may be neglected. Therefore, only the first-order DPs dynamics are formulated in differential equations, while the higher-order harmonic DPs are expressed by algebraic equations. In this way, the dynamics (state variables) from higher-order DPs are removed and are solved assuming quasi-steady-state conditions.

Following the reduced-order PDP approach [65], (4.14), (4.16) and (4.18) are kept unchanged for the fundamental frequency components, i.e., when k=1. Moreover, for $k>1$ (i.e., for harmonics

k=5, 7,…) the states are removed from (4.14), (4.16) and (4.18), yielding the algebraic equations as (4.20), (4.22), and (4.24) for ac network, transformer and rectifier load, respectively. The differential expressions of fundamental components are listed in (4.19), (4.21) and (4.23) for ac network, transformer and rectifier load, respectively.

$$L_s \frac{d}{dt}\langle i_{as}\rangle_1 + (r_s + r_{s1} + \mathrm{j}k\omega_s L_s)\langle i_{as}\rangle_1 - r_{s1}\langle i_{3as}\rangle_1 = \langle e_{as}\rangle_1, \tag{3.32}$$

$$(r_s + r_{s1} + \mathrm{j}k\omega_s L_s)\langle i_{as}\rangle_k - r_{s1}\langle i_{3as}\rangle_k = \langle e_{as}\rangle_k, k > 1; \tag{3.33}$$

$$\begin{cases} \langle v_{1as}\rangle_1 = (L_{l1} + L_m)\left(\frac{d}{dt}\langle i_{1as}\rangle_1 + \mathrm{j}k\omega_s\langle i_{1as}\rangle_1\right) + r_1\langle i_{1as}\rangle_1 + L_m\left(\frac{d}{dt}\langle i_{2as}\rangle_1 + \mathrm{j}k\omega_s\langle i_{2as}\rangle_1\right), \\ \langle v_{2as}\rangle_1 = (L_{l2} + L_m)\left(\frac{d}{dt}\langle i_{2as}\rangle_1 + \mathrm{j}k\omega_s\langle i_{2as}\rangle_1\right) + r_2\langle i_{2as}\rangle_1 + L_m\left(\frac{d}{dt}\langle i_{1as}\rangle_1 + \mathrm{j}k\omega_s\langle i_{1as}\rangle_1\right), \end{cases} \tag{3.34}$$

$$\begin{cases} \langle v_{1as}\rangle_k = (L_{l1} + L_m)\left(\mathrm{j}k\omega_s\langle i_{1as}\rangle_k\right) + r_1\langle i_{1as}\rangle_k + L_m\left(\mathrm{j}k\omega_s\langle i_{2as}\rangle_k\right), k > 1, \\ \langle v_{2as}\rangle_k = (L_{l2} + L_m)\left(\mathrm{j}k\omega_s\langle i_{2as}\rangle_k\right) + r_2\langle i_{2as}\rangle_k + L_m\left(\mathrm{j}k\omega_s\langle i_{1as}\rangle_k\right), k > 1. \end{cases} \tag{3.35}$$

$$\begin{cases} \langle v_{rec\_as}\rangle_1 = \langle v_{2as}\rangle_1, \langle i_{rec\_as}\rangle_1 = -\langle i_{s2as}\rangle_1 - \langle i_{2as}\rangle_1, \\ \langle v_{rec\_as}\rangle_1 = r_{s2}\langle i_{s2as}\rangle_1 + L_{s2}\cdot\left(\frac{d}{dt}\langle i_{s2as}\rangle_1 + jk\omega_s\langle i_{s2as}\rangle_1\right), \end{cases} \tag{3.36}$$

$$\begin{cases} \langle v_{rec\_as}\rangle_k = \langle v_{2as}\rangle_k, \langle i_{rec\_as}\rangle_k = -\langle i_{s2as}\rangle_k - \langle i_{2as}\rangle_k, k > 1, \\ \langle v_{rec\_as}\rangle_k = r_{s2}\langle i_{s2as}\rangle_k + L_{s2}\cdot jk\omega_s\langle i_{s2as}\rangle_k, k > 1. \end{cases} \tag{3.37}$$

4.3 Implementation

4.3.1 Constructing Parametric Functions of LCR

As for constructing the LCR parametric functions, it is noted that only 1st, 5th and 7th DP orders are considered here in the AC subsystem, while only 0th order DP is used for the DC subsystem. However, with its simple structure, the reduced-order PDP model can be readily augmented to include higher-order harmonics of interest, provided that dynamics if these harmonics are desired. In the parametric approach, the LCR is modeled through the relationship between the AC variables and DC variables. As recalled from Chapter 3, the parametric relationships representing the average behavior of the rectifier phase *a* are

$$\left|\langle v_{as}\rangle_k\right| = \alpha_k(z)\left|\langle v_{dc}\rangle_0\right|, k \in \{1,5,7\}; \tag{3.38}$$

$$\left|\langle i_{dc}\rangle_0\right| = \beta_0(z)\left|\langle i_{as}\rangle_1\right|; \tag{3.39}$$

$$\varphi_k(z) = \text{ang}(\langle v_{as}\rangle_k) - \text{ang}(\langle i_{as}\rangle_1), k \in \{1,5,7\}. \tag{3.40}$$

$$z = \frac{\left|\langle v_{dc}\rangle_0\right|}{\left|\langle i_{as}\rangle_1\right|}. \tag{3.41}$$

In this section, only phase *a* is presented for compactness. The numerically extracted parametric functions are depicted in Figure 4.8 and Figure 4.9. All these data are stored and tabulated in look-up table in Matlab/Simulink for the future use.

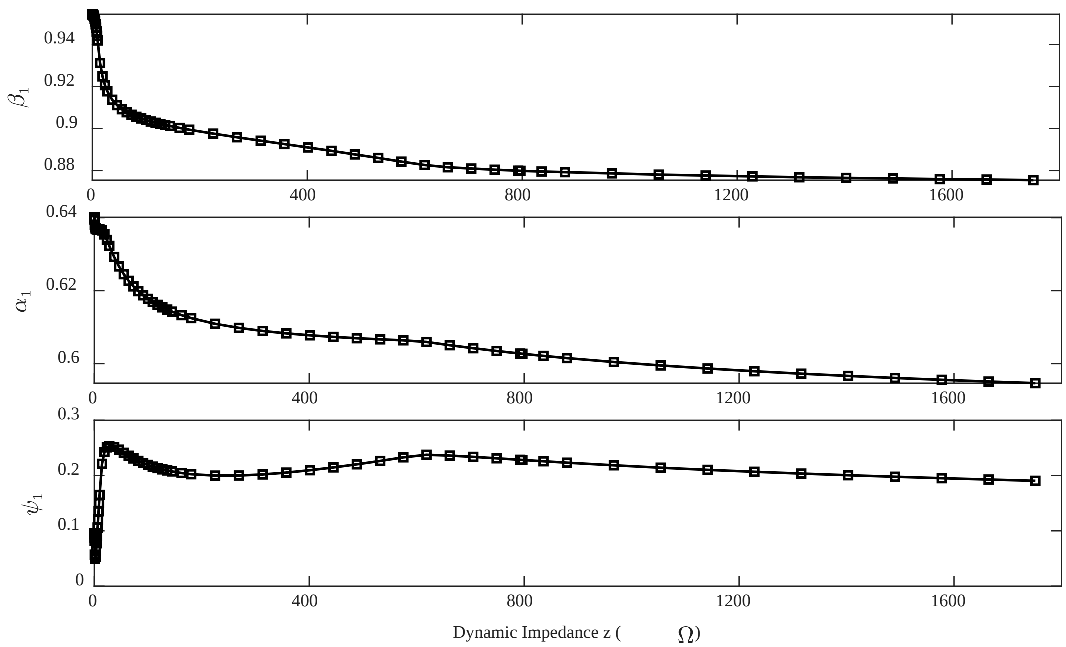

Figure 4. 8 Parametric functions $\alpha_1(z)$, $\beta_1(z)$, $\varphi_1(z)$ extracted from detailed simulations using MSS approach.

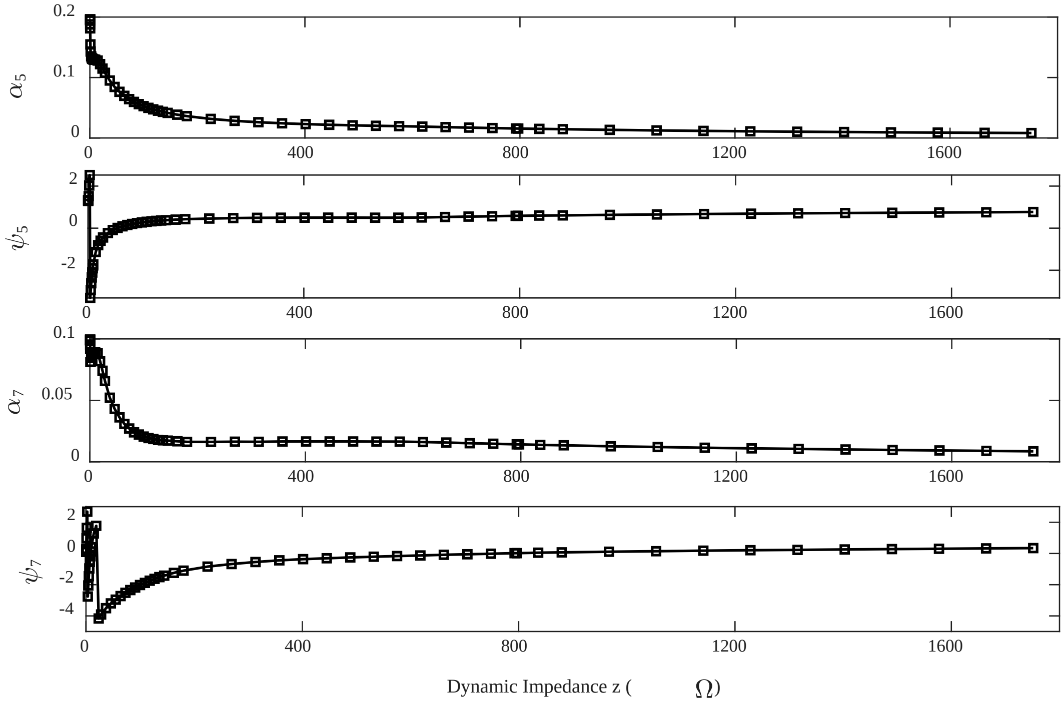

Figure 4. 9 Parametric functions $\alpha_{5,7}$(z), $\varphi_{5,7}$(z) extracted from detailed simulations using MSS approach.

4.3.2 Subsystem Interface and Implementation

For comparison, the implementation of full-order model for the single-phase equivalent circuit of the considered AC distribution system with rectifier load, shown in Figure 4.7, is depicted in Figure 4.10. The model has three parts composing the overall system: the AC system consisting of differential equations (4.14), (4.16), (4.18); the LCR system; and the DC system. Since only 0 th order component is included in DC system, the 0 th GAM-Type DP, in effect, degrades to the dynamic averaging in time-domain, as illustrated in (3.16) and (3.17).

The implementation of reduced-order model is illustrated in Figure 4.11. Since differential equations are removed from modelling the harmonic components, an algebraic loop is created by the algebraic variables $<i_{3as}>_k$, $<i_{2as}>_k$. Therefore, for the purpose of implementation in this thesis unit delays are added to break this implicit relationship and speeding up the simulation. In addition,

Figure 3.4 in Chapter 3 illustrates the interconnections between the AC and DC subsystems and the LCR model.

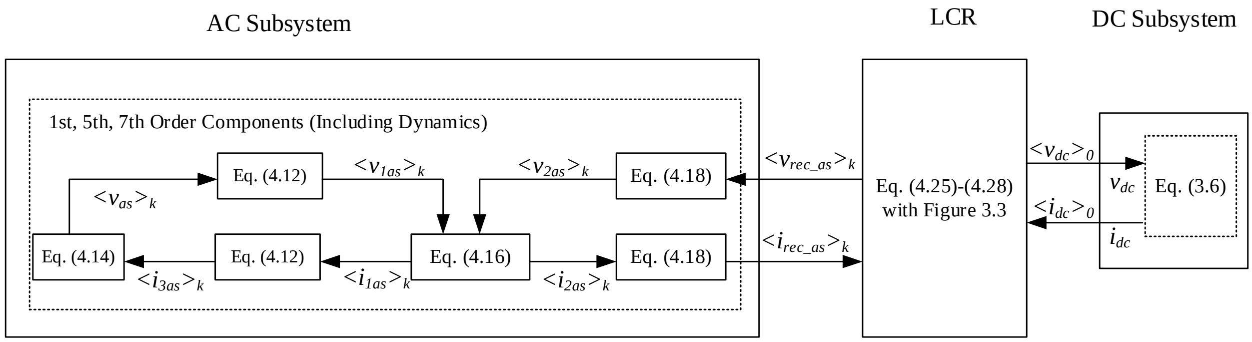

Figure 4. 10 Implementation of the full-order PDP of the AC distribution system with rectifier loads.

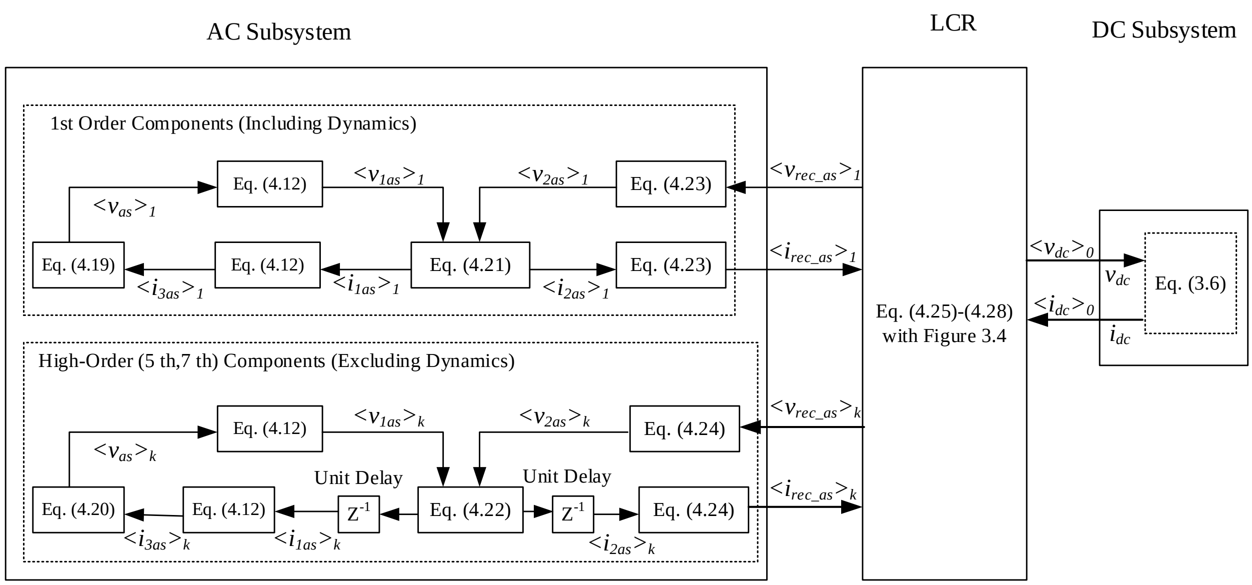

Figure 4. 11 Implementation of the reduced-order PDP of AC distribution system with rectifier loads.

The difference between the two models lay in the AC subsystem. In the reduced-order model, the AC subsystem is modelled using DAEs (4.19)-(4.24). It is noted though no algebraic loop exists in full-order model. But in this case, the simulation slows down due to dynamics of the high-order components requiring smaller time steps.

4.4 Computer Studies

To verify the reduced-order PDP model and compare its numerical performance with the full-order PDP, the subject models have been implemented in MATLAB/Simulink [32] considering 5 th and 7 th harmonics. The computer studies are carried out on the generic AC distribution system with rectifier load shown in Figure 4.6. In addition, the switching detailed model of the system is implemented using PLECS Blockset [33] in MATLAB/Simulink and is used to produce the reference solution.

A transient computer study spanning various operating conditions is selected, transiting from light load in DCM to high load in CCM-1 and to heavy load in CCM-2. In the following study, the system initially operates in DCM with a DC load of 950Ω. At t = 3s, the DC load is changed to 21Ω; and at t = 6s, the DC load is further changed to 3Ω; and the simulation runs until t = 10s. For consistency, all case studies are conducted on a PC with a 3.4GHz Intel i7-2600 CPU.

4.4.1 Steady State Analysis

To evaluate the properties of subject models to capture harmonics, it is instructive to first study their performance in steady state at different operation modes. Here, only phase a and DC voltages and currents are depicted in Figure 4.12 (DCM) and Figure 4.14 (CCM-1). The corresponding harmonic contents are displayed in Figure 4.13 and Figure 4.15 respectively. As can be seen in Figure 4.12and Figure 4.14, both PDP model and reduced-order PDP model produce similar accuracy of prediction at two different operation modes. It is also observed that the PDP model and reduced-order PDP model is capable of predicting ac system performance matching well to detailed model.

To provide a comprehensive insight into the accuracy of prediction by the subject models, the extracted harmonic contents of phase *a* current and voltage in DCM and CCM-1 are illustrated in Figure 4.13 and Figure 4.15, respectively. The PDP model and the reduced-order PDP model capture not only the fundamental component, but also the harmonic components under DCM and CCM-1 operation conditions. The harmonic contents analysis is carried out at both primary side and secondary side of the transformer, showcasing good prediction of each harmonic at two sides of the transformer by the PDP model and the reduced-order PDP model.

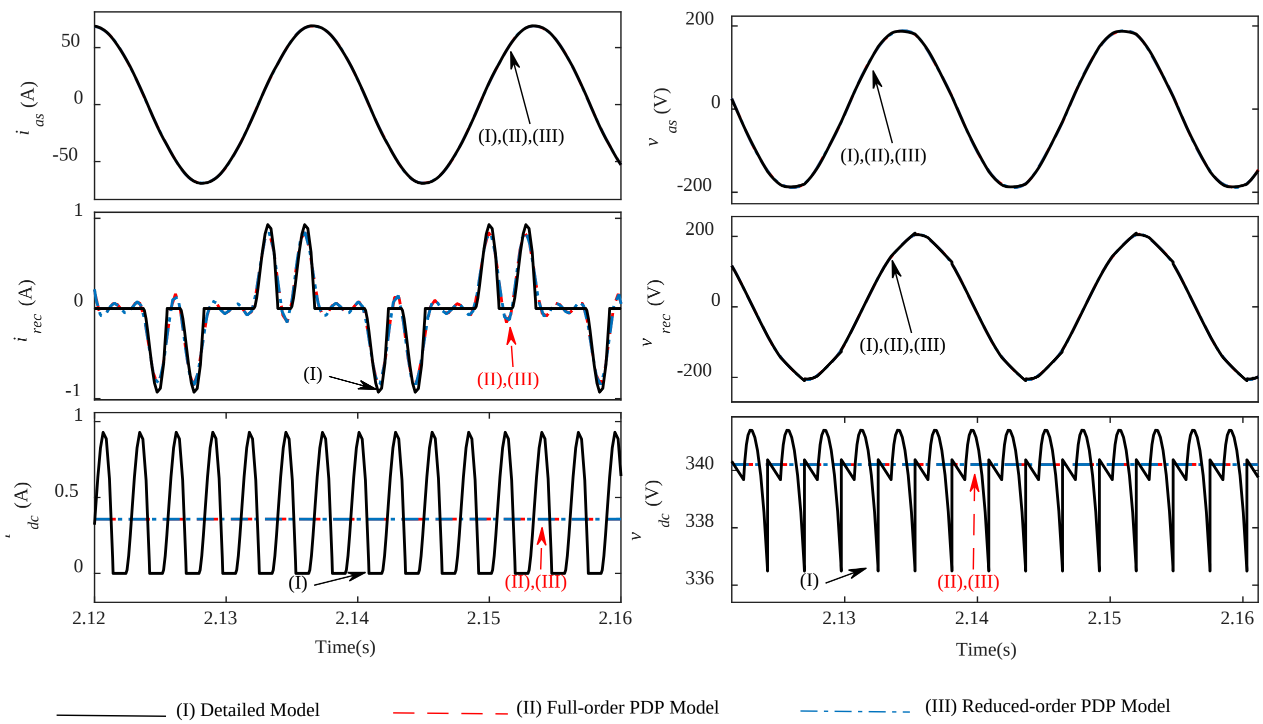

Figure 4. 12 The AC and DC subsystems variables for steady state in DCM.

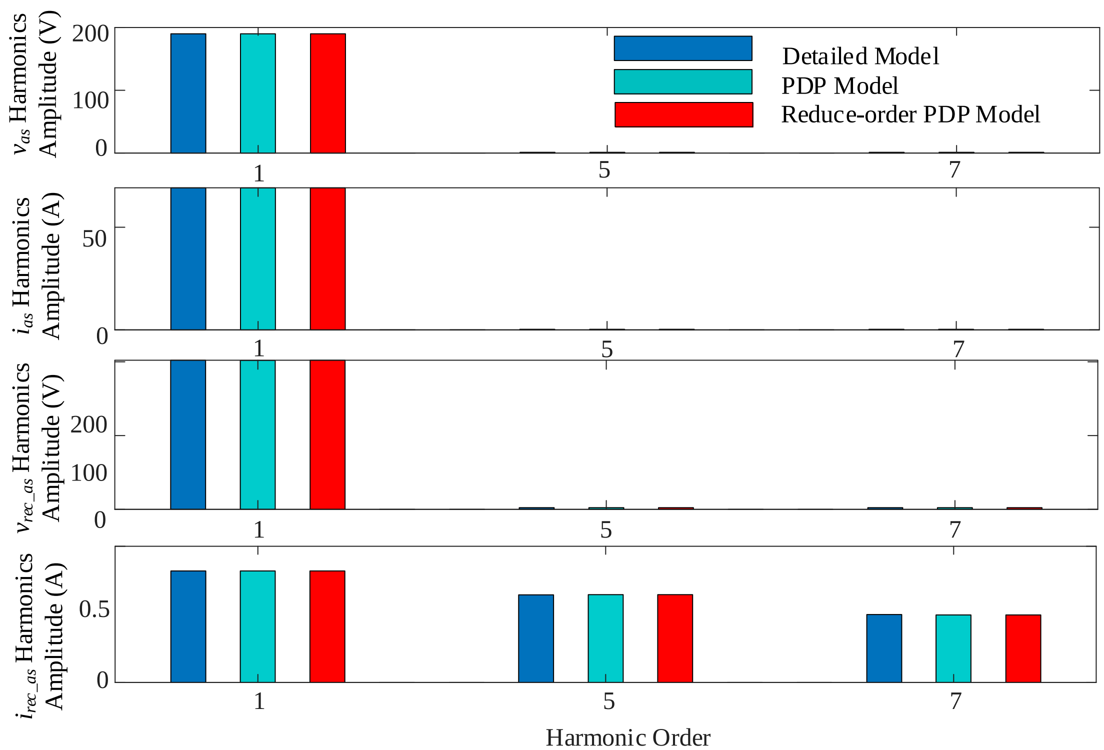

Figure 4. 12 Harmonic content analysis of phase *a* current and voltage for subject models in DCM.

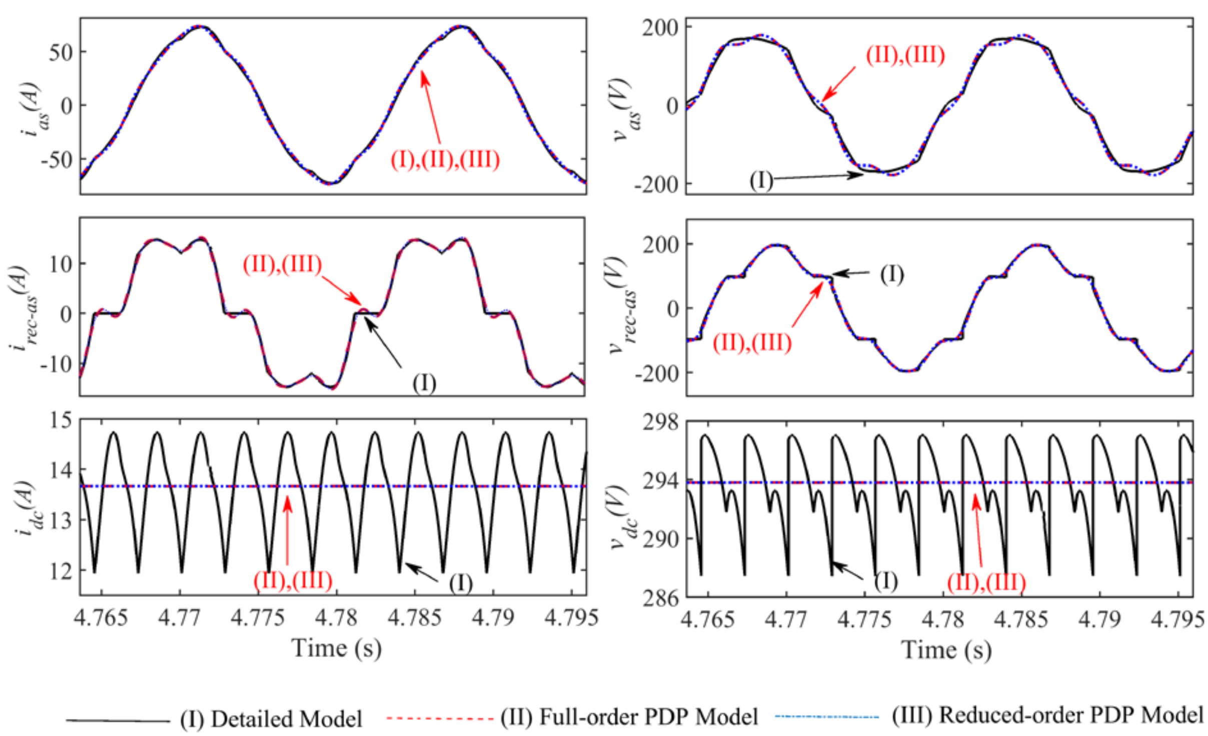

Figure 4. 13 The AC and DC subsystems variables for steady state in CCM-1.

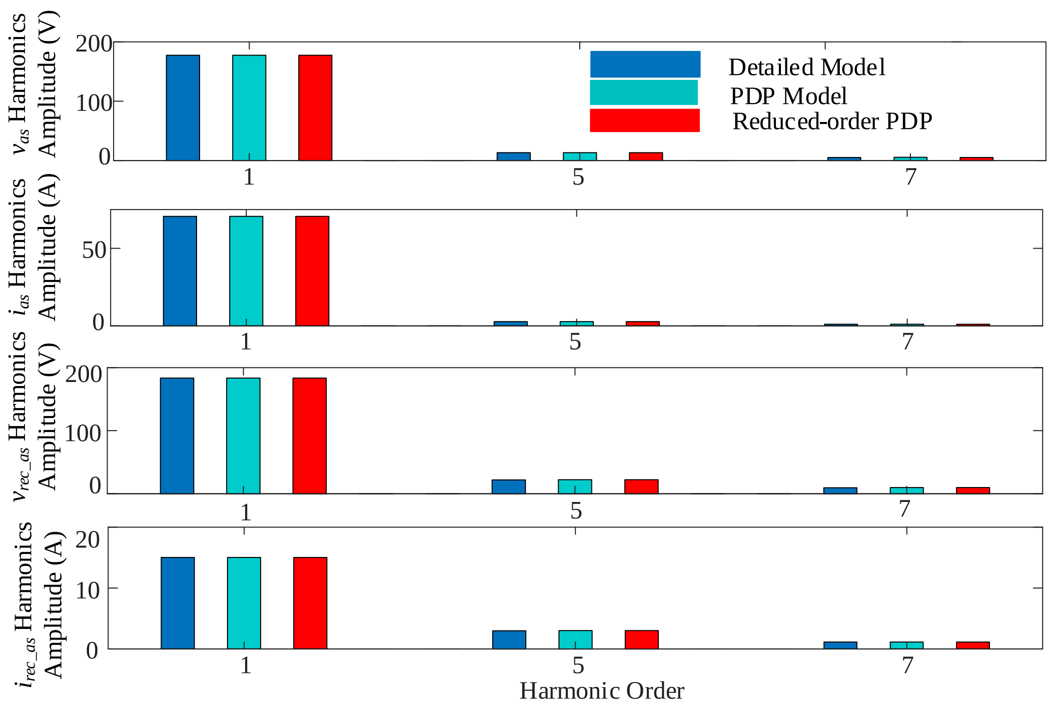

Figure 4. 14 Harmonic content analysis of phase a current and voltage for the subject models in CCM-1.

4.4.2 Large Signal Transient Response

Fragments of study shown in Figure 4.16 and 4.17 illustrate the transient response predicted by the subject models during the load changes. As shown in Figure 4.16 and Figure 4.17, the PDP model and the reduced-order PDP model can trace the dynamics of mode changes from DCM to CCM-1 and to CCM-2 very well. Therefore, it is proven that the transient response predictions by both full PDP model and reduced-order PDP model are highly consistent with the detailed model. Noticeably, the reduced-order PDP model has almost identical performance to the PDP model, which confirms the validation of the algebraic expressions for the harmonic components.

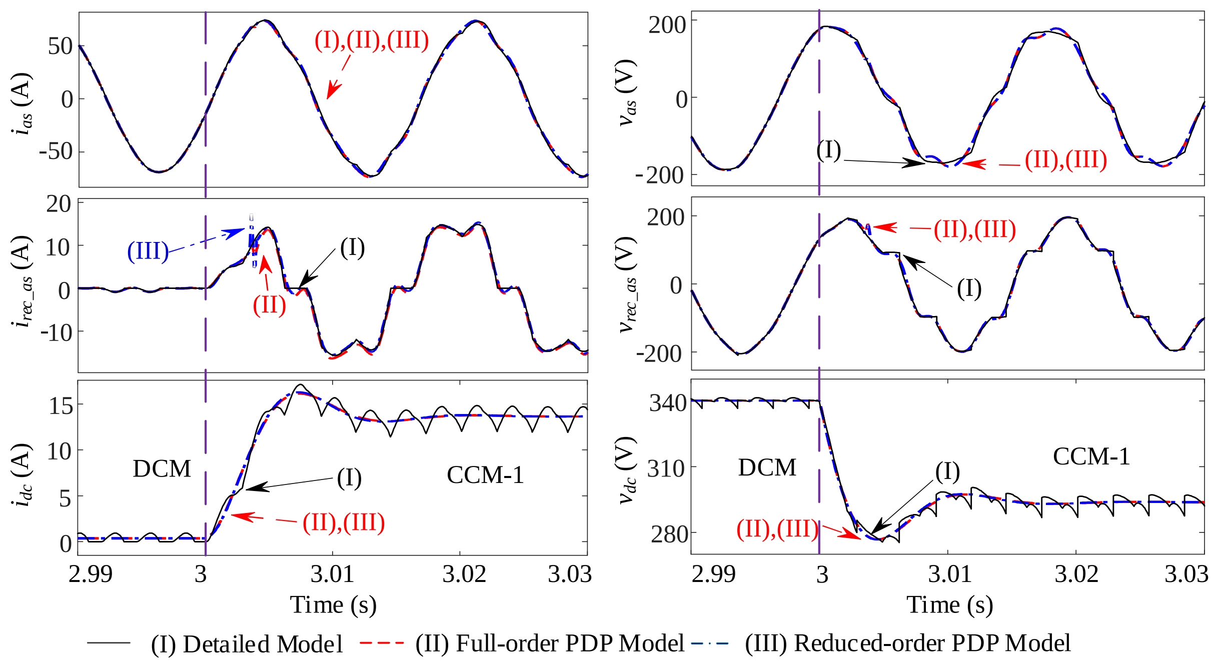

Figure 4. 15 Transient response of AC and DC variables during the transition DCM to CCM-1 modes as predicted by subject models.

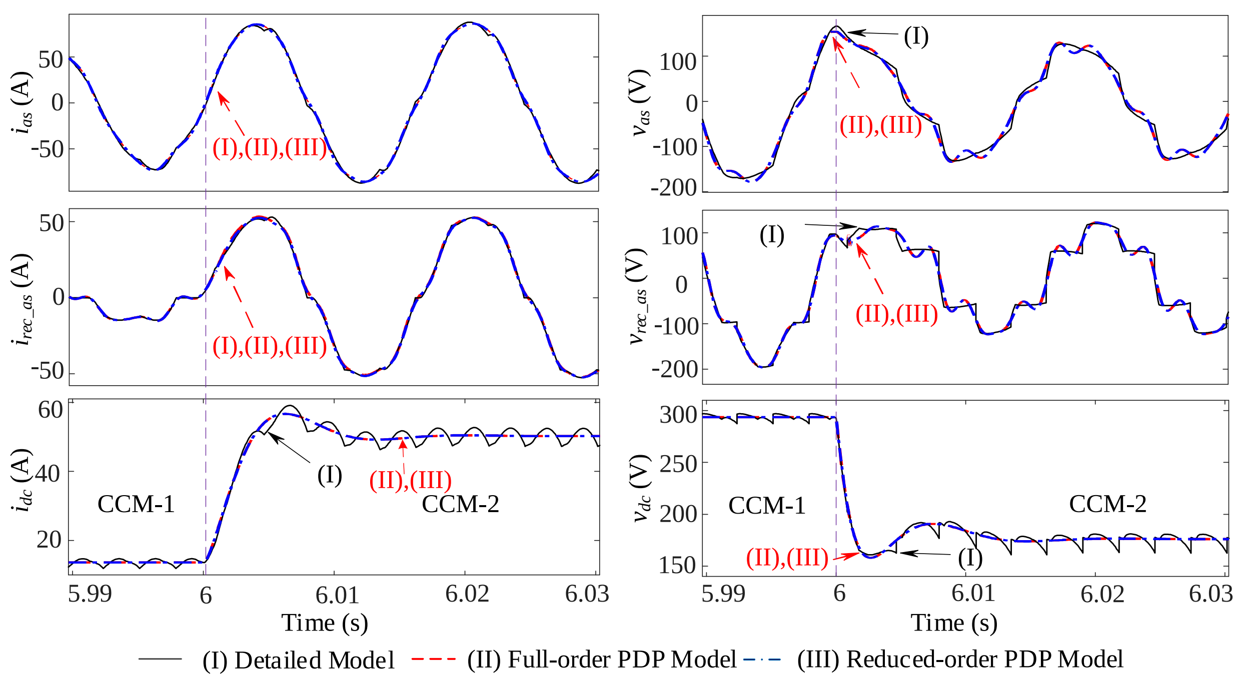

Figure 4. 16 Transient response of AC and DC variables during the transition from CCM-1 to CCM-2 mode as predicted by subject models.

4.4.3 Numerical Efficiency Analysis

To give a comprehensive comparison of the numerical efficiency, the performance of the subject models is evaluated in flexible time step studies. In the variable-step study, the two PDP models and the detailed model are executed for 10s using the ode23tb solver with max step size set to 5ms, and relative and absolute tolerances set to 1e-3, respectively. The time step sizes chosen during the simulation by the subject models are demonstrated in Figure 4.18. It is seen that the reduced-order PDP model permits largest time step size among all subject models, where it can execute at specified maximum time step size during the steady state. When the load change happens, the reduced-order model is also capable of reaching steady state quickly using comparably large steps.

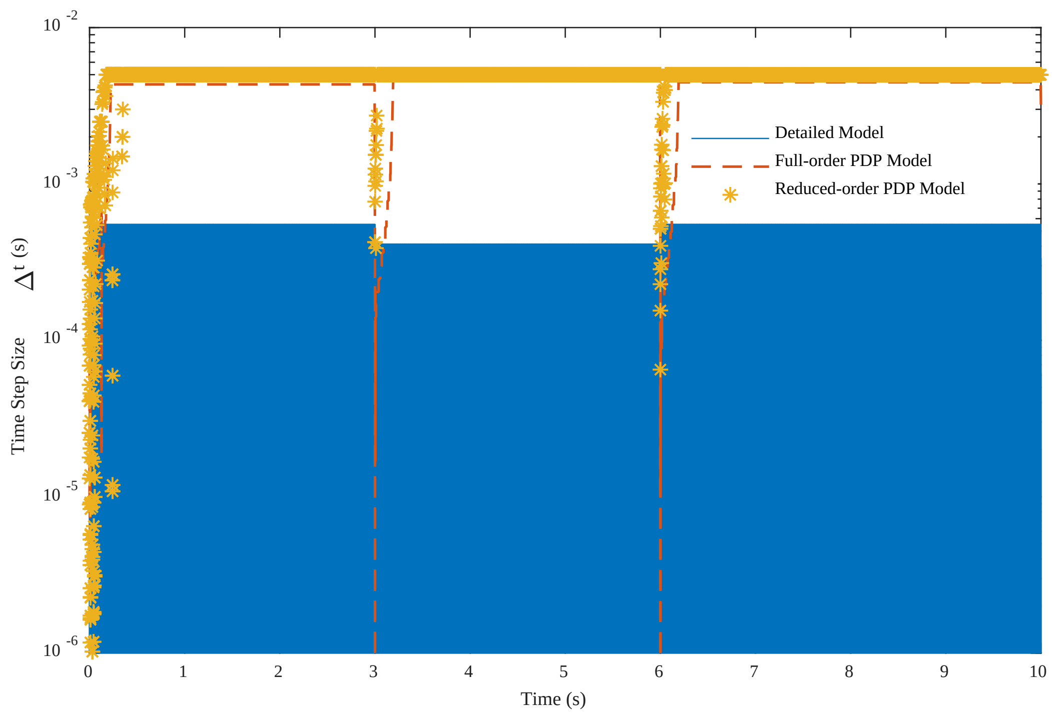

Figure 4. 17 Simulation step size taken by three subject models solved using variable-step solver in transient study.

The numerical statistics for the transient study shown in Figure 4.18 are summarized in Table 4.1, which includes the total CPU time, the total number of steps, and the average time step used by each model. As shown in Table 4.1, the detailed model uses the largest number of time steps (48,644) and consumes the most time to execute (9.14s). The full PDP model is demonstrated with superior numerical efficiency in terms of fewer time steps and less CPU time (4,049 and 1.62s, respectively). Moreover, using a combination of differential and algebraic equations to represent the DPs, the proposed reduced-order PDP model speeds up simulation by using even smaller number of time steps (2,312) and the least computation cost (0.95s). Additionally, since the reduced-order PDP model formulates transients in fundamental component only and assumes quasi steady states for harmonics, it results in much higher average time step than the full PDP model (4325.26μs vs. 2469.75μs), as shown in the last column in Table 4.1.

Table 4. 1 Numerical efficiency of the subject Models for variable time step study of 10 seconds.

Model	No. of Time Steps	Total CPU Time, s	Average Time Step, μs
Detailed Model	48644	9.14	205.58
Full-Order PDP	4049	1.62	2469.75
Reduced-Order PDP	2312	0.95	4325.26

Chapter 5: Reduced-order PDP Modelling of SM-Rectifier System with Prediction of DC Ripples

This chapter presents a numerically efficient reduced-order PDP model for integrated SM-rectifier system with more accurate prediction of DC ripples. Unlike previous cases, this chapter considers the DC ripples which is achieved through a set of additional parametric functions. The DC subsystem is modelled to accommodate any high-order component using the GAM-Type DPs solution. Next, the reduced-order dynamic phasor modelling technique is applied to CP-VBR model of the synchronous machine. The case studies in conjunction with error and efficiency analysis are presented to highlight the superior combination of numerical accuracy and efficiency of the proposed model.

A generic SM-rectifier system is considered in this chapter as depicted in Figure 5.1. To reduce DC ripples, an *LC* filter is usually added between rectifier and DC system. Without loss of generality, motor sign convention is used, and all parameters are referred to the stator side. It is assumed that the machine is magnetically linear, and that the *q*-axis leads the *d*-axis by 90 degrees [42].

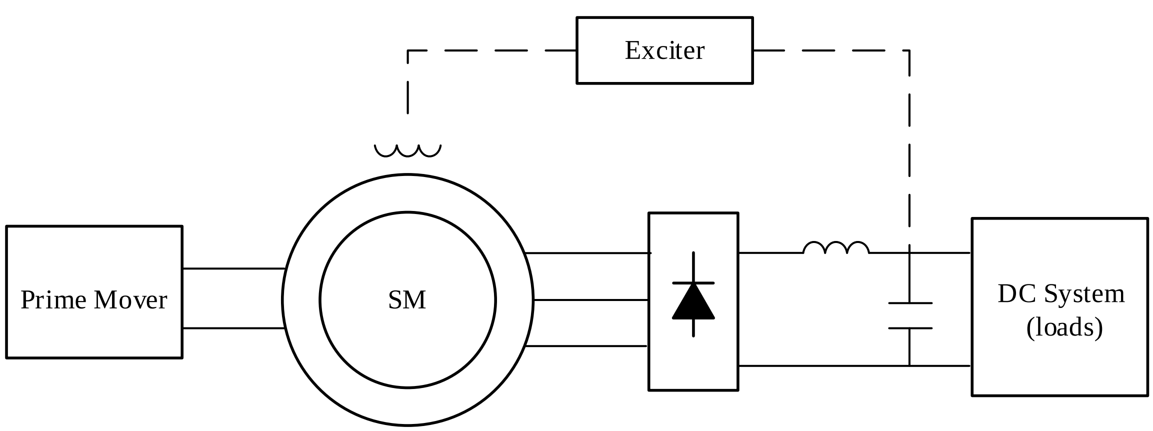

Figure 5. 1 The generic SM-rectifier system.

For the purpose of modelling, the synchronous machine represented here by its constant-parameter voltage-behind-reactance (CP-VBR) model [45]-[49] is directly interfaced with a line-commutated diode rectifier. The equivalent circuit of SM-rectifier system is illustrated in Figure 5.2 to set the stage for following discussion and modelling.

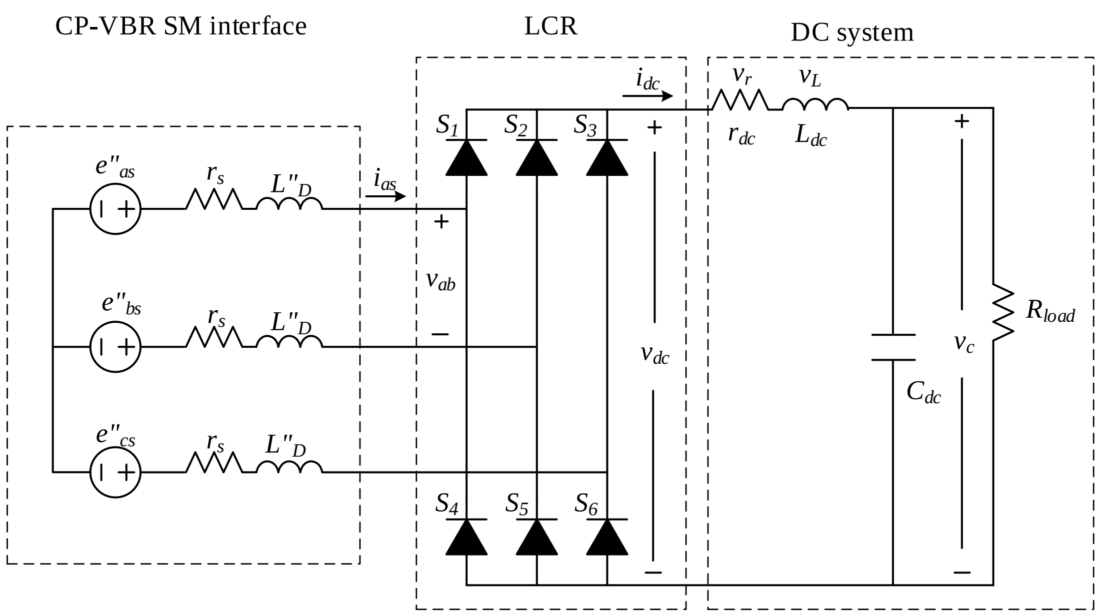

Figure 5. 2 Circuit diagram of SM-rectifier system.

5.1 DP Modelling of SM Based on CP-VBR

5.1.1 CP-VBR Model of SM in Time-Domain

The conventional Park's equivalent circuit of synchronous machine assumes that an arbitrary number of damper windings are represented in the q- and d-axes. For the purpose of modelling, all rotor windings are referred to the stator side using turns ratio [46]. Although Park's conventional representation of synchronous machine in qd coordinates is very widely used in simulation programs, it makes hard to directly interface with power electronics due to transformed stator variables [46]. Therefore, it is more convenient to represent the synchronous machine in terms of physical variables in order to achieve a direct interface between the machine and power electronics. The voltage-behind-reactance methodology has been developed which results in an interfacing stator circuit in physical variables in *abc* phase coordinates, while it represents the rotor circuits in *qd* variables. In the original VBR model [45], the inductances of the stator interfacing circuit are also rotor-position-dependent due to dynamic saliency of the rotor and the fact that the subtransient magnetizing inductance L''_{md} and L''_{mq} are not equal. In the recent literature, there have been several approaches to achieve a constant-parameter stator interfacing circuit by imposing the equality condition on subtransient magnetizing inductance L''_{md} and L''_{mq} [46], [47], [49]. Without loss of generality, in order to achieve the constant-parameter interfacing circuit in this thesis (as assumed in Figure 5.2), an approach based on adding an artificial damper winding in *q*-axis in considered here [49]. In addition, the resistance of this extra winding should be sufficiently large in order not to affect the machine's operational impedance at low frequencies. Therefore, the added leakage inductance of this added winding denoted by (M+1) is calculated as

$$L_{lkq(M+1)} = \left[\frac{1}{L''_{md}} - \frac{1}{L''_{mq}} \right]^{-1}. \tag{4.1}$$

Herein, $L_{\mathrm{lkq(M+1)}}$ represents the leakage inductance of the extra damper winding. Thus, the desired result is given as

$$L'''_{mq} = L''_{md} \tag{4.2}$$

where a triple-prime sign (''') being used to distinguish the subtransient quantities of the approximate model [47], and L'''_{mq} is defined as the new subtransient magnetizing inductance in *q*-

axis. As a consequence, a constant interfacing inductance matrix can be achieved. The final stator branch interfacing equation with constant-parameter in VBR has the following form

$$\mathbf{v}_{abcs} = \mathbf{R}_s \mathbf{i}_{abcs} + \mathbf{L}_D^{''} \frac{d}{dt} \mathbf{i}_{abcs} + \mathbf{e}_{abcs}^{''} \tag{4.3}$$

where $\mathbf{v}_{abcs}$ and $\mathbf{i}_{abcs}$ are the three-phase stator voltage and current vectors, respectively; and stator resistance matrix $\mathbf{R}_s$ and subtransient stator inductance matrix $\mathbf{L}_D^{''}$ are defined as

$$\mathbf{R}_s = diag(r_s, r_s, r_s) \ , \ \ \mathbf{L}_D^{''} = diag(L_D^{''}, L_D^{''}, L_D^{''}). \tag{4.4}$$

Herein,

$$L_D^{''} = L_{ls} + L_{md}^{''}. \tag{4.5}$$

The subtransient inductances $L_{md}^{''}$ and $L_{mq}^{'''}$ are defined as

$$L_{mq}^{'''} = L_{md}^{''} = \left[\frac{1}{L_{md}} + \frac{1}{L_{lfd}} + \sum_{j=1}^{N} \frac{1}{L_{lkdj}} \right]^{-1}. \tag{4.6}$$

Finally, the subtransient voltages $\mathbf{e}_{abcs}^{''}$ are

$$\mathbf{e}_{abcs}^{''} = \left[\mathbf{K}_s^r \right]^{-1} \left[e_q^{''} \quad e_d^{''} \quad 0 \right]^T, \tag{4.7}$$

where

$$e_q^{''} = \omega_r \lambda_d^{''} + \sum_{j=1}^{M+1} \left(\frac{L_{mq}^{'''} r_{kqj}}{L_{lkqj}^2} (\lambda_q^{''} - \lambda_{kqj}) \right) + \left(\sum_{j=1}^{M+1} \frac{r_{kqj}}{L_{lkqj}^2} \right) L_{mq}^{'''2} i_{qs}, \tag{4.8}$$

$$e_d^{''} = -\omega_r \lambda_q^{''} + \sum_{j=1}^{N} \left(\frac{L_{md}^{''} r_{kdj}}{L_{lkdj}^2} (\lambda_d^{''} - \lambda_{kdj}) \right) + \left(\frac{r_{fd}}{L_{lkd}^2} + \sum_{j=1}^{N} \frac{r_{kdj}}{L_{lkdj}^2} \right) L_{md}^{''2} i_{ds} + \frac{L_{md}^{''} v_{fd}}{L_{lfd}} + \frac{L_{md}^{''} r_{fd}}{L_{lfd}^2} (\lambda_d^{''} - \lambda_{fd}). \tag{4.9}$$

The subtransient flux linkages are defined as

$$\lambda_q^{''} = L_{mq}^{'''} \left(\sum_{j=1}^{M+1} \frac{\lambda_{kqj}}{L_{lkqj}} \right), \lambda_d^{''} = L_{md}^{''} \left(\frac{\lambda_{fd}}{L_{lfd}} + \sum_{j=1}^{N} \frac{\lambda_{kdj}}{L_{lkdj}} \right), \tag{4.10}$$

and magnetizing flux linkages are

$$\lambda_{mq} = L_{mq}^{'''} i_{qs} + \lambda_q^{''}, \lambda_{md} = L_{md}^{''} i_{ds} + \lambda_d^{''}. \tag{4.11}$$

The rotor flux linkages are expressed by following state equations,

$$\begin{aligned} \frac{d}{dt}\lambda_{kqj} &= -\frac{r_{kqj}}{L_{lkqj}}(\lambda_{kqj} - \lambda_{mq}); \; j = 1, 2, ..., M, M+1, \\ \frac{d}{dt}\lambda_{kdj} &= -\frac{r_{kdj}}{L_{lkdj}}(\lambda_{kdj} - \lambda_{md}); \; j = 1, 2, ..., N, \\ \frac{d}{dt}\lambda_{fd} &= -\frac{r_{fd}}{L_{lfd}}(\lambda_{fd} - \lambda_{md}) + v_{fd}. \end{aligned} \tag{4.12}$$

Here, M denotes number of damper windings in the q-axis, and N denotes number of damper windings in the d-axis. Finally, the electromagnetic torque can be calculated using magnetizing fluxes as

$$T_e = \frac{3P}{4}(\lambda_{mq} i_{qs} - \lambda_{md} i_{ds}). \tag{4.13}$$

So, the time-domain CP-VBR model of synchronous machine is fully defined by (5.3) for stator interfacing, (5.8)-(5.9) for subtransient voltages, (5.10)-(5.12) for flux linkages equations, (5.1) for saliency approximation, and (5.13) for electromagnetic torque.

5.1.2 GAM-Type DP Modelling of SM Based on CP-VBR

Assuming machine stator windings are sinusoidally distributed, the synchronous machine is expected to generate sinusoidal distributed air gap fluxes and sinusoidal emf's [42]. In such a case, a synchronous machine can be viewed as a power source with only fundamental frequency (60Hz).

For this reason, only first-order DP of subtransient voltage source is considered when deriving the GAM-type DP VBR model.

5.1.2.1 Full-order DP Model

Applying the GAM-type DPs technique to stator interfacing equation (5.3), the dynamic phasor model is yielded as

$$\begin{cases} \langle \mathbf{V}_{abcs} \rangle_1 = (\mathbf{R}_s + jk\omega_s \mathbf{L}_D^{"}) \cdot \langle \mathbf{I}_{abcs} \rangle_1 + \mathbf{L}_D^{"} \dfrac{d}{dt} \langle \mathbf{I}_{abcs} \rangle_1 + \langle \mathbf{E}_{abcs}^{"} \rangle_1 , \\ \langle \mathbf{V}_{abcs} \rangle_k = (\mathbf{R}_s + jk\omega_s \mathbf{L}_D^{"}) \cdot \langle \mathbf{I}_{abcs} \rangle_k + \mathbf{L}_D^{"} \dfrac{d}{dt} \langle \mathbf{I}_{abcs} \rangle_k , k = \{5, 7\}. \end{cases} \tag{4.14}$$

Herein, $<\mathbf{V}_{abcs}>_1$ and $<\mathbf{I}_{abcs}>_1$ are 1st order DPs of stator voltages and currents, respectively; $<\mathbf{V}_{abcs}>_k$ and $<\mathbf{I}_{abcs}>_k$ are kth order DPs of stator voltages and currents respectively. Besides the fundamental components, only 5th and 7th order harmonics may be dominant in synchronous machine rectifier systems [69]. As shown in the literature [6], 1st order DP of subtransient voltage source $\langle \mathbf{E}_{abcs}^{"} \rangle_1$ is obtained through

$$\langle \mathbf{E}_{abcs}^{"} \rangle_1 = \left[\mathbf{K}_{u,qdr}^{U,abc} \right] \left[e_q^{"} \quad e_d^{"} \right]^T , \tag{4.15}$$

where

$$\left[\mathbf{K}_{u,qdr}^{U,abc} \right] = \frac{1}{2} \begin{bmatrix} e^{j(\theta_r - \omega_s t)} & e^{j(\theta_r - \frac{\pi}{2} - \omega_s t)} \\ e^{j(\theta_r - \frac{2\pi}{3} - \omega_s t)} & e^{j(\theta_r - \frac{\pi}{2} - \frac{2\pi}{3} - \omega_s t)} \\ e^{j(\theta_r + \frac{2\pi}{3} - \omega_s t)} & e^{j(\theta_r - \frac{\pi}{2} + \frac{2\pi}{3} - \omega_s t)} \end{bmatrix}. \tag{4.16}$$

Due to slowly changing rotor variables even during electromechanical transients, these variables are kept in time-domain as in (5.7)-(5.12) [6]. In order to compute the rotor equations and the electromagnetic torque, the DP variables from stator branches are transformed to time-domain qd-coordinates, i.e., from $\mathbf{F}_{abcs}$ to $\mathbf{f}_{qd0s}$ ($f=\{v,i\}$). This process can be fulfilled by combining (2.20) and Park's transformation, as follows

$$\mathbf{f}_{qd0s} = 2 \cdot \mathbf{K}_s^r \cdot \mathrm{Re}\left[\sum_{k=K} \langle \mathbf{F}_{abcs} \rangle_k (t) e^{\mathrm{j}k\omega_s t} \right]. \tag{4.17}$$

In summary, the full-order constant-parameter model based on GAM (herein referred to as CP-GAM) consists of stator interfacing equations (5.14)-(5.17), subtransient voltages (5.8)-(5.9), flux linkages equations (5.10)-(5.12), saliency approximation (5.1), and electromagnetic torque (5.13).

5.1.2.2 Reduced-order DP Model

As discussed in Chapters 3 and 4, the reduced-order DP modeling technique assumes that the system transients are dominated by the first-order DP (fundamental components of variables), whereas the transients from high-order DPs (harmonic components of variables) may be neglected [65]. Therefore, the first-order components are formulated by differential equations, while the high-order components are expressed by algebraic equations. Hereby, the GAM-type DPs of stator interfacing equation are simplified as below

$$\langle \mathbf{V}_{abcs} \rangle_1 = (\mathbf{R}_s + jk\omega_s \mathbf{L}_D^{"}) \cdot \langle \mathbf{I}_{abcs} \rangle_1 + \mathbf{L}_D^{"} \frac{d}{dt} \langle \mathbf{I}_{abcs} \rangle_1 + \langle \mathbf{E}_{abcs}^{"} \rangle_1 , \tag{4.18}$$

$$\langle \mathbf{V}_{abcs} \rangle_k = (\mathbf{R}_s + jk\omega_s \mathbf{L}_D^{"}) \cdot \langle \mathbf{I}_{abcs} \rangle_k , k = \{5,7\}. \tag{4.19}$$

The first-order DP of the stator equation defines the state equation, while high-order DPs are changed to algebraic equations by eliminating high-order dynamics. In consequence, the number of state variables is reduced, thus saving computations.

5.2 Parametric DP Modelling of LCRs Considering DC Ripples

As addressed in Chapter 3, a wide range of operating conditions of LCR can be modeled by a set of parametric functions with regard to dynamic impedance, relating AC variables to DC variables in dynamic phasor representation. However, in Chapter 3, the DC subsystem has been assumed as ideal without any harmonics. In practice, the 6th and 12th harmonics are commonly found in DC side variables as the corresponding ripple.

Assuming a symmetrical AC system, the parametric relationships representing the average behavior of rectifier for phase *a* in DPs are obtained as

$$\begin{cases} \langle v_{as} \rangle_k = \alpha_k(\cdot)\left|\langle v_{dc} \rangle_0\right| e^{\mathrm{j}(\mathrm{ang}(\langle i_{as} \rangle_1)+\varphi_k)} \\ \langle v_{as} \rangle_k = \langle v_{bs} \rangle_k e^{\mathrm{j}(\frac{2k\pi}{3})} = \langle v_{cs} \rangle_k e^{\mathrm{j}(\frac{-2k\pi}{3})} \end{cases}, k \in K. \tag{4.20}$$

Here, the DPs for phase *b* and phase *c* are obtained by a phase shift of ±2*k*π/3, respectively. The 0th order DPs on the DC side are established as

$$\begin{cases} \left|\langle i_{dc} \rangle_0\right| = \beta_0(\cdot)\left|\langle i_{as} \rangle_1\right| \\ \langle i_{dc} \rangle_0 = \left|\langle i_{dc} \rangle_0\right| \end{cases}. \tag{4.21}$$

With harmonics considered in DC side, the DPs for high-order component in DC side are established as

$$\left|\langle i_{dc} \rangle_{k_{dc}}\right| = \beta_{k_{dc}}(\cdot)\left|\langle i_{as} \rangle_1\right|, k_{dc} = K_{dc}. \tag{4.22}$$

The phase angle of harmonic currents on DC side are established as

$$\varphi_{k_{dc}}(\cdot) = \mathrm{ang}(\langle i_{dc} \rangle_{k_{dc}}) - \mathrm{ang}(\langle i_{as} \rangle_1), k_{dc} \in K_{dc}. \tag{4.23}$$

Here, the angle of $<i_{as}>_1$ selected as the reference angle for the AC variables, and it is also used as the reference for DC side variables as well. Combing (5.21), (5.22) and (5.23), the DC DPs can be obtained as

$$\begin{cases} \langle i_{dc} \rangle_0 = \left| \langle i_{dc} \rangle_0 \right| = \beta_0(\cdot) \left| \langle i_{as} \rangle_1 \right| \\ \langle i_{dc} \rangle_{k_{dc}} = \beta_{k_{dc}}(\cdot) \left| \langle i_{as} \rangle_1 \right| e^{\mathrm{j}(\mathrm{ang}(\langle i_{as} \rangle_1) + \varphi_{k_{dc}})}, k_{dc} \in K_{dc} \end{cases}. \tag{4.24}$$

In (5.20)-(5.24), the parametric functions $\alpha_k(\cdot)$, $\beta_{k_{dc}}(\cdot)$,$\varphi_k(\cdot)$ and $\varphi_{k_{dc}}(\cdot)$ are dependent on the loading conditions of the LCR system. The set K={1, 5, 7} denotes the selected AC harmonics of interest, while the set K_{dc}={6, 12} denotes the selected DC harmonics of interest, respectively. The $\alpha_k(\cdot)$, $\beta_{k_{dc}}(\cdot)$,$\varphi_k(\cdot)$ and $\varphi_{k_{dc}}(\cdot)$ are obtained as functions of a so-called dynamic impedance z defined as defined in terms of DC and fundamental components as [6]

$$z = \frac{\left| \langle v_{dc} \rangle_0 \right|}{\left| \langle i_{as} \rangle_1 \right|}. \tag{4.25}$$

The methods of obtaining parametric functions can be found in [44]. It is worth mentioning that similar formulations are obtained for phase b and phase c by a phase shift of $\pm 2k\pi/3$, respectively, as shown in (5.20). The parametric functions can be obtained using the MSS approach; and all the data are stored and tabulated in look-up tables for subsequent use in Matlab/Simulink.

5.3 DP Modelling of DC Subsystem with Ripples

Contrary to the previous work [6], [65], [67], [69]-[70] where only the DC component has been included in DC side, this section includes the 6th and 12th order components in DC subsystem in order to reproduce the DC ripples. Since the 6th and 12th harmonics are commonly-found harmonics in rectifier loads in practice [71], the corresponding DPs are considered here.

The 0th order DP representation of DC subsystem can be directly compatible with the time-domain model, as mentioned in Chapter 3, for which the 0th order DPs are formulated [65], [70] as

$$\begin{cases} v_{dc} = v_c + r_{dc} i_{dc} + v_L \\ C_{dc} \cdot \dfrac{d}{dt} v_c = i_{dc} - \dfrac{v_c}{R_{load}} \\ \dfrac{d}{dt} v_L = \dfrac{1}{\tau}(L_{dc} \dfrac{d}{dt} i_{dc} - v_L) \end{cases} . \tag{4.26}$$

Herein, time constant τ should be selected small enough so that its effect at switching frequency is negligible [43].

However, based on operation features of the GAM-type DPs specified in [6], [67], [69], the high-order DPs representation of DC side is different from the 0th order. First of all, DC subsystem modelled in time-domain expressed as (5.26) can be rewritten as (5.27), after applying GAM approach.

$$\begin{cases} \langle v_{dc} \rangle_{k_{dc}} = \langle v_L \rangle_{k_{dc}} + \langle v_c \rangle_{k_{dc}} + r_{dc} \langle i_{dc} \rangle_{k_{dc}} \\ \dfrac{d}{dt} \langle v_c \rangle_{k_{dc}} = \dfrac{1}{C} \langle i_{dc} \rangle_{k_{dc}} - \left(\dfrac{1}{CR_{load}} + \mathrm{j} k_{dc} \omega_s \right) \langle v_c \rangle_{k_{dc}} \\ \dfrac{d}{dt} \langle v_L \rangle_{k_{dc}} = \dfrac{L_{dc}}{\tau} \dfrac{d}{dt} \langle i_{dc} \rangle_{k_{dc}} - \left(\dfrac{1}{\tau} + \mathrm{j} k_{dc} \omega_s \right) \langle v_L \rangle_{k_{dc}} + \left(\mathrm{j} k_{dc} \omega_s \dfrac{L_{dc}}{\tau} \right) \langle i_{dc} \rangle_{k_{dc}} \end{cases} . \tag{4.27}$$

The model is built up in DPs and should be decomposed into real and imaginary parts as followings

$$\begin{cases} \begin{bmatrix} \langle v_{dc,r} \rangle_{k_{dc}} \\ \langle v_{dc,i} \rangle_{k_{dc}} \end{bmatrix} = \begin{bmatrix} 1 & 0 & 1 & 0 \\ 0 & 1 & 0 & 1 \end{bmatrix} \begin{bmatrix} \langle v_{L,r} \rangle_{k_{dc}} \\ \langle v_{L,i} \rangle_{k_{dc}} \\ \langle v_{c,r} \rangle_{k_{dc}} \\ \langle v_{c,i} \rangle_{k_{dc}} \end{bmatrix} + \mathbf{R}_{dc} \begin{bmatrix} \langle i_{dc,r} \rangle_{k_{dc}} \\ \langle i_{dc,i} \rangle_{k_{dc}} \end{bmatrix}, k_{dc} = \{6, 12\}, \\ \mathbf{R}_{dc} = \begin{bmatrix} r_{dc} & 0 \\ 0 & r_{dc} \end{bmatrix}; \end{cases} \tag{4.28}$$

In terms of modelling the DC subsystem, i_{dc} acts as the input variable, while the voltage v_{dc} is the output variable. Moreover, the voltages across inductor L_{dc} and capacitor C can be regarded as state variables, which can be computed through below equation:

$$\frac{d}{dt}\begin{bmatrix} \langle v_{L,r} \rangle_{k_{dc}} \\ \langle v_{L,i} \rangle_{k_{dc}} \\ \langle v_{c,r} \rangle_{k_{dc}} \\ \langle v_{c,i} \rangle_{k_{dc}} \end{bmatrix} = \begin{bmatrix} -\frac{1}{\tau} & k\omega_s & 0 & 0 \\ -k\omega_s & -\frac{1}{\tau} & 0 & 0 \\ 0 & 0 & -\frac{1}{R_{load}C} & k\omega_s \\ 0 & 0 & -k\omega_s & -\frac{1}{R_{load}C} \end{bmatrix} \begin{bmatrix} \langle v_{L,r} \rangle_{k_{dc}} \\ \langle v_{L,i} \rangle_{k_{dc}} \\ \langle v_{c,r} \rangle_{k_{dc}} \\ \langle v_{c,i} \rangle_{k_{dc}} \end{bmatrix} + \begin{bmatrix} 0 & -\frac{L_{dc}k\omega_s}{\tau} & \frac{L_{dc}}{\tau} & 0 \\ \frac{L_{dc}k\omega_s}{\tau} & 0 & 0 & \frac{L_{dc}}{\tau} \\ \frac{1}{C} & 0 & 0 & 0 \\ 0 & \frac{1}{C} & 0 & 0 \end{bmatrix} \begin{bmatrix} \langle i_{dc,r} \rangle_{k_{dc}} \\ \langle i_{dc,i} \rangle_{k_{dc}} \\ \frac{d}{dt}\langle i_{dc,r} \rangle_{k_{dc}} \\ \frac{d}{dt}\langle i_{dc,i} \rangle_{k_{dc}} \end{bmatrix}.$$

(4.29)

Finally, the DC subsystem can is modeled using the DC and selected harmonic components of DPs, according to (5.27)-(5.29).

5.4 Implementation

5.4.1 Constructing Parametric Functions of LCR Considering DC Ripple

The numerically extracted parametric functions are depicted in Figure 5.3 and Figure 5.4. These functions have been calculated using the MSS approach [43]-[44], and they plotted with respect to dynamic impedance. The calculated parametric functions for DC variables are also depicted in Figure 5.5 and Figure 5.6. All these data are stored and tabulated in look-up tables for the future use in Matlab/Simulink.

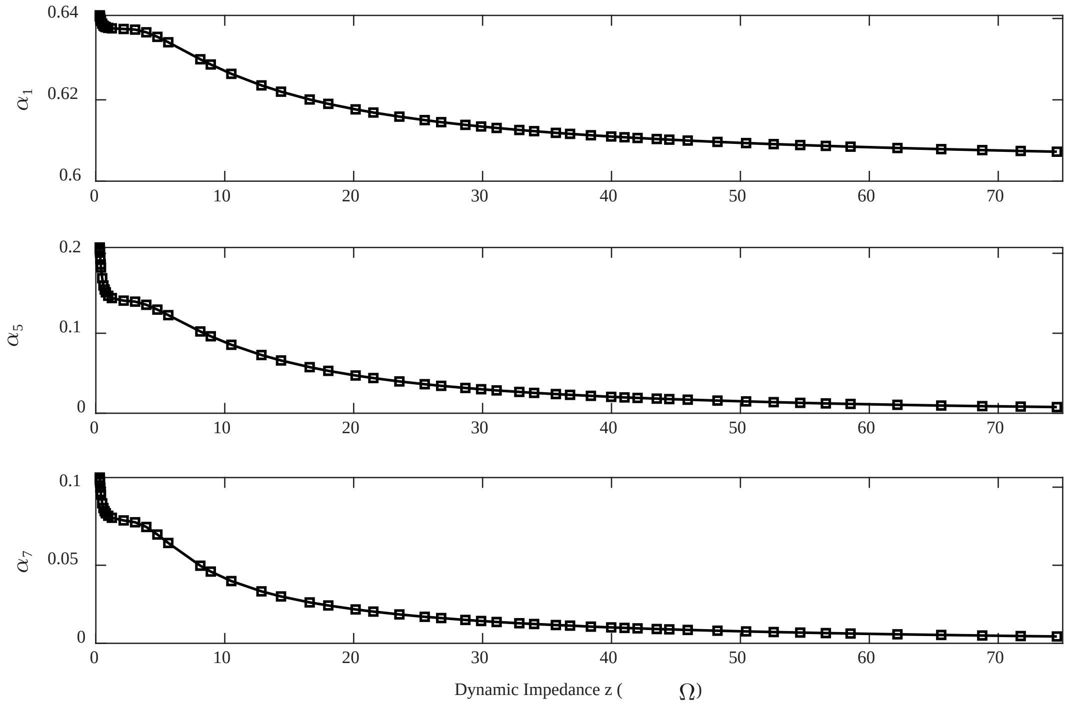

Figure 5. 3 Parametric functions $\alpha_1(z)$, $\alpha_5(z)$, $\alpha_7(z)$ extracted from detailed simulations.

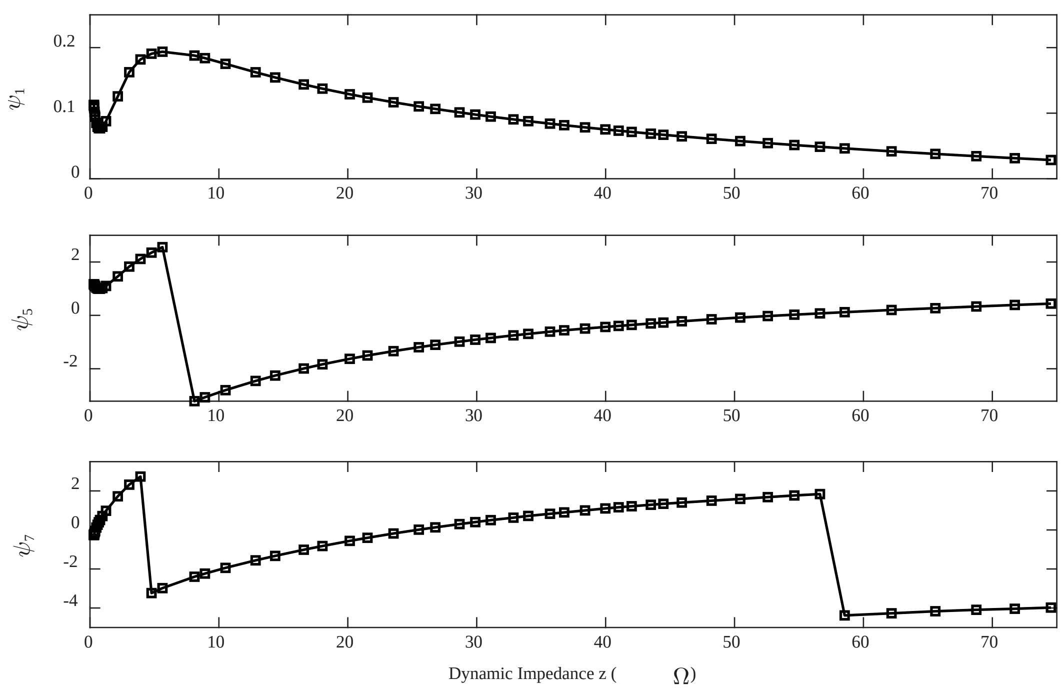

Figure 5. 4 Parametric functions $\varphi_1(z)$, $\varphi_5(z)$, $\varphi_7(z)$ extracted from detailed simulations.

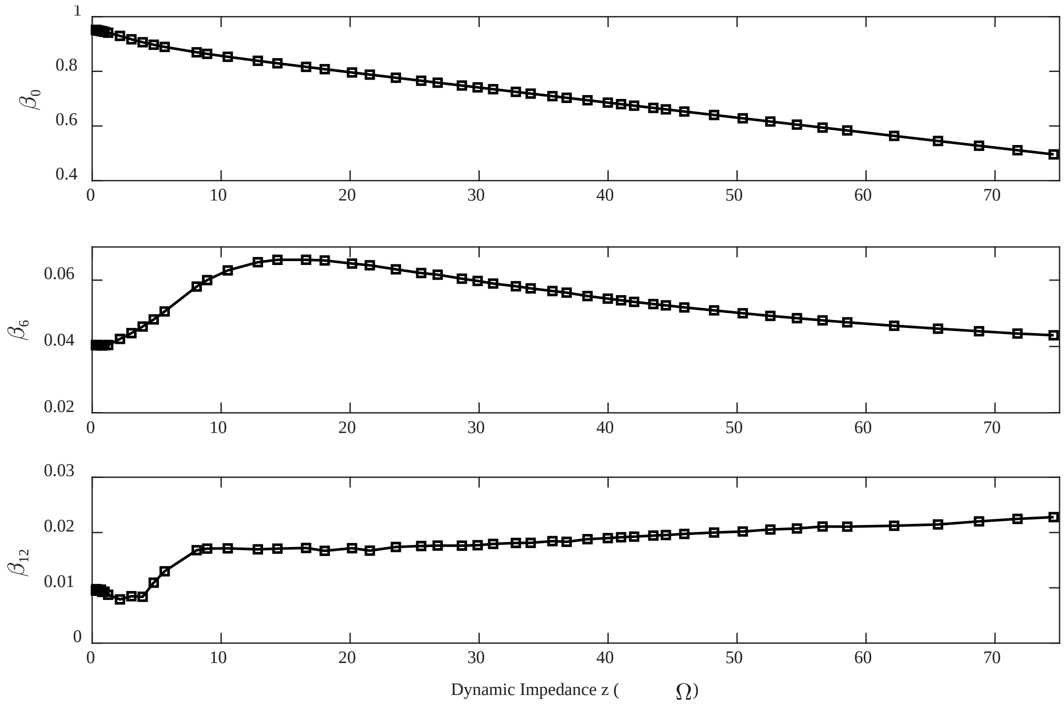

Figure 5. 5 Parametric functions β_0 (z), β_6 (z), β_{12} (z) extracted from detailed simulations.

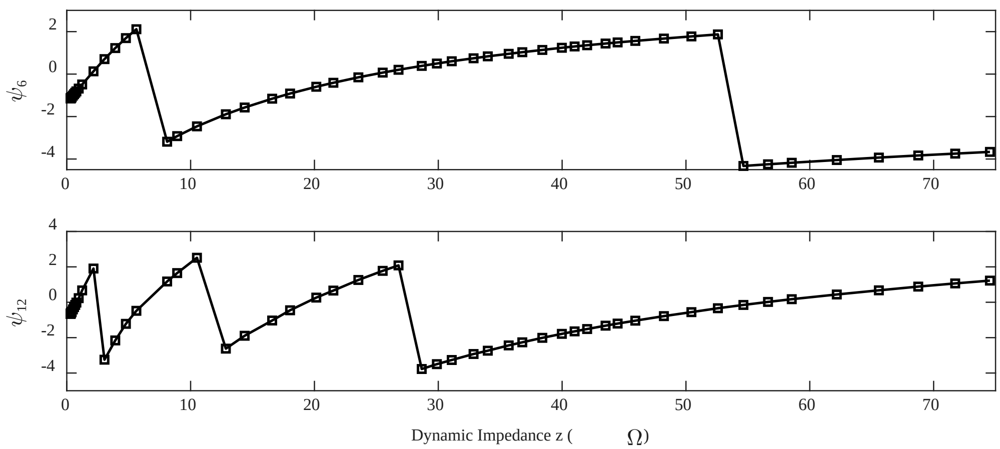

Figure 5. 6 Parametric functions φ_6 (z), φ_{12} (z) extracted from detailed simulations.

5.4.2 Subsystem Interface and Implementation

The full-order PDP modelling of the considered SM-rectifier system is composed of three parts: 1) the SM expressed as a 60hz power source using CP-VBR stator interfacing equations in

DPs representation (5.18), the rotor dynamics in time-domain representation (5.8)-(5.12); and time-domain DP interfacing equations (5.15)-(5.17), high-order DPs including dynamics by (5.14); 2) the LCR represented by (5.20), (5.22)-(5.25); and 3) the DC subsystem modeled via Differential Algebraic equations (5.26) in time domain for 0th order components and state-space equations in DPs representation (5.28), and (5.29) for high-order components. The implementation of all three subsystems is illustrated in Figure 5.7, in hybrid time-dynamic phasor domain.

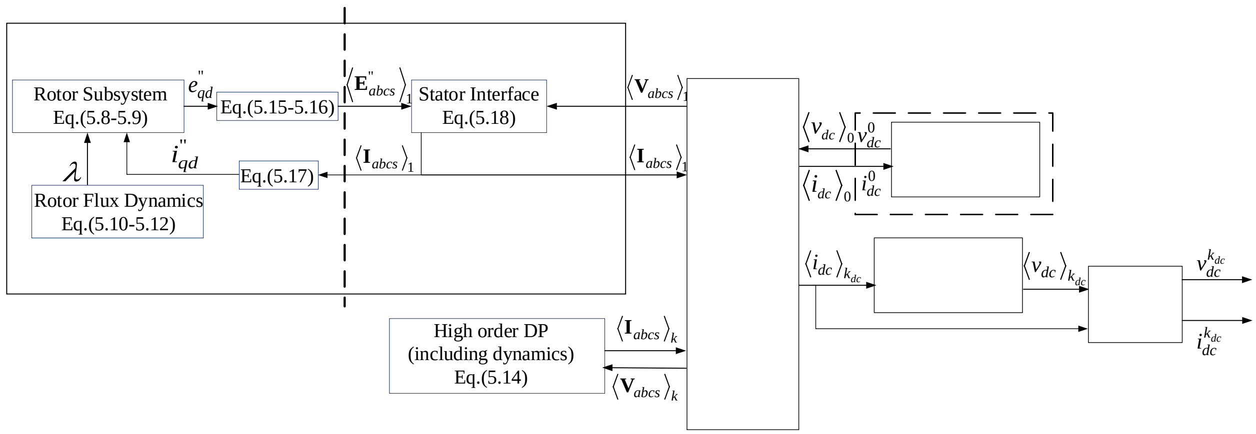

Figure 5. 7 Implementation of full-order PDP model of SM-rectifier system with prediction of DC ripple.

Since SM is assumed as a power source at fundamental frequency, compared to the full-order model, no changes are made on SM in reduced-order PDP model as depicted in Figure 5.8. However, the reduced-order model excludes the dynamics of high-order components by algebraic expressions as shown in (5.19), which is seen as the only difference.

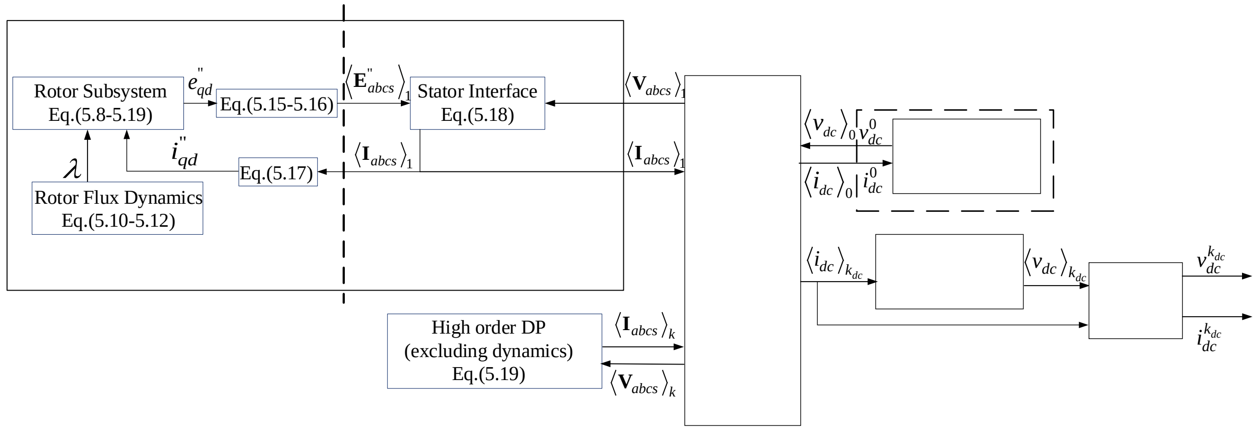

Figure 5. 8 Implementation of reduced-order PDP model of SM-rectifier system with prediction of DC ripple.

5.5 Computer Studies

In this section, computer studies are performed on the benchmark SM-rectifier system show in Figure 5. 2 with parameters as in [43]. The full-order PDP model and reduced-order PDP model have been implemented in Matlab/Simulink [32] based on Figure 5.7 and Figure 5.8, while the detailed model has been implemented in PLECS [33] and used to produce the reference solution. A case study spanning different operating modes is investigated. The system starts up in steady-state operation corresponding to common CCM-1 operating mode with a constant excitation of E_{xfd} =19.5 V and an equivalent DC load r_{dc}= 21Ω. At t = 0.5s, the DC load steps down to r_{dc}= 0.5Ω and the system runs until t = 1s operating in CCM-2 mode. For consistency, all case studies are conducted on a PC with a 3.4GHz Intel i7-2600 CPU.

5.5.1 Small-Step-Size Study

This system is first solved using the ode 23tb solver with the following settings: relative and absolute error tolerances of 10^{-4}, and maximum and minimum step sizes of 100 μs and 0.1 μs, respectively. Figure 5.9 shows the system response of phase a and DC voltages and currents as predicted by different subject models. For better illustration, three magnified fragments of Figure 5.9 that depict the system operation in CCM-1 and CCM-2 modes are also shown in more detail in Figure 5.10 and Figure 5.11, respectively.

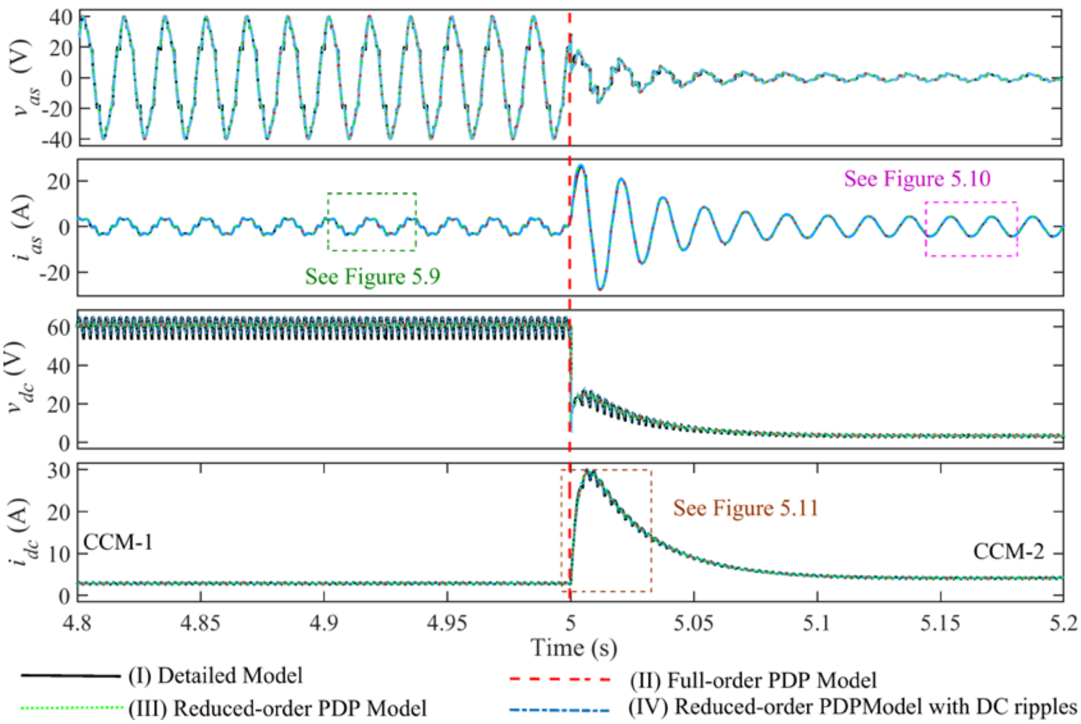

Figure 5. 9 System response to load change as predicted by the subject models.

As shown in Figure 5.10 and Figure 5.11, all three PDP models yield consistent results ain both CCM-1 and CCM-2 operating modes, in terms of phase a voltage and current. The three PDP models perform well and accurately predict phase a variables even in heavy mode CCM-2, where the voltages are highly distorted and currents are close to sinusoidal, as shown in Figure 5.11. However, the prior full-order PDP model and the prior reduced-order PDP model only capture the average value of the DC voltages and currents. At the same time, the new proposed reduced-order PDP model with DC ripple is able to reproduce the very accurate waveforms even on the DC side, as shown in Figure 5.10 and Figure 5.11. Moreover, as shown in Figure 5.12, all three PDP models match the detailed model solutions very well. From phase *a* responses, it's shown in Figure 5.12 that all three PDP models result in consistent transient responses. From DC responses, the advantageous accuracy of the new proposed PDP model is demonstrated in the way of tracking very closely the details of the reference solution of DC variables.

In addition, the accurate prediction of DC currents and voltages by the proposed model reveals sufficient and proper selection of the desired orders (0 th, 6 th,12 th) when constructing the rectifier parametric functions and building the DC subsystem model. As depicted in Figure 5.13, the FFT analysis of steady-state DC current responses also validates the proper selection of harmonic components.

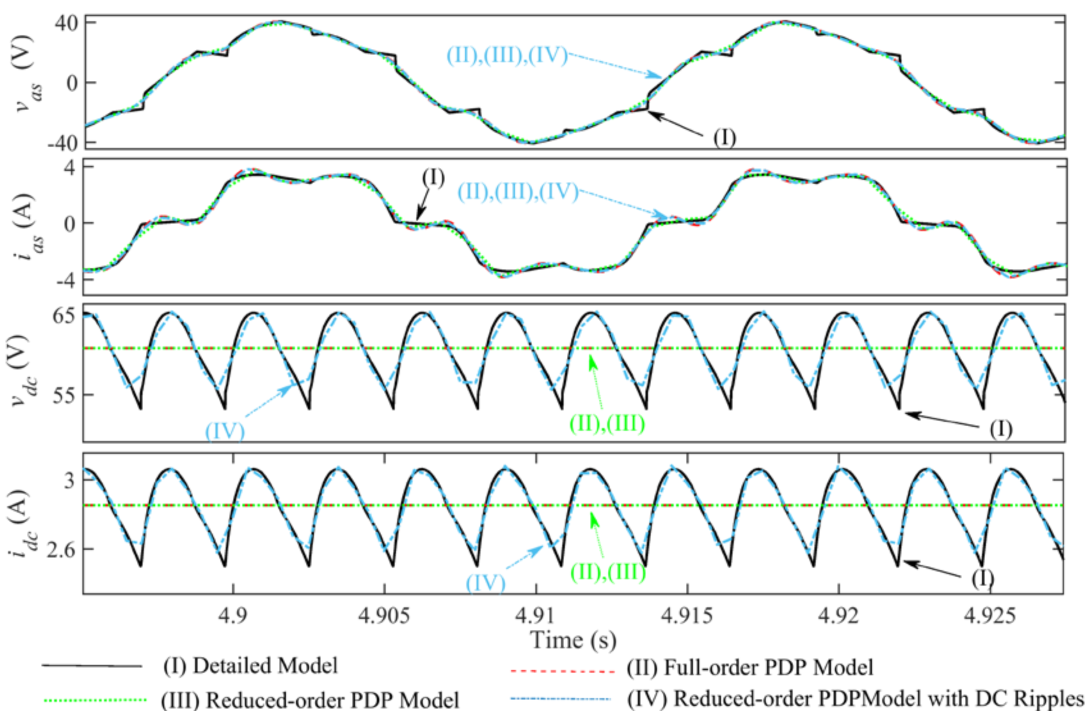

Figure 5. 10 Magnified view of system responses in steady state in CCM-1 mode.

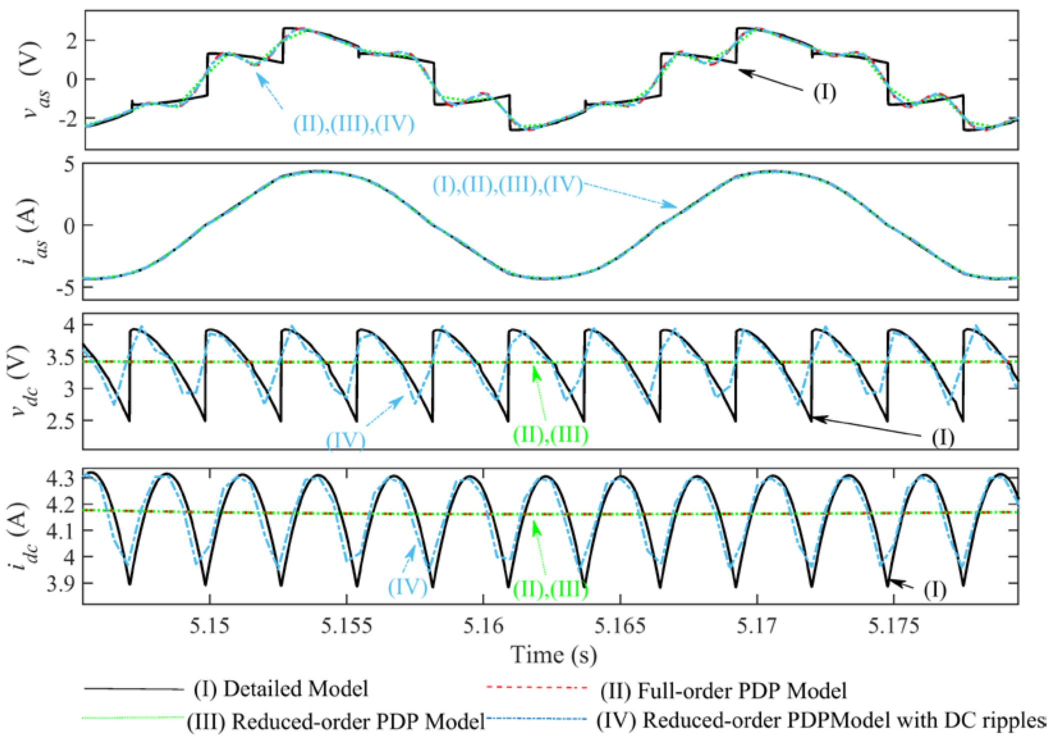

Figure 5. 11 Magnified view of system response in steady state in CCM-2 mode.

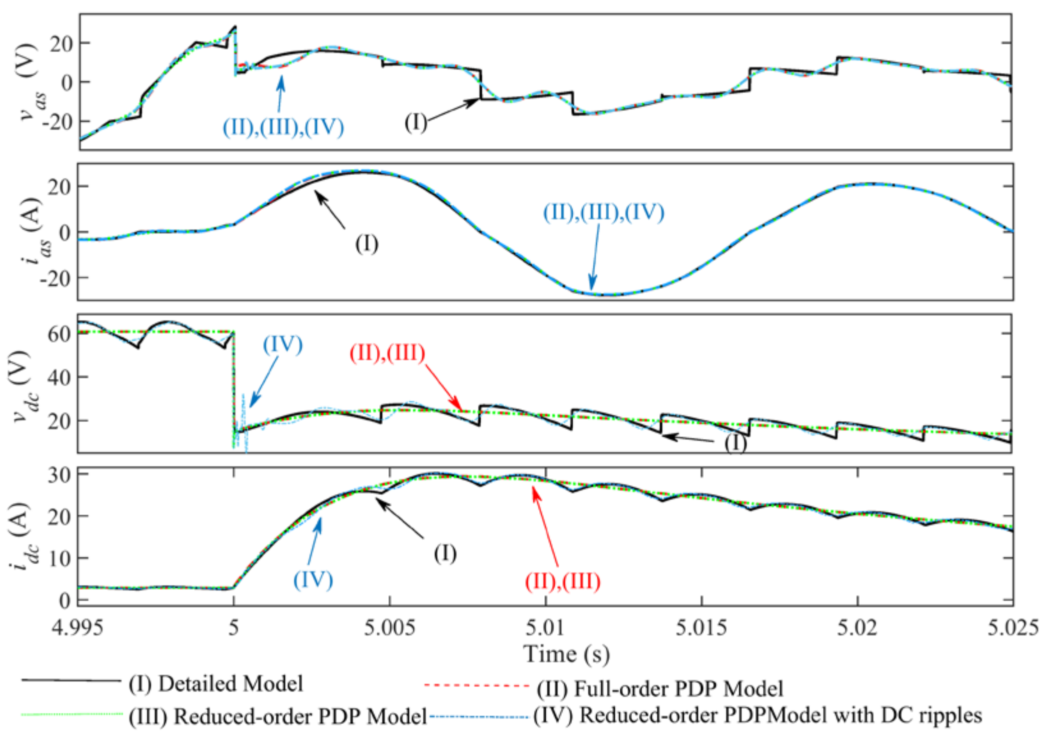

Figure 5. 12 Magnified view of transient response during change from CCM-1 to CCM-2 mode.

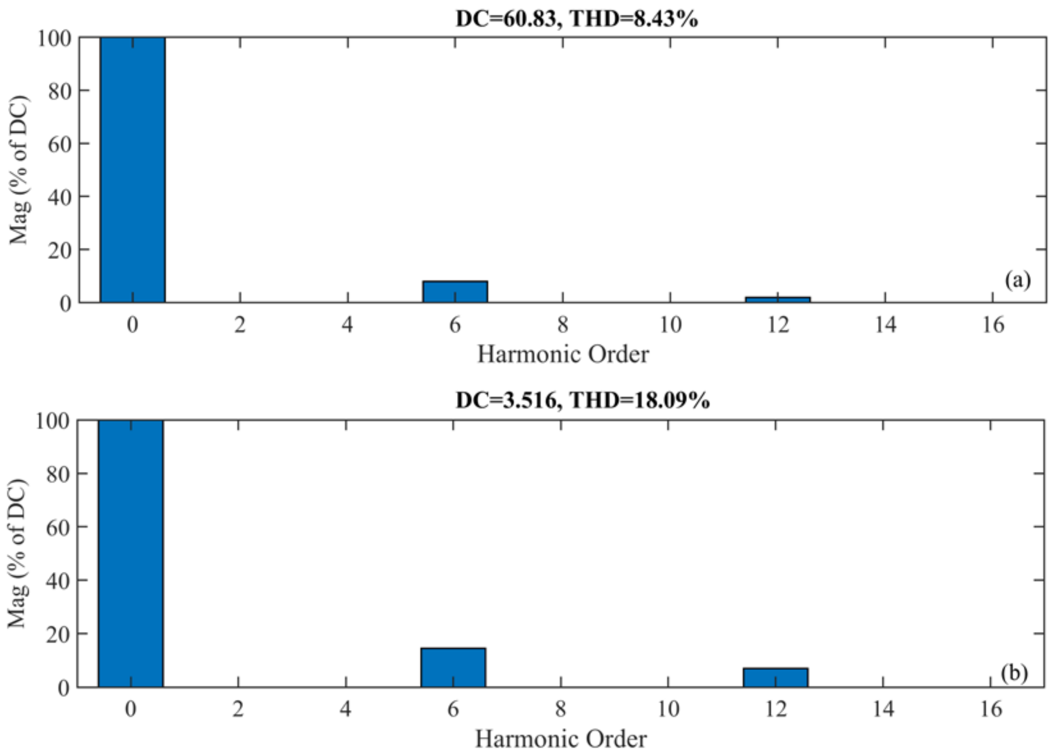

Figure 5. 13 Harmonic content of DC voltage for the considered operating modes: (a) CCM-1, (b) CCM-2.

5.5.2 Flexible-Step-Size Study

To evaluate the numerical performance, all four subject models have been used to conduct the same flexible time step case study as in Section 5.5.1 using the ode23tb solver with maximum time step size enlarged to 5 ms, and error tolerances set to 1e-3. Figure 5.14 demonstrates the time step size Δt taken by each subject model during the entire simulation. As is seen in Figure 5.14, the detailed model uses very small time steps even in steady state, which is due to constant switching of the LCR. The three PDP models can use maximum time step size in steady state. Even though the PDP models all use much smaller time steps during the transients of load changes, they are generally able to increase the step size fairly rapidly once in steady state.

Those observations can be verified in Figure 5.15. All three PDP models produce accurate AC transient response using similarly small time step size. However, during steady state, PDP models are able to simulate at relatively large time step size. In terms of DC response, reduced-order PDP model with DC Ripples considers high-order harmonics in DC side so that it can predict harmonic rings during transient period.

For quantitative analysis, Table 5.1 summarizes the number of time steps, the CPU time, and the average time step for all four subject models. As it can be seen in Table 5.1, all three PDP models have superior numerical efficiency compared to the detailed switching model with less number of steps taken and less CPU time.

At the same time, it is noted that the proposed reduced-order PDP model takes significantly fewer steps (2,283 vs. 2,862) and executes much faster (1.28s vs. 1.8s) than the full-order model. In addition, the reduced-order PDP model with ripples outperforms the full-order PDP model in terms of both the number of time steps (2,802 vs. 2,862) and the CPU time (1.64s vs. 1.8s). Due to the constantly excited transients which are present in all higher-order DPs (harmonics), the variable time step of the full-order PDP model cannot significantly increase and the average time step is only 3,494.06μs. At the same time, the reduced-order PDP model has the transients of the fundamental component only (since the harmonic DPs are solved algebraically assuming their steady state), and its average time step is much higher than that of the reduced-order PDP model with ripples (4380.20μs vs. 3568.88μs), as summarized in Table 5.1.

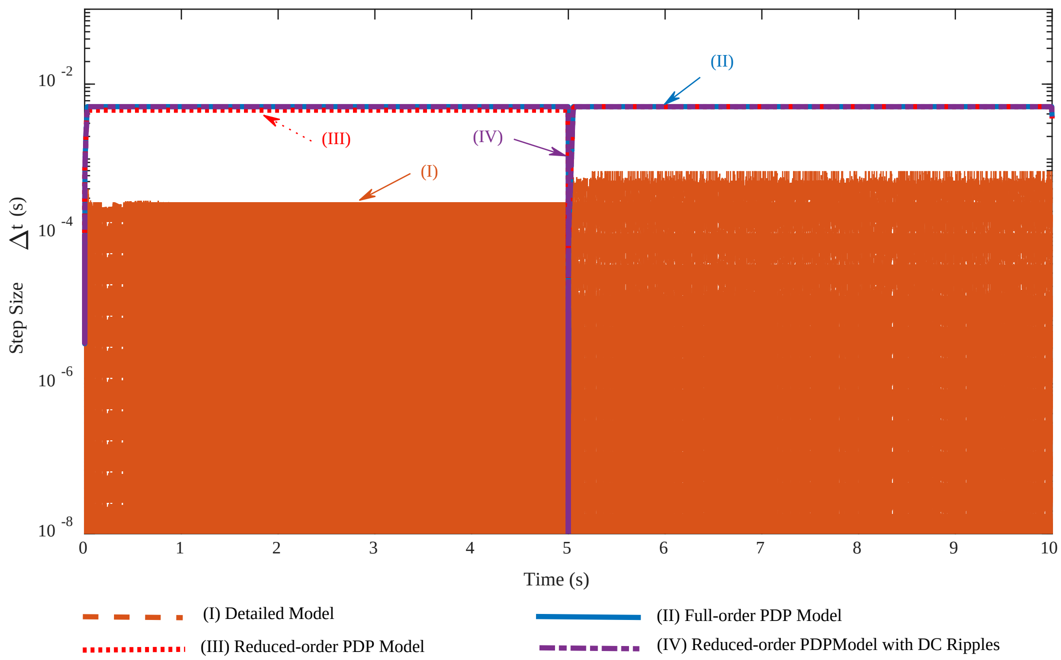

Figure 5. 14 Step size Δt as taken by subject models.

Table 5. 1 Numerical efficiency of all subject models for variable time step study of 10 seconds.

Model	No. of Time Steps	Total CPU Time, s	Average Time Step, μs
Detailed Model	74393	21.53	134.42
Full-Order PDP	2862	1.80	3494.06
Reduced-Order PDP	2283	1.28	4380.20
Reduced-Order PDP with DC Ripples	2802	1.64	3568.88

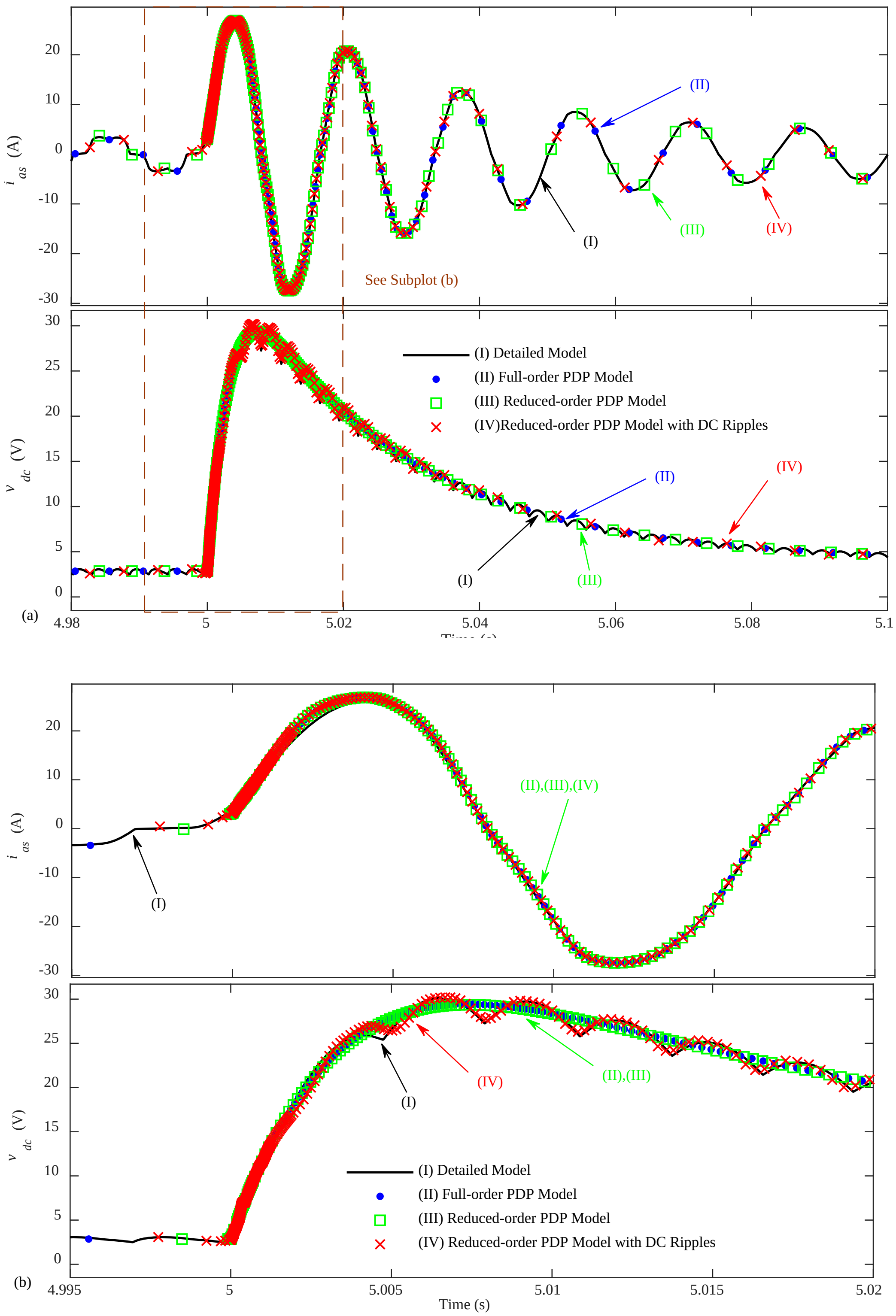

Figure 5. 15 system responses of subject models in flexible time step size study: (a) AC current i_{as} and DC voltage v_{dc}, and (b) magnified view from subplot (a).

Chapter 6: Conclusions

6.1 Summary of Contributions

The technical challenges resulting from the newly emergent integrated AC-DC power systems have also impacted the computer simulations that are required to study systems' dynamic behavior in an efficient manner. Various simulation programs and solution approaches have been developed throughout years, each aiming at investigation of specific classes of transient phenomena. A hybrid time-phasor signal representation called the dynamic phasor (DP) has been receiving increasing attention in the recent literature on system modelling and simulation techniques, due to its suitability to both electromagnetic and electromechanical transients in power systems. This thesis focuses developing innovative reduced-order GAM-Type DP modelling approach that may be suitable for various emerging AC-DC power systems to capture the dynamic behavior at reduced computational cost. The proposed novel concept of combining the differential equations (DE) and algebraic equations (AE) for DPs with harmonics is demonstrated on a series of representative example AC-DC benchmark systems, and their simulation studies and analysis of numerical performance.

To set the stage for the proposed research, Chapter 2 summarizes different simulation methods and signal representations, as needed to formulate the **Objective 1**. The two commonly-used methodologies used in EMT simulation of power systems, namely the EMTP and State-Variable (SV) based programs have been discussed in Chapter 2, with the work in this thesis being limited to SV-based tools only. The two types of dynamic phasor (DP) representations, namely the SFA and the GAM approaches have been discussed as well.

The initial **Objective 1** has been achieved in Chapter 3, where a new reduced-order parametric dynamic phasor (PDP) modelling approach has been developed and demonstrated on a generic integrated AC-DC system. The contribution of Chapter 3 lays in proposing a numerically efficient dynamic phasor modelling technique where the fundamental order DPs are formulated as differential equations; and the harmonic DPs are represented as algebraic equations. This formulation results in fewer state variables (6 state variables vs. 18 state variables) presented in Section 3.3.2, and achieves computational advantages over the previously established full-order PDP model and detailed model, as has been validated by computer studies in Section 3.5. Flexible-time-step study in Section 3.5.1 shows that compared to the full-order PDP model, the new proposed reduced-order model accelerates the simulation (1.91s vs. 0.77s) and significantly reduces the number of required time steps (10,499 vs. 2,229). In addition, since the dynamics of high-order harmonics is negligible, the elimination of differential terms almost have no effect on the simulation accuracy, which is revealed in both variable-time-step size studies and fixed-time-step size studies.

In Chapter 4, the **Objective 2** is achieved by presenting an easily-interfaced modelling technique for three-phase transformer based on the GAM and extending the reduced-order PDP method to AC distribution system with transformers and rectifier loads. Instead of deriving a single-phase equivalent circuit of a three-phase transformer, the proposed technique of Section 4.1 allows to use the winding voltages and currents directly, which facilitates the deriving single-phase equivalent circuit when the transformer windings are Δ-connected. To interface with the rest of power network, appropriate phase shift and magnitude scaling are applied to the currents and voltages. Then, the reduced-order PDP modelling technique is applied to validate the modelling accuracy and efficiency. The computer studies in Section 4.4 demonstrates fewer time steps and less CPU time is taken by the reduced-order model than by the detailed model (2,312 vs. 48,644 and 0.95s vs. 9.14s, respectively), while modelling accuracy is retained as shown in both steady state analysis and transient analysis.

The initial **Objective 3** is achieved in Chapter 5, where the DC ripples are first considered in modelling of AC-DC systems, and a reduced-order parametric dynamic phasor modelling method is extended to integrated SM-rectifier system. Section 5.1 shows a reduced-order GAM-type CP-VBR model for synchronous machine. This new model achieves a constant-parameter *abc*-phase stator-network interface, thus avoiding the time-varying inductance caused by dynamic saliency. Section 5.2 proposed the parametric functions for LCRs to include the DC ripples in the dynamics of the DC subsystem. This new set of parametric functions allows to accommodate any desired order of harmonics in both AC and DC sides, which tends to increase simulation accuracy. Modelling of DC subsystem is extended to include the high-order components using GAM-Type DPs solution, as represented in Section 5.3. Computer studies in Section 5.4 validate the new model in terms of predicting the DC ripples, as was desired in **Objective 3**. In terms of computational cost, the proposed reduced-order PDP model takes significantly fewer steps (2,283 vs. 74,393) and executes much faster (1.28s vs. 21.53s) than the detailed model. In addition, the reduced-order PDP model with ripples outperforms the full-order PDP model in terms of both the number of time steps (2,802 vs. 2,862) and CPU time (1.64s vs. 1.80s).

The proposed reduced-order PDP methodology and the new models have numerically efficient structure, which makes them ideal for including in many commonly-used EMT simulation while offering appreciable computational gains. It is envisioned that the new reduced-order PDP models presented in Chapters 3–5 will greatly benefit many researchers and engineers around the world who are working on applications of AC-DC systems, and require fast and accurate EMT simulations for system-level studies.

6.2 Future Work

To conclude this thesis, some potential areas for extension of the proposed work are discussed below:

- **Extending the reduced-order PDP model to thyristor-controlled LCR systems**

The line-commutated-rectifiers studied in this thesis are ideal with no firing control. However, the thyristor-controlled LCR systems are also utilized in many industrial applications where the rectifier can be fed from either a rotating machine or a distribution feeder/transformer. Accordingly, the thyristor firing pulses can be generated based on the sensed rotor position or filtered terminal voltages, respectively. To build up a reduced-order PDP model for thyristor-controller LCR benchmark system, more parameters and corresponding parametric functions are required.

- **Inclusion of magnetic saturation into DP modelling of rotating machines**

The SM model used in this thesis assumes a magnetic linearity. Nevertheless, magnetic saturation commonly happens in SMs in practice, which leads to changes of effective inductance as the magnetizing flux changes [42]. This requires modelling technique to adequately incorporate the effect of magnetic saturation into the general-purpose models. A future research task would be to derive an appropriate model for SM in DP-GAM domain to achieve more accurate prediction of power system transients and maintain numerical efficiency.

References

[1] R. E. P. N. for the 21st century, “Renewables 2017 Global Status Report,” Tech. Rep. 2017, REN21.

[2] “Electric Power Monthly with Data for March 2017,” U.S. Energy Information Administration (EIA), U.S. Department of Energy, Washington, DC, Jun. 2017. [Online]. Available: https://www.eia.gov/electricity/monthly/ . (Consulted on June.28, 2017).

[3] U.S. Department of Energy (DOE). (2014) Smart Grid System Report. [Online]. Available: https://www.smartgrid.gov/files/2014-Smart-Grid-System-Report.pdf (Consulted on Jun.28, 2017).

[4] N. Hatziargyriou, H. Asano, R. Iravani, and C. Marnay, “Microgrids,” *IEEE Power Energy Mag*., vol. 5, no.4, pp.78-94, Jul./Aug. 2007.

[5] D. E. Olivares, et al., "Trends in microgrid control," *IEEE Tran. Smart Grid*, vol. 5, no.4, pp. 1905-1919, Jul. 2014.

[6] Y. Huang, "Numerically Efficient Modelling and Simulation of Integrated AC-DC Power Systems using Dynamic Phasor Type Solutions," Ph.D. dissertation, Univ. British Columbia, Vancouver, BC, Canada, 2017.

[7] H. Chang, "Smart Electronic Loads for Harmonic Compensation in Future Electrical Distribution Systems," M.A.Sc. thesis, Univ. British Columbia, Vancouver, BC, Canada, 2017.

[8] “Challenges to the Integration of Renewable Resources at High System Penetration,” California Institute for Energy and Environment, Berkeley, CA, May 2014. [Oline]. Available: http://www.energy.ca.gov/2014publications/CEC-500-2014-042/CEC-500-2014-042.pdf. (Consulted on Jun.28, 2017).

[9] N. Mohan and T. M. Undeland, *Power Electronics: Converters, Applications, and Design*. New York, NY, USA: Wiley, 2007.

[10] G. Seguir, *Power Electronic Converters: AC-DC Conversion*. New York, NY, USA: McGraw-Hill, 1986.

[11] T. H. Nguyen, D. Lee and C. Kim, "A Series-Connected Topology of a Diode Rectifier and a Voltage-Source Converter for an HVDC Transmission System," *IEEE Trans. Power Electron*., vol. 29, no. 4, pp. 1579-1584, April 2014.

[12] N. Zhou, J. Wang, Q. Wang and N. Wei, "Measurement-Based Harmonic Modeling of an Electric Vehicle Charging Station Using a Three-Phase Uncontrolled Rectifier," *IEEE Trans. Smart Grid*, vol. 6, no. 3, pp. 1332-1340, May 2015.

[13] A. Cross, A. Baghramian and A. Forsyth, "Approximate, average, dynamic models of uncontrolled rectifiers for aircraft applications," *IET Power Electronics*, vol. 2, no. 4, pp. 398-409, July 2009.

[14] Z. Jin, L. Meng, J. M. Guerrero and R. Han, "Hierarchical Control Design for a Shipboard Power System With DC Distribution and Energy Storage Aboard Future More-Electric Ships," *IEEE Trans. Ind. Informat*, vol. 14, no. 2, pp. 703-714, Feb. 2018.

[15] J. Sun, "Impedance-based stability criterion for grid-connected inverters," *IEEE Trans. Power Electron*., vol 26, no.11, pp. 3075-3078, Nov. 2011.

[16] M. Amin and M. Molinas, "Understanding the origin of oscillatory phenomena observed between wind farms and HVdc systems," *IEEE Trans. Emerg. Sel. Topics Power Electron.*, vol. 5, no. 1, pp. 378-392, March 2017.

[17] X. Wang, F. Blaabjerg and W. Wu, "Modelling and analysis of harmonic stability in an AV power-electronics-based power system," *IEEE Trans. Power Electron*., vol.29, no.12, pp. 6421-6432, Dec. 2014.

[18] J. Arrillaga and N.R. Watson, *Computer Modelling of Electrical Power Systems*, 2nd ed. Chichester, UK: John Wiley&Sons, Ltd, 2001.

[19] P.W. Sauer and M. A. Pai, *Power System Dynamics and Stability*, Prentice-Hall, 1998.

[20] P. Kundur, *Power System Stability and Control*. New York: McGraw-Hill, 1994.

[21] Y. Huang, L. Dong, S. Ebrahimi, N. Amiri and J. Jatskevich, "Dynamic Phasor Modeling of Line-Commutated Rectifiers with Harmonics Using Analytical and Parametric Approaches," *IEEE Trans. Energy Convers*., vol. 32, no. 2, pp. 534–547, Jun. 2017.

[22] S. Chiniforoosh, H. Atighechi, A. Davoudi, J. Jatskevich, A.Yazdani, S. Filizadeh, S. Sseedifard, J. A. Martinez, V. Sood, K. Strunz, J. Mahseredjian, and V. Dinavahi, "Dynamic Average Modeling of Front-End Diode Rectifier Loads Considering Discontinuous Conduction Mode and Unbalanced Operation," *IEEE Trans. Power Del*., vol. 27, no. 1, pp. 421–429, Jan. 2012.

[23] S. Henschel, "Analysis of electromagnetic and electromechanical power system transients with dynamic phasors," Ph.D. dissertation, Univ. British Columbia, Vancouver, BC, Canada, 1999.

[24] P. Zhang, J.R. Marti, and H. Dommel, "Shifted-frequency analysis for EMTP simulation of power-system dynamics," *IEEE Trans. Circuit Syst*. I: Reg. Papers, vol. 57, no. 9, pp. 2564-2574, Sep. 2010.

[25] S. Sanders, J. Noworolski, X. Liu and G. Verghese, “Generalized averaging method for power conversion circuits,” *IEEE Trans Power Electron*., vol. 6, no. 2, pp. 251–259, Apr. 1991.

[26] V. Venkatasubramanian, “Tools for dynamic analysis of the general large power system using time-varying phasors,” *Int. J. Elec. Power Energy Syst*., vol. 16, no.6, pp. 365-376, Dec. 1994.

[27] J. R. Martí, H. W. Dommel, B. D. Bonatto and A. F. R. Barrete, “Shifted Frequency Analysis (SFA) concepts for EMTP modelling and simulation of Power System Dynamics,” in *Proc. 18th Power Systems Computation Conf*., Wroclaw, Poland, Aug. 2014.

[28] T. H. Demiray, “Simulation of power system dynamics using dynamic phasors models,” Ph.D. dissertation, Swiss Fed. Inst. Technol., Zurich, Switzerland, 2008.

[29] T. Yang, “Development of dynamic phasors for the modelling pf aircraft electrical power systems,” Ph.D. dissertation, Univ. Nottingham, Nottingham, UK, 2013.

[30] T. Yang, S. Bozhko, J.M. Le-Peuvedic, G. Asher and C.I. Hill, “Dynamic phasor modelling of multi-generator variable frequency electrical power systems,” *IEEE Trans. Power Syst*., vol. 31, no. 1, pp. 563-571, Jan. 2016.

[31] “*PSCAD/EMTDC X4 On-line Help*,” Manitoba HVDC Research Centre and RTDS Technologies Inc., Winnipeg, MB, Canada, 2016. [Online]. Available: http://www.pscad.com. (Consulted on Jun.28,2017).

[32] *MATLAB 7(R2016b)*, The MathWorks Inc., Natick, MA, USA, 2016.

[33] PLECS Blockset, Plexim GmbH, Zurich, Switzerland, 2016. [Online]. Available: http://www.plexim.com/products/plecs_blockset.

[34] A. M. De Broe, S. Drouilhet, and V. Gevorgian, " A peak power tracker for small wind turbines in battery charging applications," *IEEE Trans. Energy Convers*., vol. 14, no. 4, pp. 1630-1635, Dec. 1999.

[35] A. Emadi, M. Ehsani, and J.M. Miller, *Vehicular Electric Power Systems: Land, Sea, Air, and Space Vehicles*. New York, NY, USA: Marcel Dekker, 2004.

[36] M. Barnes, D. Van Hertem, S. P. Teeuwsen, and M. Callavik, "HVDC systems in smart grids," in *Proc. IEEE*, to appear.

[37] Larry Lawhead, Randy Hamilton, John Horak, "Three Phase Transformer Winding Configurations and Differential Relay Compensation", presented at 60 th Annual Georgia Tech Protective Relay Conference, USA, 2006.

[38] S. Chiniforoosh, H. Atighechi, A. Davoudi, J. Jatskevich, A.Yazdani, J. A. Martinez, S. Sseedifard, D.C. Aliprantis, V. Sood, "Steady-state and dynamic performance of Front-End Diode Rectifier Loads as predicted by dynamic average-value models," *IEEE Trans. Power Del*., vol. 28, no. 3, pp. 1533-1541, Jul. 2013.

[39] H. Visser and P. van den Bosch, "Modelling of periodically switched networks," *Proc. IEEE PESC*, pp. 67-73, 1991.

[40] P. W. Lehn, "Exact modelling of the voltage source converter," *IEEE Trans. Power Del*., vol. 17, no. 1, pp. 217-222, Jan. 2002.

[41] K. L. Lian, B. K. Perkins and P. W. Lehn, "Harmonic Analysis of a Three-Phase Diode Bridge Rectifier Based on Sampled-Data Model," *IEEE Trans. Power Del*., vol. 23, no. 2, pp. 1088-1096, Apr. 2008.

[42] P. C. Krause, O. Wasynczuk, and S. D. Sudhoff, *Analysis of Electric Machinery and Drive Systems*, 2nd ed. Piscataway, NJ, USA: IEEE Press, 2002.

[43] J. Jatskevich, S. D. Pekarek and A. Davoudi, “Parametric dynamic average-value model of synchronous machine-rectifier system,” *IEEE Trans. Energy Convers*., vol. 21, no. 1, pp. 9-18, Mar. 2006.

[44] J. Jatskevich, S. D. Pekarek and A. Davoudi, “Fast procedure for constructing an accurate dynamic average-value model of synchronous machine-rectifier systems,” *IEEE Trans. Energy Convers*., vol. 21, no. 2, pp. 435–441, Jun. 2006.

[45] S. D. Pekarek, O. Wasynczuk, and H. J. Hegner, “An efficient and accurate model for the simulation and analysis of synchronous machine/converter systems,” *IEEE Trans. Energy Convers*., vol. 13, no. 1, pp.42-48, Mar. 1998.

[46] S. D. Pekarek and E. A. Walters, “An accurate method of neglecting dynamic saliency of synchronous machines in power electronic based systems,” *IEEE Trans. Energy Convers*., vol. 14, no. 4, pp.1177-1183, Dec. 1999.

[47] M. Chapariha, L. Wang, J. Jatskevich, H. W. Dommel, and S. D. Pekarek, “Constant-parameter R-L branch equivalent circuit for interfacing AC machine models in state-variable-based simulation packages,” *IEEE Trans. Energy Convers*., vol. 27, no. 3, pp. 634-645, Sep. 2012.

[48] F. Therrien, M. Chapariha, and J. Jatskevich, “Pole selection procedure for explicit constant-parameter synchronous machine models,” *IEEE Trans. Energy Convers*., vol. 29, no. 3, pp. 790-792, Sep. 2014.

[49] M. Chapariha, F. Therrien, J. Jatskevich, and H. W. Dommel, “Explicit formulations for constant-parameter voltage-behind-reactance interfacing of synchronous machine models,” *IEEE Trans. Energy Convers*., vol. 28, no. 4, pp. 1053-1063, Dec. 2013.

[50] L. Wang, J. Jatskevich, V. Dinavahi, H. W. Dommel, J. A. Martinez, K. Strunz, M. Rioual, G. W. Chang, and R. Iravani, "Methods of interfacing rotating machine models in transient simulation programs," *IEEE Trans. Power Del*., vol. 25, no. 2, pp. 891-903, Apr. 2010.

[51] R. H. Park, "Two-reaction theory of synchronous machines generalized method of analysis: part I," *Trans. Amer. Instit. Electr. Eng*., vol. 48, no. 3, pp. 716-727, Jul. 1929.

[52] P. Zhang, J. R. Marti, and H. W. Dommel, "Synchronous machine modelling based in shifted frequency analysis," *IEEE Trans. Power Syst*., vol. 22, no. 3, pp. 1139-1147, Aug. 2007.

[53] H. W. Dommel, *EMTP Theory Book*, MicroTran Power System Analysis Corporation, Vancouver, Canada, May 1992.

[54] Andrea T. J. Marti, "The Application of Shifted Frequency Analysis in Power System Transient Stability Studies ," M.A.Sc. thesis, Univ. British Columbia, Vancouver, BC, Canada, 2018.

[55] C. P. Steinmetz, *Theoretical Elements of Electrical Engineering*, McGraw-Hill, Inc., 1915.

[56] Salam, Md A., et al., *Fundamentals of Electrical Circuit Analysis*, Springer Singapore, Singapore, 2018.

[57] L. Cohen, *Time-Frequency Analysis*, New York: Prentice-Hall, 1995.

[58] F. Yahyaie and P. W. Lehn, "On Dynamic Evaluation of Harmonics Using Generalized Averaging Techniques," *IEEE Trans. Power Syst*., vol. 30, no. 5, pp. 2216–2224, Sep. 2015.

[59] B. Wu, *High-Power Converters and AC Drives*. Piscataway, NJ: IEEE Press, 2006.

[60] F. Wang, et al., “Analysis and design optimization of diode front-end rectifier passive components for voltage source inverters,” *IEEE Trans. Power Electron.*, vol. 23, no. 5, pp. 2278-2289, Sep. 2008.

[61] J. G. Hwang, P. W. Lehn, and M. Winkelnkemper, “A generalized class of stationary frame-current controllers for grid-connected ac-dc converters,” *IEEE Trans. Power Del.*, vol. 25, no. 4, pp. 2742-2751, Oct. 2010.

[62] M. E. Haque, M. Negnevitsky, and K. M. Muttagi, “A novel control strategy for a variable-speed wind turbine with a permanent-magnet synchronous generator,” *IEEE Trans. Ind. Appl.*, vol. 46, no. 1, pp. 331-339, Jan./Feb. 2010.

[63] R. S. Bhide, S. V. Kulkarni, and P. B. Bhandarkar, “Analysis for five-legged transformer used for parallel operation of rectifiers by coupled circuit field approach,” *IEEE Trans. Power Del.*, vol. 26, no. 2, pp. 607-616, Apr. 2011.

[64] Y. Suh, H. Park, Y. Lee, and P. K. Steimer, “A power conversion system for AC furnace with enhanced arc stability,” *IEEE Trans. Ind. Appl.*, vol. 46, no.6, pp. 2526-2535, Nov./Dec. 2010.

[65] X. Liang, Y. Huang, J. Xia and J. Jatskevich, "Reduced-order Parametric Dynamic Phasor Modeling of Line-commutated-rectifier Systems," in *Proc. IEEE PES General Meeting.*, Atlanta, USA, Aug. 2019.

[66] Sen. P. C., *Principles of Electric Machines and Power Electronics*, 3rd ed. Hoboken, NJ: John Wiley & Sons, Ltd, 2014.

[67] Y. Huang, S. Ebrahimi, N. Amiri, Z. Shan and J. Jatskevich, “Parametric dynamic phasor modeling of thyristor-controlled rectifier systems including harmonics for various

operating modes," *IEEE Trans. Energy Convers*., vol. 32, no. 4, pp. 1626-1629, Dec. 2017.

[68] S. Ebrahimi, N. Amiri, H. Atighechi, Y. Huang, L. Wang and J. Jatskevich, "Generalized parametric average-value model of line-commutated rectifiers considering AC harmonics with variable frequency operation," *IEEE Trans. Energy Convers*., vol. 33, no. 1, pp. 341-353, Mar. 2018.

[69] Y. Huang, H. Chang, S. Rezaee, and J. Jatskevich, "Parametric dynamic phasor modeling of synchronous machine-rectifier systems for integrated AC-DC microgrids," in *Proc. IEEE Power Energy Soc. Gen. Meet.*, Chicago, IL, USA, Jul. 2017, pp.1-5.

[70] X. Liang, Y. Huang, S. Ebrahimi and J. Jatskevich, "Reduced-Order parametric dynamic phasor modeling of AC distribution systems with rectifier loads," *2019 IEEE 28th International Symposium on Industrial Electronics (ISIE)*, Vancouver, BC, Canada, 2019, pp. 165-170.

[71] P. Mattavelli, G. C. Verghese, and A.M. Stankovic, "Phasor dynamics of thyristor-controlled series capacitor systems," *IEEE Trans. Power Syst*., vol. 12, no. 3, pp. 1259-1267, Aug. 1997.

[72] E. Hairer, S.P.Norsett, and G. Wanner, "*Solving Ordinary Differential Equations I; Nonstiff Problems*," Springer-Verlag, Berlin, 1993.

[73] E. Hairer, S.P.Norsett, and G. Wanner, "*Solving Ordinary Differential Equations II; Stiff Differential-Algebraic Problems,* " Springer-Verlag, Berlin, 1996.

[74] L. F. Shampine, M. W. Reichelt, "*The MATLAB ODE Suite*," *SIAM Journal on Scientific Computing*., vol. 18, no. 1, pp. 1-22, 1997.

[75] U. M. Ascher, L. R. Petzold, "*Computer Methods for Ordinary Differential Equations and Differential-Algebraic Equations*," *SIAM*, 1998.

[76] M. E. Hosea, L. F. Shampine, "*Analysis and implementation of TR-BDF2*," *Applied Numerical Mathematics*, vol. 20, Iss. 1–2, pp. 21-37, 1996,

Appendices

Appendix A   Parameters of LCR Benchmark System

System parameters [6]: $V_{line} = 480V$, $f_s = 60Hz$, $r_s = 0.2\Omega$, $L_s = 10mH$, $r_{dc} = 0.5\Omega$,$L_{dc} = 1.33mH$, $C_{dc} = 500uF$.

Appendix B Parameters of AC Distribution System with Rectifier loads

AC sub-system parameters:

V_{line} = 600V, f_s = 60Hz, r_s = 0.2Ω , L_s = 10mH, r_{s1} =5Ω, r_{s2} = 0.5Ω, L_{s2} = 0.01H.

DC sub-system parameters [25]:

r_{dc} = 0.5Ω ,L_{dc} = 1.33mH, C_{dc} = 500uF.

Transformer parameters:

r_1 =0.4Ω, r_2 = 0.1Ω, L_{l1} = 0.002 H, L_{l2} = 0.001 H, L_m = 98H, Turns Ratio=4:3.

Appendix C Parameters of SM-Rectifier system

Synchronous machine parameters:

835 MVA, 26 kV, 0.85 power factor, 2poles, 3600 r/min, J=0.0658e^6 J·s^2, r_s=0.00243 Ω, X_{ls}=0.1538 Ω, X_{mq}=1.3032 Ω, r_{kq1}=0.00144 Ω, X_{lkq1}=0.6578 Ω, r_{kq2}=0.0068 Ω, X_{lkq2}=0.07602 Ω, X_{md}=1.3032 Ω, r_{fd}=0.0075Ω, X_{lfd}=0.1145 Ω, r_{kd}=0.0108 Ω, X_{lkd}=0.06577 Ω.

DC sub-system parameters:

r_{dc} = 0.32Ω ,L_{dc} = 1.19mH, C_{dc} = 2.28uF.